

ผลของภาวะการทำงานของสารสังเคราะห์สังกะสีออกไซด์ด้วยกระบวนการเฟรนช์  
เพื่อมุ่งสู่การผลิตอนุภาคขนาดนาโน



นาย ชวลิต สมมติวัฒน์

วิทยานิพนธ์นี้เป็นส่วนหนึ่งของการศึกษาตามหลักสูตรปริญญาวิศวกรรมศาสตรมหาบัณฑิต

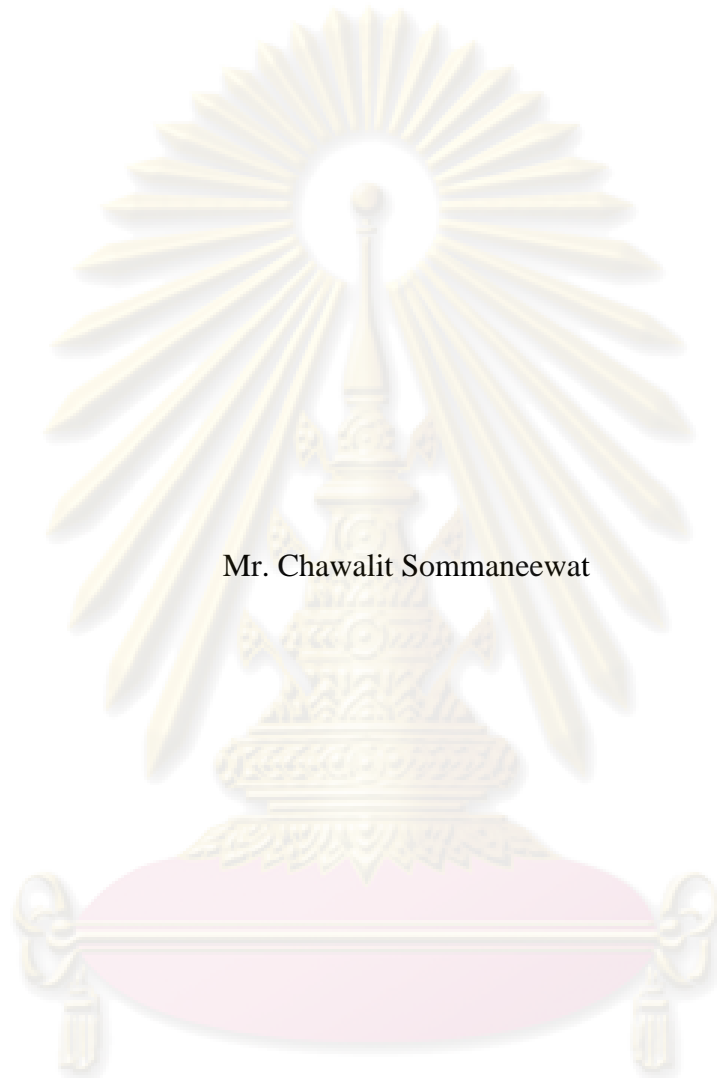
สาขาวิชาวิศวกรรมเคมี ภาควิชาวิศวกรรมเคมี

คณะวิศวกรรมศาสตร์ จุฬาลงกรณ์มหาวิทยาลัย

ปีการศึกษา 2551

ลิขสิทธิ์ของจุฬาลงกรณ์มหาวิทยาลัย

EFFECTS OF OPERATING CONDITIONS FOR ZINC OXIDE SYNTHESIS VIA  
FRENCH PROCESS TOWARD PRODUCTION OF NANOPARTICLES



Mr. Chawalit Sommaneevat

A Thesis Submitted in Partial Fulfillment of the Requirements  
for the Degree of Master of Engineering Program in Chemical Engineering  
Department of Chemical Engineering

Faculty of Engineering

Chulalongkorn University

Academic Year 2008

Copyright of Chulalongkorn University

Thesis Title EFFECTS OF OPERATING CONDITIONS FOR ZINC OXIDE SYNTHESIS VIA FRENCH PROCESS TOWARD PRODUCTION OF NANOPARTICLES

By Mr. Chawalit Sommaneeawat

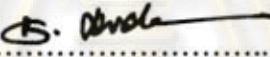
Field of study Chemical Engineering

Advisor Assistant Professor Varong Pavarajarn, Ph.D.

Co-Advisor Associate Professor Tawatchai Charinpanitkul, D.Eng.

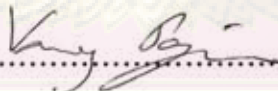
---


Accepted by the Faculty of Engineering, Chulalongkorn University in Partial Fulfillment of the Requirements for the Master's Degree

  
..... Dean of the Faculty of Engineering  
(Associate Professor Boonsom Lerthirunwong, Dr.Ing.)


THESIS COMMITTEE

  
..... Chairman  
(Professor Piyasan Praserthdam, Dr.Ing.)

  
..... Advisor  
(Assistant Professor Varong Pavarajarn, Ph.D.)

  
..... Co-Advisor  
(Associate Professor Tawatchai Charinpanitkul, D.Eng.)

  
..... Examiner  
(Assistant Professor Joongjai Panpranot, Ph.D.)

  
..... External Examiner  
(Chanchana Thanachayanont, Ph.D.)

ชวลิต สมมณีวัฒน์ : ผลของภาวะการทำงานของการสังเคราะห์สังกะสีออกไซด์ด้วยกระบวนการเฟรนช์เพื่อ  
มุ่งสู่การผลิตอนุภาคนาโน. (EFFECTS OF OPERATING CONDITIONS FOR ZINC OXIDE  
SYNTHESIS VIA FRENCH PROCESS TOWARD PRODUCTION OF NANOPARTICLES),  
อ. ที่ปรึกษาวิทยานิพนธ์หลัก: ผศ.ดร. วงศ์ ปวราจารย์, อ. ที่ปรึกษาวิทยานิพนธ์ร่วม: รศ.ดร. ธวัชชัย ชริน  
พาศิขกุล, 82 หน้า.

ปัจจุบันการสังเคราะห์สังกะสีออกไซด์อนุภาคนาโนได้รับความสนใจกันอย่างแพร่หลายเนื่องจาก  
สังกะสีออกไซด์มีคุณสมบัติที่เยี่ยม คือ เป็นสารกึ่งตัวนำ และมีค่าแบนด์แก๊ปกว้างประมาณ 3.37 อิเล็กตรอน โวลต์  
ซึ่งสามารถนำไปประยุกต์ใช้กับอุตสาหกรรมได้หลากหลาย เช่น อุตสาหกรรมอิเล็กทรอนิกส์ อุตสาหกรรม  
เครื่องสำอางค์ อุตสาหกรรมยาง เป็นต้น สังกะสีออกไซด์สามารถมีได้หลายรูปร่าง เช่น รูปร่างที่เป็นแท่ง รูปร่างที่เป็น  
หลอด รูปร่างที่เป็นก้านสี่ก้าน เป็นต้น ซึ่งรูปร่างที่แตกต่างกันนี้ ทำให้สังกะสีออกไซด์มีสมบัติที่แตกต่างกันไป  
การสังเคราะห์สังกะสีออกไซด์นั้นสามารถทำได้หลายวิธี โดยวิธีที่นิยมผลิตในเชิงอุตสาหกรรมได้แก่กระบวนการ  
เฟรนช์ ซึ่งมีความได้เปรียบวิธีอื่นคือ สามารถทำการผลิตได้อย่างต่อเนื่องและผลิตภัณฑ์ที่ได้มีความบริสุทธิ์สูง

ในงานวิจัยนี้ได้ศึกษาถึงอิทธิพลของตัวแปรที่ใช้ในการสังเคราะห์เพื่อหาสภาวะที่เหมาะสมในการสังเคราะห์  
อนุภาคสังกะสีออกไซด์ระดับนาโนเมตรที่มีขนาดและรูปร่างที่สม่ำเสมอ โดยตัวแปรที่ทำการศึกษา ได้แก่ อุณหภูมิที่  
ใช้ในการระเหยสังกะสี อัตราการไหลของแก๊สไนโตรเจนซึ่งทำหน้าที่นำพา ความเข้มข้นของแก๊สออกซิเจนที่ใช้ทำ  
ปฏิกิริยา ปริมาณไอสังกะสีที่ใช้ในการทำปฏิกิริยา และเวลาในการทำปฏิกิริยาออกซิเดชัน ซึ่งจากผลการทดลองพบว่า  
อนุภาคสังกะสีออกไซด์ระดับนาโนเมตรนั้นมีรูปร่างที่น่าสนใจ คือ รูปร่างที่เป็นทรงกลมและรูปร่างที่เป็นก้านสี่ก้าน  
นอกจากนี้ยังพบรูปร่างที่คล้ายหวี และรูปร่างที่เป็นก้านหลายก้าน โดยรูปร่างของอนุภาคสังกะสีออกไซด์เปลี่ยนจาก  
อนุภาคทรงกลมเป็นก้านสี่ก้าน เมื่ออุณหภูมิที่ใช้ในการระเหยเพิ่มสูงขึ้น ส่วนรูปร่างที่คล้ายหวีและรูปร่างที่เป็นก้าน  
หลายก้านนั้นสามารถพบได้เมื่อปริมาณ ไอสังกะสีที่ทำปฏิกิริยามีค่าลดลงและเวลาที่ใช้ในการทำปฏิกิริยาออกซิเดชันมี  
ค่าน้อย

ศูนย์วิทยทรัพยากร

ภาควิชา.....วิศวกรรมเคมี.....ลายมือชื่อนิสิต.....  
สาขาวิชา.....วิศวกรรมเคมี.....ลายมือชื่อ.ที่ปรึกษาวิทยานิพนธ์หลัก.....  
ปีการศึกษา.....2551.....ลายมือชื่อ.ที่ปรึกษาวิทยานิพนธ์ร่วม.....



## 5070257921 : MAJOR CHEMICAL ENGINEERING

KEYWORD: ZnO NANOPARTICLES / FRENCH PROCESS / TETRAPODS / GROWTH MECHANISM

CHAWALIT SOMMANEEWAT: EFFECTS OF OPERATING CONDITIONS FOR ZINC OXIDE SYNTHESIS VIA FRENCH PROCESS TOWARD PRODUCTION OF NANOPARTICLES. ADVISOR: ASST. PROF. VARONG PAVARAJARN, Ph.D., CO-ADVISOR: ASSOC. PROF. TAWATCHAI CHARINPANITKUL, D.Eng., 82 pp.

Recently, synthesis of ZnO nanoparticles has been widely interested because of their excellent properties in a semiconductor and a wide direct band gap of 3.37 eV which can apply to the several industrial applications such as electronics, pharmaceutical industry, and rubber industry. ZnO has various morphologies such as nanorod, nanotube and tetrapod. These morphologies lead to the difference in properties. ZnO could be synthesized by various methods. The commercial ZnO is mostly manufactured via the French process, which is a continuous process capable of producing high purity product.

In this research, the effects of operating conditions on the size and the shape of ZnO nanoparticles were experimentally investigated. These parameters include evaporation temperature, nitrogen gas flow rate, oxygen concentration, amount of zinc vapor, and the oxidation time. From the experimental results, it could be clearly observed that size and morphology of the ZnO nanoparticles are strongly dependent upon mixing ratio of zinc vapor and oxygen gas. ZnO nanoparticles change from spherical shape to tetrapod shape when the evaporation or oxidation temperature is increased. The nanocombs were found when amount of zinc vapor was decreased and the multipods were found under the short oxidation time.

Department: .....Chemical Engineering.....Student's Signature: *Chawalit Sommaneeawat*  
 Field of Study: .....Chemical Engineering.....Advisor's Signature: *Varong Pavarajarn*  
 Academic Year: .....2008.....Co-advisor's Signature: *Tawatchai Charinpanitkul*

## ACKNOWLEDGEMENTS

The author is very thankful to my thesis advisor and co-advisor, Asst Prof. Varong Pavarajarn, and Assoc Prof. Tawatchai Charinpanitkul Department of Chemical Engineering, Chulalongkorn University, for their introducing me to this interesting project, and for their helpful and stimulated suggestions, deep discussion and encouraging guidance throughout the course of this work. Furthermore, the author is also thankful to Prof. Piyasan Prasertthdam, Asst. Prof. Joongjai Panpranot and Dr. Chanchana Thanachayanont for their simulative comments and participation as my thesis committee.

Furthermore, the author would like to acknowledge financial support from the Thailand Research Fund (TRF) under the TRF-Master Research Grant to support this work and Univenture Public Co., Ltd. to support zinc foil as raw material.

Most of all, the author wishes to thank the members of the Center of Excellence on Catalysis and Catalytic Reaction Engineering, Department of Chemical Engineering, Faculty of Engineering, Chulalongkorn University for their assistance.

Finally, the author would like to express his highest gratitude to his parents who always pay attention to his all the times for suggestions and their wills. The most success of graduation is devoted to his parents.

ศูนย์วิทยทรัพยากร  
จุฬาลงกรณ์มหาวิทยาลัย

# CONTENTS

	Page
<b>ABSTRACT (THAI)</b> .....	iv
<b>ABSTRACT (ENGLISH)</b> .....	v
<b>ACKNOWLEDGEMENTS</b> .....	vi
<b>CONTENTS</b> .....	vii
<b>LIST OF TABLES</b> .....	x
<b>LIST OF FIGURES</b> .....	xi
 <b>CHAPTER</b>	
<b>I INTRODUCTION</b> .....	1
1.1 Background .....	1
1.2 Objectives of Research .....	3
1.3 Scope of Research .....	3
1.4 Benefits of Research .....	3
<b>II FUNDAMENTAL KNOWLEDGE AND LITERATURE REVIEW</b> .....	4
2.1 Zinc Oxide (ZnO) .....	4
2.2 Crystal Structure and Lattice Parameters of Zinc Oxide .....	5
2.3 Properties of Zinc Oxide .....	6
2.4 Commercial ZnO Synthesis .....	7
2.4.1 French Process .....	7
2.4.2 American Process .....	9

<b>CHAPTER</b>	<b>Page</b>
2.5 Generation of Particles by Reaction in Gas Phase .....	9
2.6 Synthesis of ZnO Nanostructures .....	10
2.6.1 Vapor Transport Synthesis .....	11
2.6.1.1 Effect of Reaction Temperature ... ..	12
2.6.1.2 Effect of Carrier Gas .....	13
2.6.1.3 Effect of Oxygen Concentration .....	14
2.6.1.4 Effect of Substrate .....	15
2.6.2 Other Synthesis Methods .....	16
2.7 Condensation and Evaporation.....	17
2.7.1 Homogeneous Nucleation .....	17
2.7.2 Heterogeneous Nucleation.....	18
2.7.3 Evaporation.....	19
2.8 Growth Mechanisms of ZnO .....	20
2.8.1 Vapor-Solid Process .....	20
2.8.2 Vapor-Liquid-Solid Process .....	21
<b>III EXPERIMENTAL</b> .....	<b>23</b>
3.1 Raw Material .....	23
3.2 Experimental Procedures.....	24
3.2.1 Effect of Evaporation Temperature ( $T_{\text{evp}}$ ) .....	27
3.2.2 Effect of Nitrogen Flow Rate .....	27
3.2.3 Effect of Oxygen Concentration .....	27
3.2.4 Effect of Amount of Zinc Vapor .....	28
3.2.5 Effect of Oxidation Time .....	28



<b>CHAPTER</b>	<b>Page</b>
3.3 Sample Characterization.....	29
3.3.1 Scanning Electron Microscope (SEM) .....	29
3.3.2 X-ray Diffractometer (XRD) .....	30
3.3.3 Particle Size Distribution Analysis (PSD) .....	31
<b>IV RESULTS AND DISCUSSION</b> .....	<b>32</b>
4.1 Effect of Evaporation Temperature ( $T_{\text{evp}}$ ) .....	32
4.2 Effect of Carrier Gas Flow Rate .....	40
4.3 Effect of Oxygen Concentration.....	46
4.4 Effect of Amount of Zinc Vapor .....	51
4.5 Effect of Oxidation Time.....	57
<b>V CONCLUSIONS AND RECOMMENDATIONS</b> .....	<b>59</b>
5.1 Conclusions .....	59
5.2 Recommendations for Future Work .....	60
<b>REFERENCES</b> .....	<b>61</b>
<b>APPENDICES</b> .....	<b>66</b>
APPENDIX A Calculation of Partial Pressure.....	67
APPENDIX B Temperature Profile Inside Reactor .....	69
APPENDIX C Size Distribution of ZnO Nanostructures.....	70
APPENDIX D Quantity of ZnO Deposited at Different Position.....	74
APPENDIX E List of Publication .....	77
<b>VITA</b> .....	<b>82</b>

**LIST OF TABLE**

Page

<b>Table 2.1</b> Properties of wurtzite zinc oxide .....	6
--	---



ศูนย์วิทยทรัพยากร  
จุฬาลงกรณ์มหาวิทยาลัย

## LIST OF FIGURES

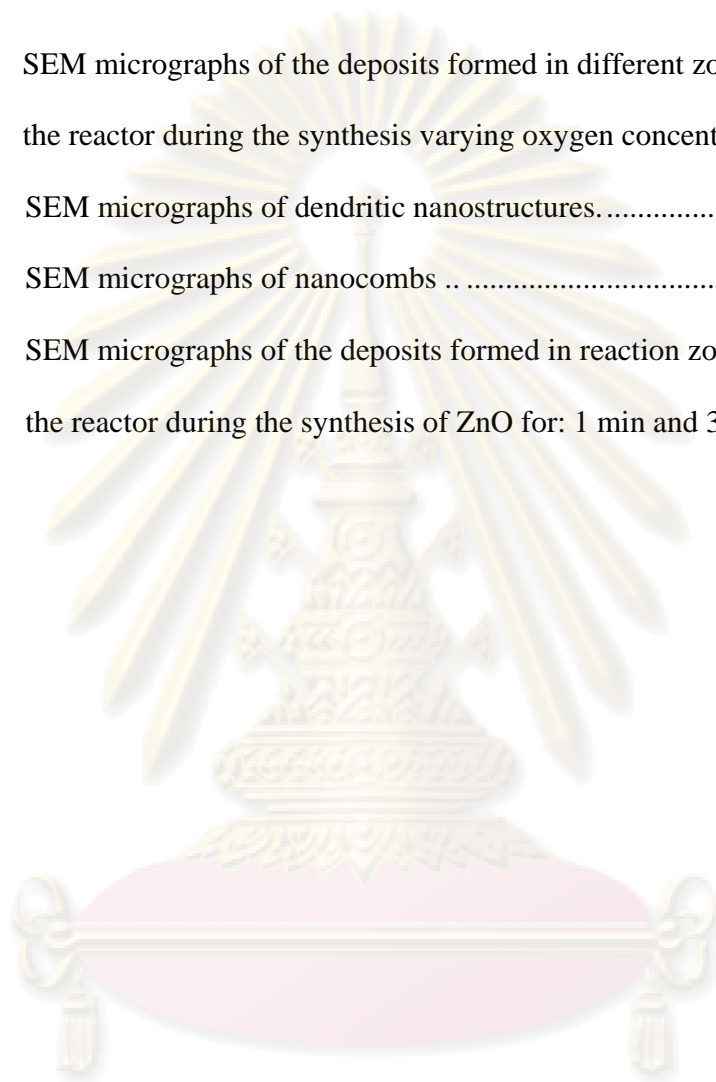
		Page
<b>Figure 2.1</b>	Zinc oxide powder.....	4
<b>Figure 2.2</b>	The hexagonal wurtzite structure of ZnO.....	5
<b>Figure 2.3</b>	The rock salt and zinc blende phase of ZnO .....	5
<b>Figure 2.4</b>	Schematic of French process .....	8
<b>Figure 2.5</b>	Mechanisms of particle formation and growth from vapor-phase precursors.....	10
<b>Figure 2.6</b>	Schematic of VLS process.....	21
<b>Figure 3.1</b>	Zinc foils as raw material .....	23
<b>Figure 3.2</b>	A horizontal tube furnace and a ceramic tube reactor .....	24
<b>Figure 3.3</b>	Dry chamber and wet chamber .....	25
<b>Figure 3.4</b>	Two filter holders .....	25
<b>Figure 3.5</b>	Schematic diagram for the experimental set up .....	26
<b>Figure 3.6</b>	Scanning electron microscope (SEM).....	29
<b>Figure 3.7</b>	X-ray diffraction (XRD) .....	30
<b>Figure 3.8</b>	Particle size analyzer.....	31

	Page
<b>Figure 4.1</b> Schematic diagram sets up for studying the effect of $T_{\text{evp}}$ .....	33
<b>Figure 4.2</b> Particle size distribution of ZnO nanoparticles by zinc evaporation temperature .....	34
<b>Figure 4.3</b> XRD patterns of ZnO nanoparticles synthesized various temperatures, collected by filters .....	34
<b>Figure 4.4</b> SEM micrographs of ZnO nanoparticles collected by filter..... $T_{\text{evp}}= 600^{\circ}\text{C}$ , $T_{\text{evp}}= 700^{\circ}\text{C}$ , $T_{\text{evp}}= 800^{\circ}\text{C}$ , and $T_{\text{evp}}= 900^{\circ}\text{C}$	36
<b>Figure 4.5</b> Partial pressure of zinc vapor and oxygen by varying evaporation temperature .....	37
<b>Figure 4.6</b> SEM micrographs of the deposits formed in different zones of the reactor in synthesis at evaporation temperature $800^{\circ}\text{C}$ .....	38
<b>Figure 4.7</b> SEM micrographs of the deposits formed in the dry and wet chamber zones dry chamber $T_{\text{evp}}= 700^{\circ}\text{C}$ , wet chamber $T_{\text{evp}}= 700^{\circ}\text{C}$ dry chamber $T_{\text{evp}}= 800^{\circ}\text{C}$ , wet chamber $T_{\text{evp}}= 800^{\circ}\text{C}$ .....	39
<b>Figure 4.8</b> SEM micrographs of ZnO nanoparticles by varying nitrogen flow rate.....	41

	Page
<b>Figure 4.9</b> Partial pressure of oxygen by varying nitrogen flow rate .....	42
<b>Figure 4.10</b> Particle size distribution of ZnO nanoparticles by varying nitrogen flow rate.....	43
<b>Figure 4.11</b> SEM micrographs of the deposits formed in different zones of the reactor during the synthesis using nitrogen flow rate of 3 L/min, 4 L/min and 5 L/min .....	44
<b>Figure 4.12</b> SEM micrographs of the deposits formed in the dry and wet chamber zones synthesized using nitrogen flow rate of 3 L/min, 4 L/min and 5 L/min .....	45
<b>Figure 4.13</b> Schematic diagram sets up for studying the effect of oxygen concentration.....	46
<b>Figure 4.14</b> SEM micrograph of ZnO nanoparticles with varying oxygen concentration.....	47
<b>Figure 4.15</b> SEM micrographs of the deposits formed in different zones of the reactor during the synthesis using oxygen concentration of 1%, 1.5% and 2% by mole.....	49
<b>Figure 4.16</b> SEM micrographs of the deposits formed in the dry and wet chamber zones synthesized varying oxygen concentration.....	50



<b>Figure 4.17</b>	SEM micrographs of the deposits formed in different zones of the reactor during the synthesis varying oxygen concentration .....	52
<b>Figure 4.18</b>	SEM micrographs of dendritic nanostructures.....	53
<b>Figure 4.19</b>	SEM micrographs of nanocombs ..	56
<b>Figure 4.20</b>	SEM micrographs of the deposits formed in reaction zone of the reactor during the synthesis of ZnO for: 1 min and 30 min....	58



ศูนย์วิทยทรัพยากร  
จุฬาลงกรณ์มหาวิทยาลัย

# CHAPTER I

## INTRODUCTION

Nanosized materials have been attractive in their potential uses for both interconnect and functional units in fabricating electronic, optoelectronic, electrochemical and electromechanical nanodevices. In the past few years, many efforts have been devoted to develop various nanoscaled materials. The change in electrical and optical properties are target for wide varieties of potential applications.

Zinc oxide (ZnO) is a polar inorganic crystalline material with many applications, mostly as electronic and photonic materials, because of its wide direct band gap of 3.37 eV (Liu et al., 2003). Potential applications of ZnO include UV photodetection, transparent electronics, humidity sensors, gas and chemical sensors, microlasers, memory array, coating, catalysts, and biomedical applications (Zhang et al., 2005). For these applications, it is preferred that size and shape of ZnO are controlled (Fan et al., 2004).

There have been numerous reports on the synthesis of ZnO nanostructures. ZnO is probably the richest family of nanostructures among all materials, both in structures and properties. Various processes have been applied to synthesize ZnO nanowire arrays, such as metal organic chemical vapor-phase epitaxy (MOCVD), infrared irradiation, thermal evaporation and thermal decomposition, laser assisted vapor-liquid-solid growth, electrochemical deposition, sol-gel method and hydrothermal process. Among them, the vapor-based routes, such as thermal evaporation, MOCVD, and laser assisted vapor-liquid-solid growth show a great versatility in synthesizing various ZnO nanostructure. Up to now, various ZnO nanostructures, including nanowires, nanobelts, tetrapods nanobridges and nanonails, nanopropellers, hierarchical nanostructure, nanowall, nanorings and nanosprings, nano-polyhedral cages and shells, have been synthesized. In the vapor-based route,

zinc species in vapor state come from the evaporation of pure zinc powder, zinc oxide powders, organic compound, or the mixture of zinc oxide with other material powders. The composition of the source materials, pressure and growth atmosphere, reaction temperature, substrate and catalysts can drastically change the morphology and nanostructure of grown ZnO. (Ren et al., 2007).

A huge majority of commercial zinc oxide is manufactured using the French process, a four-decade old technology, which is the cheapest and highly productive method to mass-produce ZnO (Mahmud et al., 2006). Various precursors have been used for the gas phase synthesis of ZnO that include Zn metal, diethyl zinc and more recently, organometallic precursors such as heterocubane. Due to its low melting point and low cost, zinc metal precursor is preferred and has been extensively used for thin film fabrication. However, precise size and shape control have not been achieved for large scale synthesis of powders (Bacsa et al., 2007).

In this present work, the process parameters that lead to efficient shape control in the synthesis of ZnO nanoparticles via the French process using zinc metal as precursor were investigated. This research thesis aims to control the process parameters such as evaporation temperature, carrier gas flow rate (nitrogen gas), concentration of oxygen in the system, amount of zinc vapor and oxidation time. Dependence of size and shapes of ZnO nanoparticles on such operating parameters was investigated and discussed.

ศูนย์วิทยทรัพยากร  
จุฬาลงกรณ์มหาวิทยาลัย

### **Objectives of research**

1. To investigate effects of process parameters on the morphology of ZnO synthesized by the French process.
2. To propose the growth mechanism of zinc oxide nanoparticles based on the experimental results.

### **Scopes of research**

1. Determine optimum conditions for the preparation of ZnO nanoparticles via the French process by varying
  - Temperature of reaction
  - Flow rate of carrier gas
  - Concentration of oxygen in the system
  - Amount of zinc vapor
  - Oxidation time
2. The ZnO nanoparticles will be characterized by the following techniques
  - X-ray Diffraction (XRD) for determining lattice parameters.
  - Scanning Electron Microscopy (SEM) for to observing the size and shape of ZnO.

### **Benefits of research**

1. Understand the optimum process conditions for zinc oxide nanoparticles synthesis via the French process.
2. Understand the growth mechanism of zinc oxide nanoparticles.

## CHAPTER II

### FUNDAMENTAL KNOWLEDGE AND LITERATURE REVIEW

#### 2.1 Zinc Oxide (ZnO)

Zinc oxide is a unique modern material. It has such an array of properties that it continues to increase in usefulness in many of the ever-widening fields of science and technology. It is a chemical compound with formula ZnO. It is nearly insoluble in water but soluble in acid or alkalis. It is a fluffy, white powder commonly known as zinc white as shown in Figure 2.1. Crystalline ZnO exhibits the piezoelectric effect and its color will change from white to yellow when heated, and come back to white when cooled down. ZnO will decompose into zinc vapor and oxygen at around 1975°C.



**Figure 2.1** Zinc oxide powder



## 2.2 Crystal Structure and Lattice Parameters of Zinc Oxide

At ambient pressure and temperature, ZnO crystallizes in the wurtzite structure, as shown in Figure 2.2. This is a hexagonal lattice characterized by two interconnecting sublattices of  $\text{Zn}^{2+}$  and  $\text{O}^{2-}$  such that each Zn ion is surrounded by a tetrahedral of O ions. In addition to the wurtzite phase, ZnO is also known to crystallize in the cubic zinc blende and rocksalt structures, which are illustrated in Figure 2.3. Zinc blende ZnO is stable only by growth on cubic structures, while the rocksalt structure is a high-pressure metastable phase forming at pressure about 10 GPa, and can not be epitaxially stabilized. Theoretical calculations have indicated that the wurtzite form is energetically preferable compared to zinc blende and rocksalt.

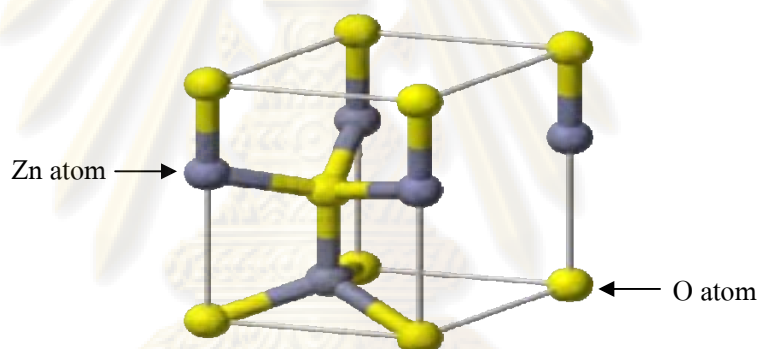


**Figure 2.2** The hexagonal wurtzite structure of ZnO.

Ref: [www.answers.com](http://www.answers.com)

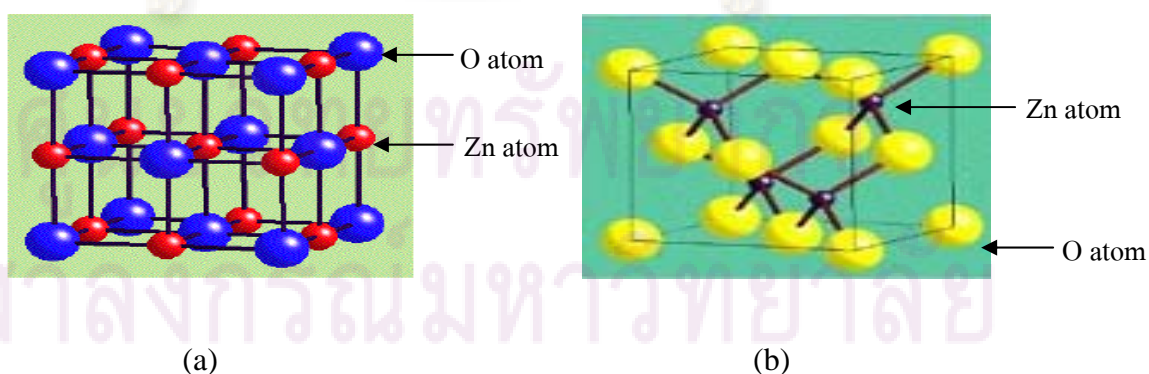


**Figure 2.3** The rock salt (a) and zinc blende (b) phase of ZnO.

Ref: [www.chem.ox.ac.uk](http://www.chem.ox.ac.uk) and [www.icis.cnr.it](http://www.icis.cnr.it)

### 2.3 Properties of Zinc Oxide

Zinc oxide is an n-type semiconductor with a band gap of 3.37 eV and the free exciton energy of 60 meV, which makes it very high potential for room temperature light emission. This also gives zinc oxide strong resistance to high temperature electronic degradation during operation. Therefore, it is attractive for many optoelectronic applications in the range of blue and violet light as well as UV devices for wide range of technological applications. Zinc oxide also exhibits dual semiconducting and piezoelectric properties. The other properties are given in Table 2.1.

Table 2.1 Properties of wurtzite zinc oxide

<i>Property</i>	<i>Value</i>
Lattice parameters at 300 K	
<i>a</i>	0.32495 nm
<i>c</i>	0.52069 nm
<i>a/c</i>	1.602 (ideal hexagonal structure is 1.633)
Density	5.606 g/cm <sup>3</sup>
Melting point	1975°C
Thermal conductivity	130 W/m.K
Linear expansion coefficient (°C)	<i>a</i> : 6.5 x 10 <sup>-6</sup> <i>c</i> : 3.0 x 10 <sup>-6</sup>
Static dielectric constant	8.656
Energy gap	3.37 eV, direct
Exciton binding energy	60 meV

Zinc oxide occurs in nature as mineral. Zinc oxide is prepared in industrial scale by vaporizing zinc metal and oxidizing the generated zinc vapor with preheated air. Zinc oxide has numerous industrial applications. It is a common white pigment in paints. It is used to make enamel, white printing ink, white glue, opaque glasses, and floor tiles. It is also used in batteries, electrical equipments, piezoelectric devices, cosmetics, dental cements, and pharmaceutical applications such as antiseptic and astringent. Other applications are the use as flame retardant, and UV absorber in plastics. Nevertheless, the current major application of zinc oxide is in the preparation of most zinc salts.

## **2.4 Commercial ZnO Synthesis**

### *2.4.1 French Process*

In French process zinc metal is vaporized in suitable containers by external heating, after which the vapor is burned in air in an adjoining off-take pipe or combustion chamber to form fine zinc oxide powder. Temperature and speed of mixing of air and vapor are important factors in the control of particle size. The higher temperature bring about the finer particles size of the resulting ZnO product. For the commercial practice, the system (Figure 2.4) is consisted of a graphite crucible placed inside a cylindrical firebrick furnace. The design is a muffle type whereby hot flame from a burner heats up the crucible by convection, and heat is transferred to the zinc ingots (inside the crucible) via conduction through the graphite lining. Zinc melts at 420°C with heat of fusion of 6.67 kJ/mol, boils at 907°C with heat of vaporization of 114.2 kJ/mol, and its critical temperature is 3107°C. The crucible is covered with a graphite lid in order to pressurize the zinc vapor trapped inside the crucible. Once the lid orifice is removed, the pressure difference causes the zinc vapor to purge out and it is instantaneously oxidized by ambient air. The zinc vapor has a nozzle temperature of 1100-1400°C and a nozzle speed of about 8-12 m/s (calculated). An enclosure is sometimes built around the combustion chamber in order to control the oxygen-to-zinc ratio and to stabilize the temperature.

Oxidation of zinc oxide and the growth of zinc oxide crystals take place in the combustion area. The temperature from 1100°C to 800°C drop within seconds between the crucible orifice and the top part of the conical suction hood (Figure 2.4(a)). Despite the highly nonuniform crystallization nature of this rapid *subminute* growth process, a large variety of nanostructure of ZnO, which includes nanorods, nanoplates, nanoboxes, irregularly shaped particles (ISPs), polyhedral drums and nanomallets can be formed. Mahmud et al. synthesized ZnO by the French process. The morphologies of ZnO were rod, polyhedral drum, irregularly-shaped particles, nanoplate, nanobox, and nanomallet [Mahmud et al. 2005].

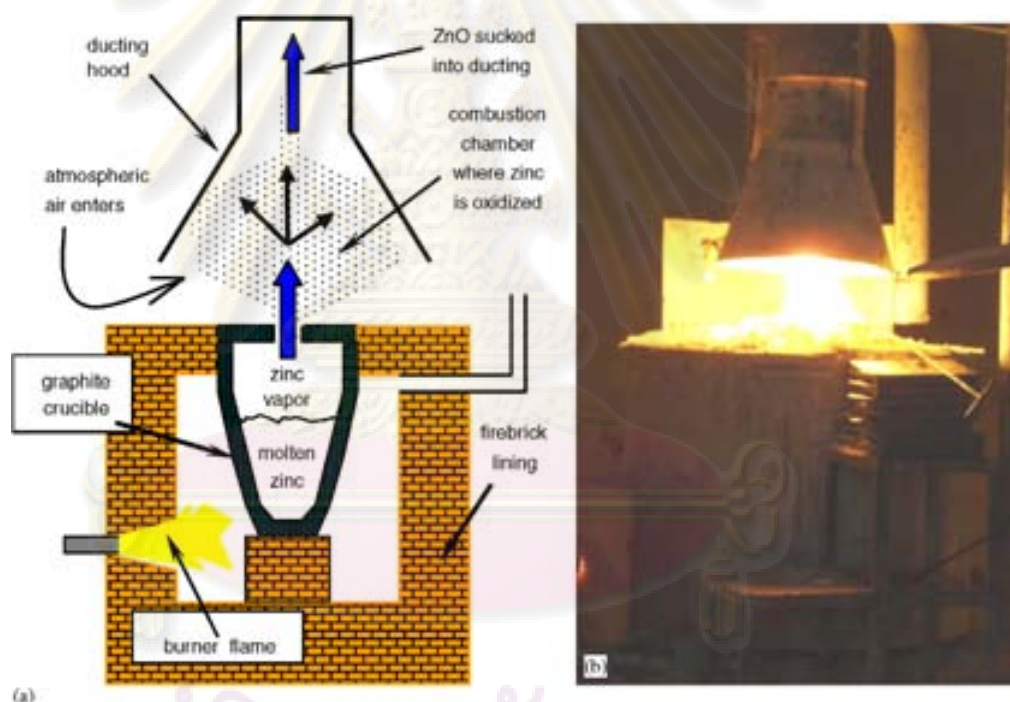


**Figure 2.4** (a) Schematic of French process furnace and (b) furnace in operation. [Mahmud et al. 2005]

The powder is collected by filtration through a multiplicity of textile bags. Frequent shaking of the bags prevents excessive cake build-up and drops the oxide into collection receptacles. In some plants, the baghouse is preceded by a series of settling chamber or baffled tunnels, in which the bulk of the production is collected. In either case, the oxide can be collected on a grade basis. The fluffiest product is gathered at the farthest distance from the combustion area. Preparation of zinc oxide

from metal permits considerable flexibility in control of particle size, particle shape, and product purity. For example, average particle size may range from 0.1 micron to several microns. The larger sizes are produced by maintaining the oxide at elevated temperature for longer period of time.

#### *2.4.2 American Process*

For American process, oxidized ores or roasted sulfide concentrates are mixed with coal (anthracite) and smelted in a Wethreill-type flat-bed or other type of furnace. The coal and the products of partial combustion, particularly carbon monoxide, reduce the ore to zinc vapor. In the off-take pipe, the vapor together with the gases from the coal, are burned under controlled conditions and piped to the baghouse, where the zinc oxide is collected. The american process oxide is characterized by the presence of sulfur compounds in zinc, such as zinc-based sulfates preferred by some producers of rubber and paint products.

### **2.5 Generation of Particles by Reaction in Gas Phase**

Particles synthesis from vapor phase involves the processes of seed generation and particle growth. The processes involving in particles synthesis from the vapor phase are summarized in Figure 2.5. Seed particles are frequently produced by a burst of homogeneous nucleation of vapor phase species. Growth can involve the processes of physical vapor deposition (PVD) or chemical vapor deposition (CVD) of vapor phase species or coagulation, which is the collisional aggregation of small particles to form larger ones. The latter process dominates when large numbers of particles are formed in the nucleation burst. Coagulation of the solid particles often results in the formation of agglomerates particles comprised of the large the number of smaller primary particles. Such agglomerate formation frequently begins after a period of coalescent coagulation in high-temperature regions of the reactor, leading to a relatively uniform primary particle size which is sometime misinterpreted as evidence that coalescent has ceased. Instead, coagulation accelerates once agglomerates begin



to form due to the increased projected areas that result from agglomerate formation. Strong bonds can form between the primary particles by solid phase sintering, leading to hard agglomerates that are often difficult to disperse.

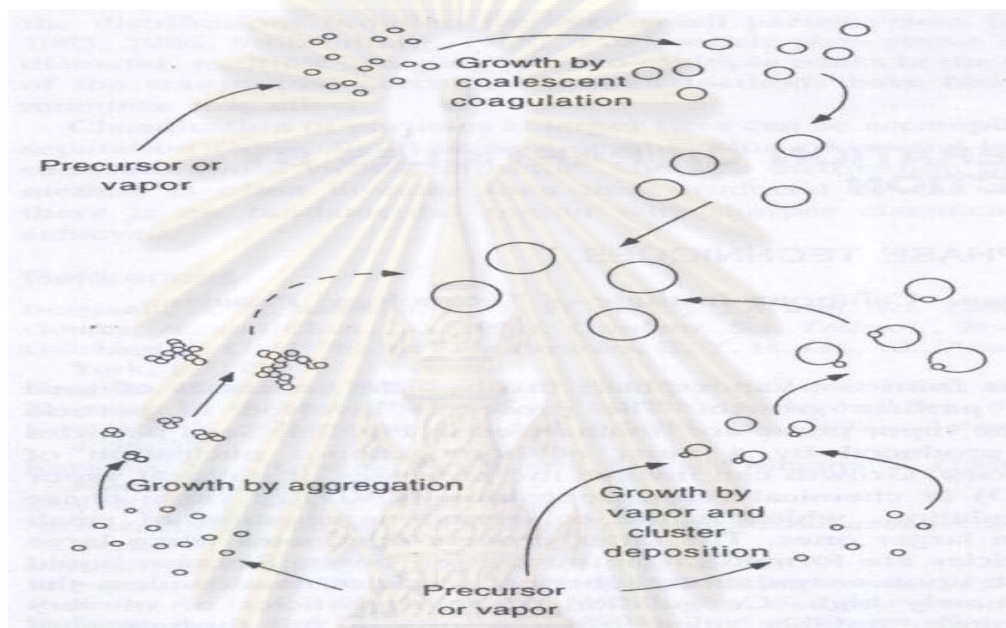


**Figure 2.5** Mechanisms of particle formation and growth from vapor-phase precursors.

## 2.6 Synthesis of ZnO Nanostructures

Various methods have been used for the production of ZnO nanostructures. They can be grouped in two main categories: high-temperature techniques, such as chemical vapor deposition, pulsed-laser deposition and thermal evaporation where the growth temperature is higher than 400°C, and chemical solution methods at around 100°C. The first category utilizes expensive equipment and is energy consuming, while the latter often requires liquid-phase coating of the substrates with ZnO seeds, which is a quite complex procedure.

### *2.6.1 Vapor Transport Synthesis*

The most common method to synthesize ZnO nanostructures utilizes a vapor transport process. In such a process, Zn and oxygen are transported and react with each other, forming ZnO nanostructures. There are several ways to generate Zn and oxygen vapor. Decomposition of ZnO is a direct and simple method, however, it is limited to very high temperature ( $\sim 1400^\circ\text{C}$ ). Another direct method is to heat up Zn powder under oxygen flow. This method facilitates relative low growth temperature ( $500\text{-}700^\circ\text{C}$ ), but the ratio between the Zn vapor pressure and oxygen pressure needs to be carefully controlled in order to obtain desired ZnO nanostructures. It has been observed that the change of this ratio contributes to a large variation on the morphology of nanostructures. The indirect methods to provide Zn vapor include metal-organic vapor phase epitaxy, in which organometallic Zn compound, diethyl-zinc for example, is used under appropriate oxygen or  $\text{N}_2\text{O}$  flow. Also in the widely used carbothermal method, ZnO powder is mixed with graphite powder as source material. At about  $800\text{-}1100^\circ\text{C}$ , graphite reduces ZnO to form Zn and  $\text{CO}/\text{CO}_2$  vapors, which later react together and result in ZnO nanocrystals. The advantages of this method lie in that the existence of graphite significantly lowers the decomposition temperature of ZnO.

There are several processing parameters such as temperature, pressure, carrier gas (including gas species and its flow rate), substrate and evaporation time period, which can be controlled and need to be selected properly before and/or during the thermal vaporization. The selection of source temperature selection mainly depends on the volatility of the source materials. Usually, it is slightly lower than the melting point of the source material. The pressure is determined according to the evaporation rate or vapor pressure of the source materials. The local temperature determines the type of product that will be obtained. It is also noted that the thermal evaporation process is very sensitive to the concentration of oxygen in the growth system.

### 2.6.1.1 Effect of Reaction Temperature

Singh et al. (2005) investigated the nucleation and growth of zinc oxide nanostructure in a catalyst free synthesis. The ZnO nanostructures were formed by evaporation of Zn in O<sub>2</sub> and Ar atmosphere in a single-zone furnace under two temperature regions, region A (~1173-1073 K) and region B (~873-773 K). The ZnO in this investigation were nanotetrapods, nanorods, nanoflowers, and nanostructures. Initially ZnO was formed and transformed to ZnO<sub>x</sub> through the loss of oxygen leading to the creation of oxygen vacancies. The evidence for the formation of ZnO<sub>x</sub> was found through variation of lattice parameters determined from XRD pattern. The ZnO<sub>x</sub> nuclei lead to the growth of several ZnO nanostructures. The formation of various ZnO nanostructures have been advanced in terms of formation of ZnO<sub>x</sub> and their distributions, as well as temperature and oxidation conditions.

Bacsa et al. (2007) studied the process parameters that lead to efficient shape control in the synthesis of high purity mono-disperse and non-agglomerated nanorods of ZnO via a one-step gas-to-particle conversion in an aerosol using zinc metal as precursor. The process parameters that controlled shape of ZnO in the synthesis were temperature of the zinc vapor, and the use of a cross flow of air that oxidizes Zn metal, which also prevented agglomeration. Zn metal powder was evaporated at various temperatures (850-950°C) under argon atmosphere. After the temperature was stable at the desired value, air (500-3000 sccm) was introduced into the furnace and the argon flow was increased to 1300 sccm. The synthesized ZnO consisted of tetrapod-type particles where needles grow from a faceted seed particle. The other was rod-like structure growing outward from plates. The nanorods had diameters varying from 8-30 nm at their tips and they were over 1 μm in length. From transmission electron microscopy images of ZnO nanorods, single crystal of nanorods was observed. The nanorod show ten times higher absorption for UV radiation when compared to commercial nanoscale ZnO powders.

Singh et al. (2007) synthesized nanotetrapods and nanorods by a simple thermal evaporation of Zn powder under simultaneous flow of oxygen and argon gases in two-zone furnace in two different temperature regions. ZnO nanotetrapod-like structure was formed in region I where the growth temperature was 850-700°C. It can be noticed that highly uniform tetrapod-like nanostructure was formed. They consisted of four nanorod (arms) with the diameter varying from ~60-150 nm and length from ~1-4  $\mu\text{m}$ . ZnO nanorods were found to grow in region II where growth temperature varied from ~500 to 400°C. The diameter of ZnO nanorods normally ranged from ~30 to 60 nm and their length from ~2 to 5  $\mu\text{m}$ . High growth temperature resulted in large-diameter ZnO nanotetrapods whereas low temperature region resulted in the formation of small diameter of ZnO nanorods.

#### 2.6.1.2 Effect of Carrier Gas

Chen et al. (2004) synthesized zinc oxide nanoparticles by varying carrier gas flow rate in the carbothermal reduction process. As the carrier gas flow rate was increased to 50 sccm, uniform tetrapod-shaped ZnO crystals were formed on inner wall of the quartz tube located downstream of the carrier gas. The diameter of the tetrapods legs was about 250-800 nm, and they were 700 nm to 2  $\mu\text{m}$  in length. Reduction of the dimensions of the tetrapods could be achieved by increasing the carrier gas flow rate to 70 sccm. When the carrier gas flow rate was further tuned to 90 sccm, ZnO nanowires were fabricated on the inner wall of quartz tube. The diameter of the nanowires ranged from 60 to 120 nm and their lengths were 10-40  $\mu\text{m}$ . Consequently, the morphology of the products could be controlled by adjusting the carrier gas flow rate.

Cheng et al. (2006) synthesized zinc oxide tetrapod-like nanostructures by thermal evaporation of Zn powder at different flow rates of argon (150, 180, or 240 sccm). Results showed that the flow rate of argon gas had a comparatively great influence on the morphology of ZnO nanostructures. As the flow rate was increased, morphology of nano-ZnO changed from an initial mixture of tetrapod, nanowire, nanosheet, and nanodendritic forms to a uniform tetrapod-like morphology. At the

lower flow rate of 150 sccm, it was found that the morphologies of nano-ZnO were disordered, consisting of nanowires, nanodendrites, nanosheets, and nanoparticles. At the rate of 180 sccm, the main as-grown product was multipod-like ZnO, including four-leg, five-leg, or six-leg forms. When the rate was increased to 240 sccm, tetrapod-like nanostructures with uniform morphology were obtained.

### 2.6.1.3 Effect of Oxygen Concentration

Ramgir et al. (2006) synthesized ZnO nanostructures using pure Zn metal. Zn metal was heated at a temperature of 950°C for 2 h. A flow rate of 100 sccm of Ar and 20 sccm of O<sub>2</sub> (20% v/v) resulted in a novel multipod structure that was collected on a substrate kept downstream, where the temperature was between 200 and 500°C. The number of arms of the multipods was between 4 and 16. All arms had a common origin with varying length from 10 to 80 μm. In addition, the white fluffy microwires were collected on the substrate containing the Zn vapor source. The wires were polydispersed in nature with width varying from 200 nm to 3 μm and length from 50 to 200 μm. At slightly lower flow rate of 5% (v/v) of O<sub>2</sub>, ZnO spheres were collected as a gray powder at the same temperature zone. These structures were polydispersed in nature with size varying between 200 nm and 5 μm. The amount of oxygen in the gas mixture was found to govern the final structure of ZnO.

Park et al. (2006) studied formation of ZnO nano-wire by a thermal evaporation method. Zn granules were placed in an alumina boat. The boat was inserted in a horizontal tube furnace. The furnace temperature was maintained in the range of 700-1000°C for 0.5-2 h. The oxygen contents were adjusted from 0.5 to 5 vol% by mass flow controller. ZnO nanowires were synthesized by changing oxygen content in the purging gas. ZnO nanostructures were produced when oxygen content in the carrier gas was about 1.6-2.0 vol% O<sub>2</sub>, while it was not produced when oxygen contents was above 2.5 vol%. Several different types of ZnO were formed at various temperatures. ZnO nanorod, ZnO nanowire, and ZnO nanoneedle were synthesized at 700, 800 and 900°C, respectively. Shape of the nanostructure was changed from rod to wire and then needle as the temperature was increased. ZnO nanostructures showed



different PL properties depending upon their morphology. Nanowire emitted strong light in the green visible region, nanorod emitted strong light in the blue and ultraviolet region.

Wang et al. (2008) studied the effects of oxygen partial pressure on the microstructures and photocatalytic activity of ZnO nanoparticles prepared by evaporation-condensation method. In the experiment, the inner temperature of the chamber was fixed at a constant 1273 K, whereas the oxygen partial pressure was maintained at different levels (700-800, 1500-1600, 1800-1900 and 2200-2300 Pa) by adjusting the gas flux ratio of Ar:O<sub>2</sub>. ZnO nanoparticles obtained were mixture of two different shapes: a majority of irregular-shape particles and few tetrapod particles. The average diameter of the irregular-particles was about 100 nm. The branch of the tetrapod particles prepared at oxygen partial pressure of 700-800 Pa was longer and smaller than that prepared at higher oxygen partial pressure ranging from 1500 to 2300 Pa, indicating the potential effects of oxygen partial pressure on shape of the products. XPS peaks comparing ZnO samples prepared at 700-800 and at 2200-2300 Pa showed that the quantity of oxygen vacancies on the surface of ZnO nanoparticles decreased gradually with the increase of oxygen partial pressure from 700 Pa to the highest value of 2300 Pa. Furthermore, the optimal photocatalytic activity was observed at the products prepared at 1800-1900 Pa, which indicated that the optimum content of surface oxygen vacancies was repaired for expected in the heterogeneous photocatalysis.

#### 2.6.1.4 Effect of Substrate

Xu et al. (2004) synthesized ZnO nanowires and nanorod arrays on various substrates by thermally evaporating and oxidizing the ZnCl<sub>2</sub> powder at 350-500°C, using a method based on the vapor-phase transport process. Gold- and copper-coated silicon slices were put downstream at the opening of the inner slender quartz tube. The temperature of the substrates was set to 500°C. The temperature of the source region was 350°C. A grey layer of product covered the surface of the substrate surface after 30 min reaction. The nanowires grown on gold-coated silicon showed a uniform



diameter of about 40 nm, and the nanorods on copper-coated silicon grew upwards to form flower-like arrays. From the PL spectrum, the nanorods fabricated on Cu-catalysed substrate radiated strong UV emission, in addition to the green light which was emitted at much higher intensity green than that for nanorods on the Au-catalysed substrate. This indicated that more defects existed in the nanorod array fabricated on Cu-coated silicon wafer.

Sun et al. (2008) synthesized ZnO microtube arrays on a Si substrate coated with a composite of fluororesin and SiO<sub>2</sub> powder by making use of a simple one-step thermal evaporation process. The commercial Zn powder was heated to 650°C at a rate of 50°C/min, and kept at 650°C for 15 min. Grayish ZnO products were formed on the substrate. The ZnO tubes with an outer diameter in a range of 1-3 μm had a length of several tens micrometers. The wall thickness was in the range from 0.5 μm to 1.5 μm. It was found that fluororesin was the most important factor for the growth of the ZnO microtubes, and the well-aligned ZnO tubes could be fabricated when the thickness of the composite coating was between 0.1 mm and 1 mm. This novel approach in which fluororesin was adopted to tune the growth of ZnO crystals may become one of the effective methods to control the shape of ZnO nano- /micro-size structures.

### *2.6.2 Other Synthesis Methods*

Although the vapor transport process is the dominant synthesis method for growing semiconducting nanostructures such as ZnO, GaN and Si nanowires, other growth methods such as electrodeposition, sol-gel, polymer assisted growth have been developed in parallel. These methods provide the possibility of forming ZnO nanostructures at low temperature. For example, in an electrodeposition method, anodic aluminum oxide membrane (AAM) with highly ordered nanopores has been used as a template for the growth of zinc nanowires array via electrodeposition. Then the nanowire array can be oxidized at 300°C for 2 hours to obtain ZnO nanowire array [Y. Li et al (2000)]. In a sol-gel synthesis method, AAM has also been used as the template that was immersed into a suspension containing zinc acetate for 1 minute, then heated in air at 120°C for 6 hours. ZnO nanofibers were eventually obtained after

removing the AAM template [Miao et al (2002)]. This sol-gel process was further improved by an electrochemical method in order to obtain nanorods with diameter smaller than 50 nm. These methods are complementary to the vapor transport synthesis of ZnO nanostructure, and also employ less severe synthesis conditions, which provide great potential for device application.

## 2.7 Condensation and Evaporation

The formation and growth of aerosol particles by condensation is the principal method of aerosol production in nature and is the most important mass-transfer process between the gas phase and the particulate phase. This process usually requires a supersaturated vapor and is initiated by the presence of small particles (nuclei) or ions that serve as sites for particle formation.

### 2.7.1 Homogeneous Nucleation

*Homogeneous nucleation* is the formation of particles from a supersaturated vapor without the assistance of condensation nuclei or ion. The process is also called *self-nucleation*. This type of particle formation is rare for water vapor in the atmosphere, but it can be readily produced in the laboratory to study the process of formation and growth. Even in unsaturated vapor, the attractive forces between molecules, such as van der Waals forces, lead to the formation of molecular clusters. The clusters are formed continuously, but they are unstable and continuously disintegrate. When the vapor is supersaturated, the number concentration of clusters increases to the point where they collide with one another frequently. This process is similar to coagulation, except that the “agglomerates” disintegrate soon after being formed. The greater the supersaturation, the greater the number concentration of clusters and the more frequent is the formation of transient “agglomerates” having a size exceeds  $d^*$  ( $d^*$  is Kelvin diameter). Once such an “agglomerate” exceeds  $d^*$ , even momentarily, it becomes stable and grows by condensation to form a large particle. For a given temperature, the supersaturation required for this event to happen occurs at

a well-defined point called the *critical saturation ratio*. In photochemical smog formation, certain gas phase reactions are promoted by ultraviolet light and form low-vapor-pressure reaction products. Because of their low vapor pressure, these products exist at high supersaturation and form particle by homogeneous nucleation. When an increase in aerosol mass concentration occurs in the atmosphere by this mechanism, it is called *gas-to-particle conversion*.

Since a stable droplet is formed when the droplet diameter exceeds  $d^*$  for a particular saturation ratio. The droplet has passed a threshold and will grow by condensation. The rate of growth depends on the saturation ratio, particle size and particle size relative to the gas mean free path. When a particle first starts to grow, its size will likely be less than the mean free path. For this condition, the rate of particle growth is governed by the rate of random collisions between the particle and the vapor molecules. For particles larger than the gas mean free path, the growth depends, not on the rate of random molecule collisions, but on the rate of diffusion of molecules to the droplet surface.

### 2.7.2 Heterogeneous Nucleation

Heterogeneous nucleation or nucleated condensation is a process of particle formation and growth that is promoted by the presence of condensation nuclei or ions. Whereas the homogeneous nucleation usually requires saturation ratio of 2-10, the heterogeneous nucleation can occur at supersaturations of only a few percent.

Insoluble nuclei can provide a passive site for the condensation of supersaturated vapor. At a given level of supersaturation, an insoluble nucleus with a wettable surface will have an adsorbed layer of vapor molecules on its surface. If its diameter is greater than  $d^*$ , the nucleus will behave like a droplet of that size and grow by condensation. However, the actual situation is more complicated because ability of particle to nucleate condensation depends on many factors, including its size, shape, chemical composition, surface structure and surface charge.

### 2.7.3 Evaporation

Evaporation is the process whereby atoms or molecule in a liquid state (or solid state if the substance sublime) gain sufficient energy to enter the gaseous state. The thermal motion of a molecule of liquid must be sufficient to overcome the surface tension and evaporate, that is, the kinetic energy must exceed the work function of cohesion at the surface. Evaporation therefore, proceeds more quickly at high temperature, at higher flow rates between the gas and liquid phase and in liquid phase with lower surface tension (i.e. higher vapor pressure). Because gas has less order than liquid or solid, and thus the entropy of the system is increased, which always required energy input. These mean that the enthalpy change for evaporation ( $\Delta H_{\text{evaporation}}$ ) is always positive. So evaporation is a cooling process.

Factors that influence rate of evaporation include:

- Concentration of the substance evaporating in the air. If the air already has a high concentration of the evaporating substance, then the given substance will evaporate more slowly.
- Concentration of other substances in the air. If the air is already saturated with other substances, it can have a lower capacity for the evaporating substance.
- Flow rate of air or any gas. This is in part related to the concentration pointed above. If the fresh air is moving over the substance all the time, then the concentration of the substance in the air is less likely to go up with time, thus encouraging faster evaporation. In addition, molecules in motion have more energy than those at rest. So, the stronger the flow air, the greater the evaporating power of the air molecules.
- Temperature of the substance. If the substance is hotter, then evaporation will become faster.
- Inter-molecular force, the stronger the forces keeping the molecules together in the liquid or solid state, the more energy that must be input in order to evaporate them.

## 2.8 Growth Mechanisms of ZnO

According to the difference in nanostructure formation mechanisms, the extensive used vapor transport process can be categorized into the catalyst free vapor-solid (VS) process and catalyst assisted vapor-liquid-solid (VLS) process.

### 2.8.1 Vapor-Solid Process

Synthesis utilizing VS process is usually capable of producing rich variety of nanostructures, including nanowires, nanorods, nanobelts and other complex structures. In this process, the nanostructures are produced by condensing directly from vapor phase. For ZnO synthesis via VS process, Zn atoms were continuously evaporated from the source material during the heating process. In the presence of oxygen, the Zn vapor absorbs on the surface of a reactor quartz tube and reacts with oxygen to form ZnO nuclei. As the reactant concentration increases, the ZnO nuclei individually grows in upward direction in the form of nanostructures.

Sekar et al. (2005) synthesized ZnO nanowires by oxidation of Zn-coated substrate at 600°C. Sea-urchin-like nanostructure, consisting of straight nanowires of ZnO with blunt faceted ends and a sudden reduction in diameter projecting out, was observed. This structure had diameters of 30-60 nm and lengths of 2-4 μm. The crystal growth mechanism consists of two stages, i.e., nucleation and growth. When the Zn-coated Si (1 0 0) substrate is heated at 500°C, the metal Zn powders were first melted and aggregated to form the micro-sized Zn nucleus on the surface of the Si substrate. After the introduction of oxygen into the reaction chamber at 600°C, the oxygen reacted with the outer surface of the previously formed Zn nucleus and formed nanosized ZnO nuclei on the surface of these Zn nucleus. Since a metal catalyst was not used, a liquid alloy was not formed. Instead, as the aggregated Zn nucleus became supersaturated, the liquid Zn reacted with oxygen and formed ZnO nuclei at the interface. These ZnO nuclei individually grew in the upper direction in the form of ZnO nanowires. The nuclei thus played a crucial role in the growth of ZnO nanowires, which grew till the Zn source was almost used up. So, from each zinc droplet, there is

an origination of several ZnO nanowires which led to the formation of the sea-urchin-like structure.

### 2.8.2 Vapor-Liquid-Solid Process

Controlled growth of ZnO nanowires/nanorods/nanotubes has been achieved by catalyst assisted VLS process. In this process, various nanoparticles or nanoclusters are used as catalysts, such as Au, Cu, Co, and Sn. Figure 2.6 shows a schematic representation of a typical VLS process. The formation of eutectic alloy droplet occurs at each catalyst site, followed by the nucleation and growth of solid ZnO nanowire due to the supersaturation of the liquid droplet. Incremental growth of the nanowire taking place at the droplet interface constantly pushes the catalyst upward. Thus, such growth method inherently provides site-specific nucleation at each catalytic site. The typical characteristic of VLS process is the presence of metal particles capped at the end of grown structures.

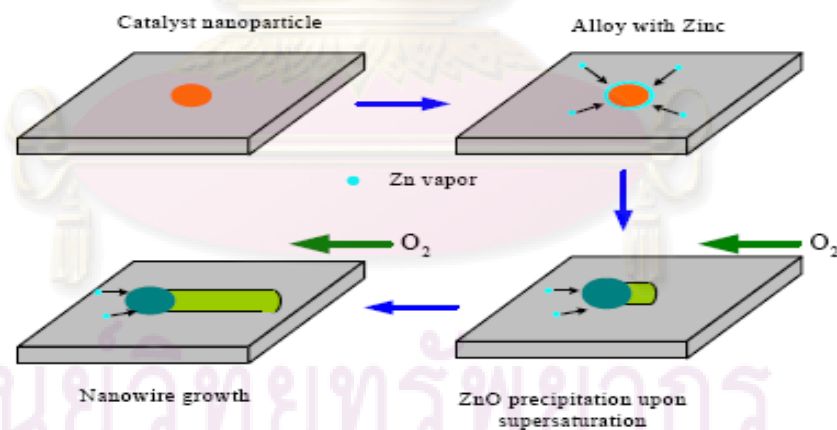
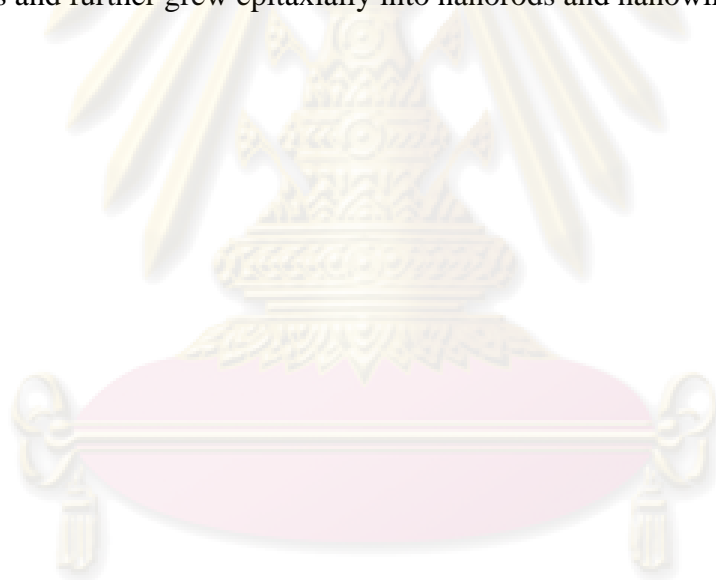


**Figure 2.6** Schematic of VLS process [Zhiyong Fan and Jia G. Lu].



Xu et al. (2004) synthesized ZnO nanowires and nanorod arrays fabricated on various substrates (gold-coated silicon and copper-coated silicon) by thermally evaporating and oxidizing the  $\text{ZnCl}_2$  powder at 350-500°C, by a method based on the vapor-phase transport process. The growth process of the catalyst-assisted nanostructural crystals followed the vapor-liquid-solid (VLS) mechanism in general. With a temperature of 350°C,  $\text{ZnCl}_2$  powder at the source region was evaporated and carried into the higher temperature region. On the substrate surface, the vapor reacted with metallic catalyst and condensed into liquid zinc-alloy catalyst nanodroplet. Each droplet acted as a nucleus that was energetically favored to adsorb incoming zinc vapor and further influenced the morphology of the ZnO nanostructures. When the droplet became supersaturated, the metallic zinc recombined with oxygen to form ZnO nanocrystals and further grew epitaxially into nanorods and nanowires.



ศูนย์วิทยทรัพยากร  
จุฬาลงกรณ์มหาวิทยาลัย

## CHAPTER III

### EXPERIMENTAL

The synthesis of zinc oxide nanoparticles by French process using zinc as source material is explained in this chapter. The chemicals, samples preparation and characterization techniques are also explained.

#### 3.1 Raw Material

Zinc foils as shown in Figure 3.1, which were used as raw materials for the synthesis of ZnO in this research, were obtained from Univenture Co., Ltd. The purity of zinc is higher than 99.995%.



**Figure 3.1** Zinc foils as raw material.

### 3.2 Experimental Procedures

ZnO nanoparticles were synthesized by thermally evaporating Zn foils and consequently reacting with oxygen in air without the presence of catalyst. The system consisted of a ceramic tube reactor (110 cm in length, 6.2 cm in the outer diameter) placed inside a horizontal tube furnace, as shown in Figure 3.2. The number of smaller ceramic tubes (5 cm in length, 4.8 cm in the outer diameter) were placed inside the ceramic tube reactor to collect ZnO deposited within the system to observe the growth mechanism of ZnO. One end of the ceramic tube was connected to gas inlets and the other end was connected to a rotary vacuum pump through a series of product collecting means, i.e., a dry chamber, a wet chamber and filters respectively, as shown in Figure 3.3–3.4.

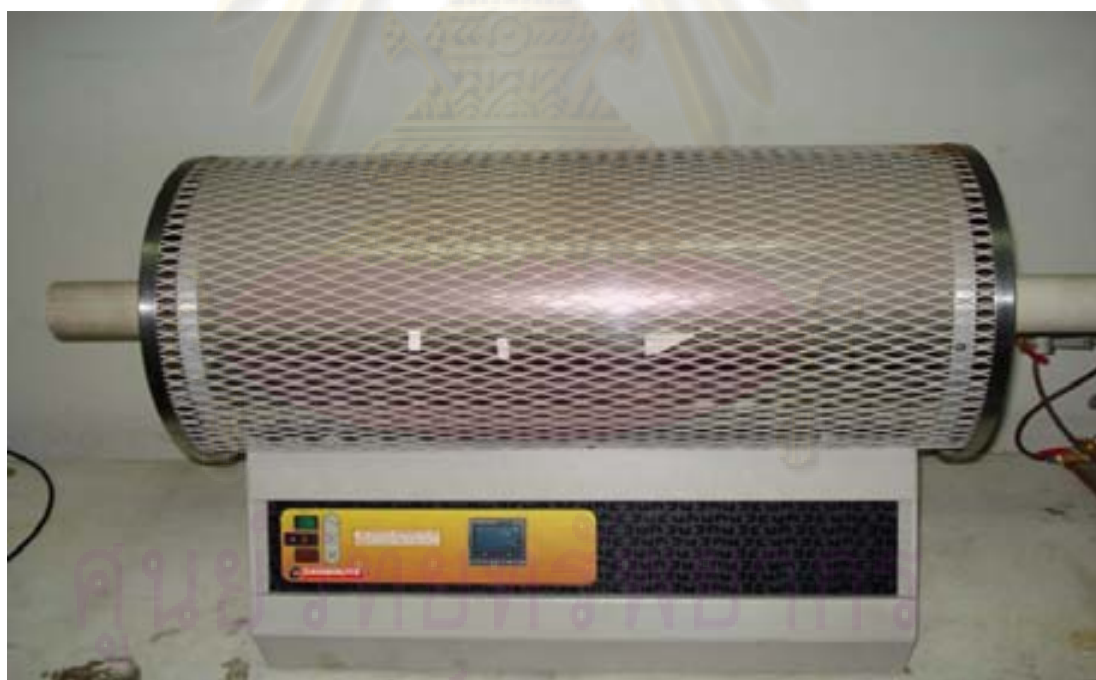


**Figure 3.2** A horizontal tube furnace and a ceramic tube reactor.

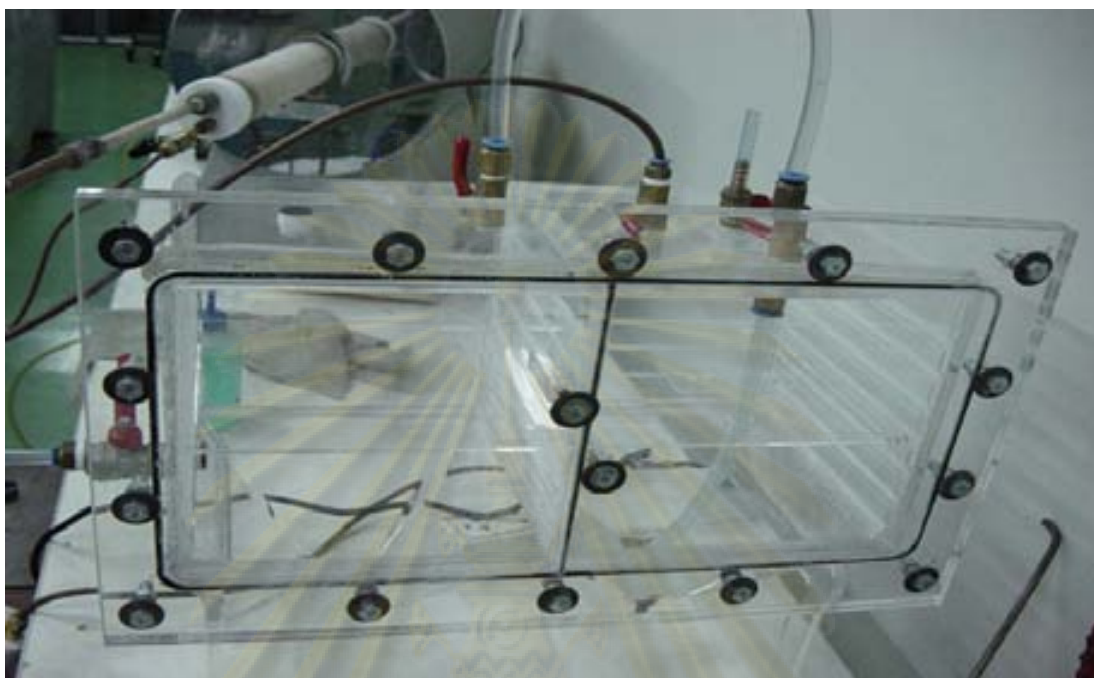


**Figure 3.3** Dry chamber and wet chamber for collecting the product coming out from the reactor.



**Figure 3.4** Two filter holders installed at the outlet of the collecting chamber.

The whole system is shown in Figure 3.5. For each experiment, about 7 g of zinc foils were loaded into an alumina boat placed at the center of the horizontal tube furnace which is an evaporation zone. Then the reactor was evacuated to the low pressure and subsequently filled with nitrogen gas back to 1 atm before heating up to desired temperature. Nitrogen gas was also continuously supplied to the reactor during the heat up process to purge residual oxygen in reactor. When the furnace reached the desired temperature, air was supplied to the reactor to initiate the reaction. The flow rate of both nitrogen and air were controlled by flow meters. The pressure within the system was kept at 1 atm by means of the vacuum pump. After 2 h, the oxygen supply was cut off and the furnace was cooled down to room temperature.

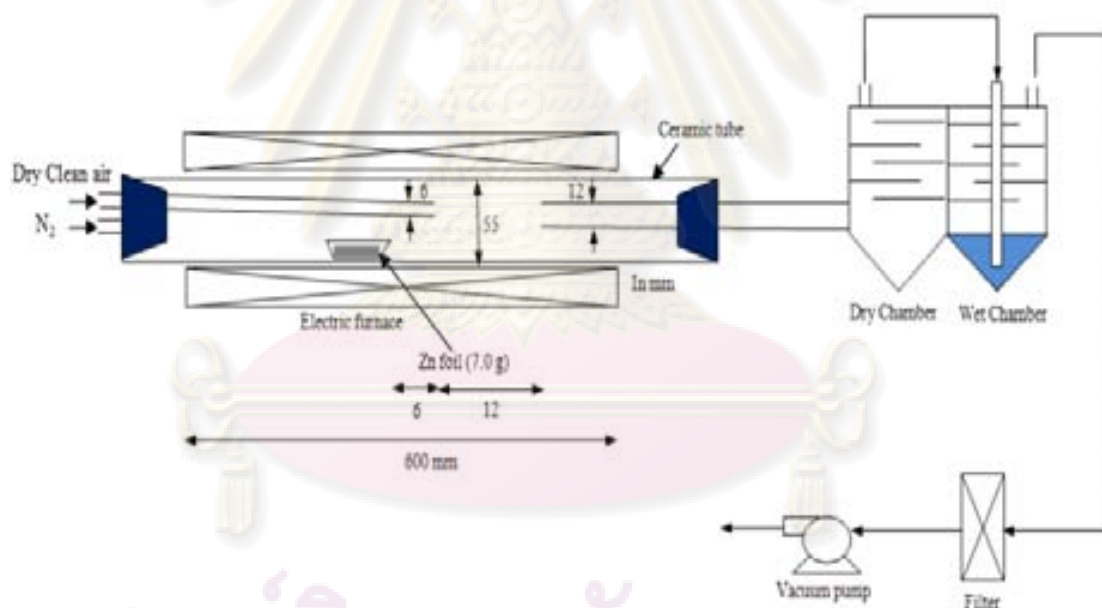


**Figure 3.5** Schematic diagram for the experimental set up.

ศูนย์วิจัยทรัพยากร  
จุฬาลงกรณ์มหาวิทยาลัย

The investigation of this work was separated into 5 parts as follow.

### *3.2.1 The Effect of Evaporation Temperature*

In this part, the effects of zinc evaporation temperature on morphology, size and particle size distribution of the synthesized ZnO were studied. Therefore, the temperature of the tube furnace used for the synthesis of ZnO nanoparticles was varied from 600, 700, 800 and 900°C. The flow rates of nitrogen gas and air were kept constant at 5 L/min and 0.6 L/min, respectively.

### *3.2.2 The Effect of Nitrogen Flow Rate*

The nitrogen flow can dilute the partial pressure of zinc that subsequently affects morphology of the synthesized ZnO. Therefore, nitrogen flow rate was varied to investigate this effect. The maximum and the minimum flow rate were 5 and 3 L/min, respectively. For this set of experiment, the zinc evaporation temperature was fixed at 800°C and air flow rate was kept at 0.6 L/min.

### *3.2.3 The Effect of Oxygen Concentration*

According to literature reviews, the oxygen concentration could determine the ratio of reactant which affects the synthesized ZnO. Thus, oxygen concentration was also varied in our experiment set up (1, 1.5 and 2 % by mole). The evaporation temperature was fixed at 800°C for these experiments.

ศูนย์วิทยทรัพยากร  
จุฬาลงกรณ์มหาวิทยาลัย



### *3.2.4 The Effect of Amount of Zinc Vapor*

The effect of amount of zinc vapor was studied by varying the cross sectional area of the alumina boat at 4, 12, and 20 cm<sup>2</sup> respectively. The zinc evaporation temperature was fixed at 800°C at the heating rate of 10°C/min. The reaction was conducted for 5 min, whereas air and nitrogen flow rate was kept at 0.6 and 5 L/min respectively.

### *3.2.5 The Effect of Oxidation Time*

The effect of oxidation time was studied by varying the feeding time of air at 1 and 30 min. The zinc evaporation temperature was fixed at 800°C at the heating rate of 10°C/min. Air and nitrogen flow rate was kept at 0.6 and 5 L/min respectively.



ศูนย์วิทยทรัพยากร  
จุฬาลงกรณ์มหาวิทยาลัย

### 3.3 Sample Characterization

The instruments used to characterize properties of the synthesized ZnO included Scanning Electron Microscope (SEM) model Hitachi S-3400N, X-ray Diffractometer (XRD) model SIEMENS D5000, and Particle Size Distribution Analysis (PSD) Mastersizer S, respectively.

#### 3.3.1 Scanning Electron Microscopy (SEM)

Morphology and size of the synthesized zinc oxide were observed by using SEM at a research laboratory collaborated between Mektec Manufacturing Corporation (Thailand) Ltd and Chulalongkorn University. SEM specimens were prepared by taking the ZnO powder on SEM substrate, and then directly placing the piece onto a conductive platinum coated microscope grid. The specimens were loaded into a sample chamber, and observations were immediately started using image catcher scanner for taking the photos. A photo of the scanning electron microscopy machine is shown in Figure 3.6.



**Figure 3.6** Scanning Electron Microscope (SEM).

### 3.3.2 X-Ray Diffraction (XRD)

X-ray diffraction (XRD) analysis of zinc oxide was performed by a SIEMENS D5000 diffractometer at the Center of Excellence on Catalysis and Catalytic Reaction Engineering, Chulalongkorn University as shown in Figure 3.7. The X-ray diffractometer was connected to a personal computer with Diffract AT version 3.3 program. The ZnO sample was spreaded on the slide and then set in the equipment which provide X-ray beam for the analysis. The measurement was carried out by using  $\text{CuK}\alpha$  radiation with Ni filter. The condition of the measurement is shown as followed:

$2\theta$  range of detection :  $20 - 80^\circ$

Resolution :  $0.04^\circ$

Number of Scan : 10



**Figure 3.7** X-Ray Diffraction (XRD).

### 3.3.3 Particle Size Distribution Analysis (PSD)

The particle size and particle size distribution of the samples were analyzed by using laser scattering particle size distribution analyzer at the Center of Excellence on Particle Technology, Faculty of Engineering, Chulalongkorn University as shown in Figure 3.8. In the sample preparation, 0.2 g zinc oxide powder was added into 10 cm<sup>3</sup> of 0.2% hexasodium metaphosphate solution, then ultrasonic for 30 min. Finally, the prepared sample was added into 800 cm<sup>3</sup> of water and measured the particle size.



**Figure 3.8** Particle size analyzer.

ศูนย์วิจัยทรัพยากร  
จุฬาลงกรณ์มหาวิทยาลัย

## CHAPTER IV

### RESULTS AND DISCUSSION

The aim of this research is to study the process parameters which affect the morphology and size of ZnO nanoparticles synthesized from French process such as effect of evaporation temperature, carrier gas flow rate, oxygen concentration, amount of zinc vapor and oxidation time. Effect of each process variable was thoroughly investigated and then reported and discussed in this chapter.

#### 4.1 Effect of Zinc Evaporation Temperature ( $T_{\text{evp}}$ )

In French process, zinc ingots are heated at 1100-1400°C to generate zinc vapor. The evaporation temperature is much higher than the boiling point of zinc (907°C) so that it can generate a lot of zinc vapor. However, amount of fuel used for the evaporation is plentiful. Moreover, high concentration of zinc vapor tends to inhibit the formation of zinc oxide nanoparticles. Thus, we tried to investigate the effect of zinc evaporation temperature, in the range below the boiling point of zinc, on the morphology and size of synthesized ZnO nanoparticles. The schematic diagram of experimental set up for this section is shown in Figure 4.1. The evaporation temperature was varied from 600 to 900°C. Air and nitrogen gas were introduced into the reactor at fixed flow rate 0.6 and 5 L/min respectively. Synthesized ZnO nanoparticles were collected in the reactor tube, at the surface of the collecting chambers and the filters. The products were characterized by SEM and XRD.

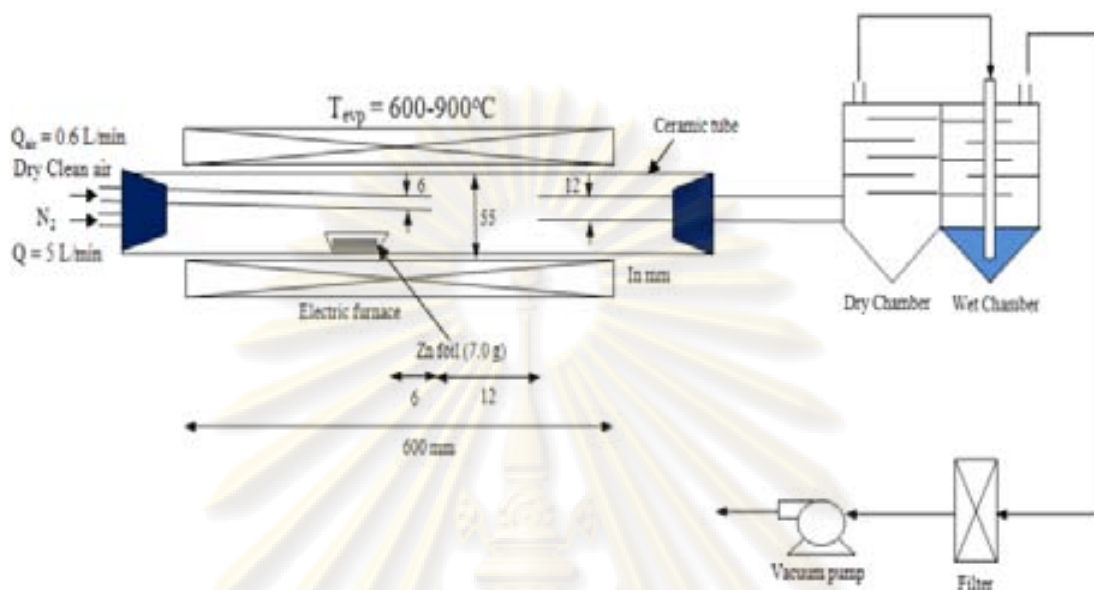


**Figure 4.1** Schematic diagram for experimental sets up for studying the effect of  $T_{\text{evp}}$ .

Figure 4.2 shows particle size distribution of ZnO nanoparticles synthesized at various zinc evaporation temperature. It is found that particle size of ZnO synthesized, using the evaporation temperature of  $600^{\circ}\text{C}$  is small than that of ZnO synthesized at  $700\text{-}800^{\circ}\text{C}$ . The average size of ZnO nanoparticles which collected at the filters synthesized by the evaporation temperature of  $600$ ,  $700$  and  $800^{\circ}\text{C}$ , is  $1.153$ ,  $1.453$  and  $1.684\ \mu\text{m}$  respectively. Figure 4.3 shows the XRD patterns of ZnO nanoparticles at  $T_{\text{evp}} = 600^{\circ}\text{C}$ ,  $700^{\circ}\text{C}$ , and  $800^{\circ}\text{C}$  respectively. All diffraction peaks can be indexed to the known hexagonal wurtzite structure of ZnO. No diffraction peak from Zn or other impurity phases is found in any sample, confirming that the products are pure ZnO. The crystallinity of ZnO becomes higher with the increasing evaporation temperature, witnessed from high intensity of XRD peaks.

จุฬาลงกรณ์มหาวิทยาลัย



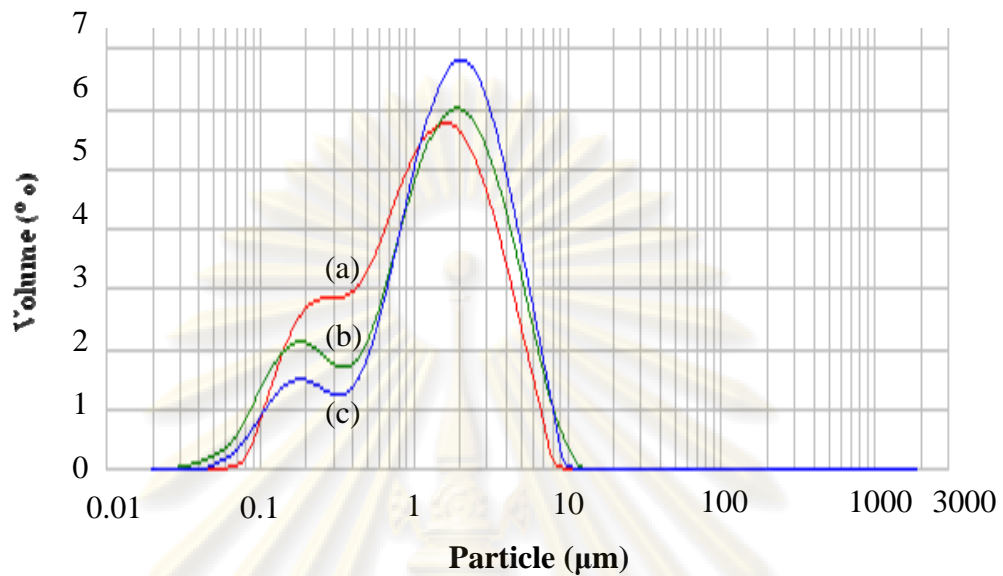


**Figure 4.2** Particle size distribution of ZnO nanoparticles synthesized by zinc evaporation temperature ( $T_{\text{evp}}$ ) of: (a) 600°C, (b) 700°C, (c) 800°C.

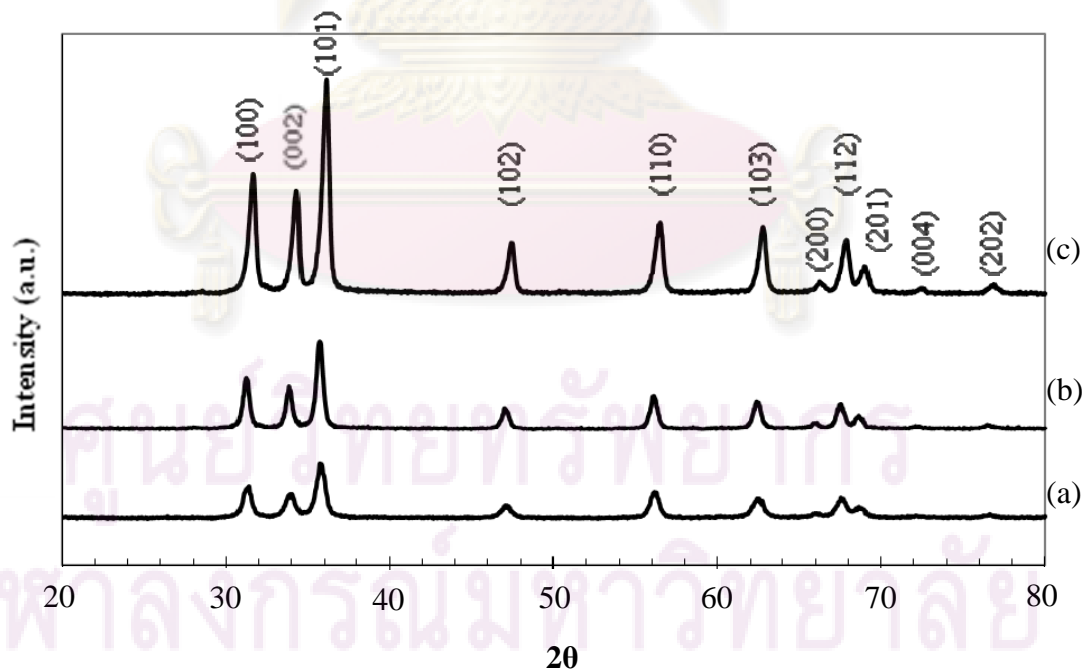


**Figure 4.3** XRD patterns of ZnO nanoparticles synthesized various temperatures, collected by filters: (a)  $T_{\text{evp}} = 600^\circ\text{C}$ , (b)  $T_{\text{evp}} = 700^\circ\text{C}$  and (c)  $T_{\text{evp}} = 800^\circ\text{C}$ .

Morphology of the synthesized ZnO nanoparticles was also determined by scanning electron microscopy (SEM). SEM micrographs in Figure 4.4 show that ZnO nanoparticles collected at filters is rather spherical in shape when the evaporation temperature is 600 or 700°C. However, tetrapods are sparsely found at 700°C. The morphology of the ZnO nanoparticles shifts from spherical into tetrapods, as the reaction temperature is raised from 600 to 800°C. It should be noted that the highest temperature employed in this work is still lower than the boiling point of zinc. The increasing temperature not only affects the generation of zinc vapor, but also increases mobility of the growth species on the surface of the crystals, which allows the growth along the preferential *c*-axis and results in product as tetrapods. According to our experimental results, it should be pointed out here that tetrapods and spherical products are grown in two temperature regimes, namely ~800-900°C and ~600-700°C. The diameter and length of ZnO nanoparticles were measured by an image processing program (SemAfore 4.0), which randomly selected about 50 particles from SEM images. The diameter of sphere varies in the range from 80 to 120 nm. The diameter and the length of the legs of the pods are in the range of 60-90 nm and 270-350 nm, respectively. Regarding particle size measurement techniques, PSD technique and SEM employ different principle to measure the particle size. PSD technique uses scattering of light from particle to calculate the particle size based on the assumption that particles are spherical. SEM technique, on the other hand, gives the actual morphology of the particle. Since morphology of ZnO in this research is not spherical, the size measurement from SEM images has more representative meaning than PSD results. However, it should be noted that the SEM images were taken from small amount of samples, which may not totally represent the whole population of the samples. Therefore, many SEM images were taken from one sample to ensure uniformity of the results.

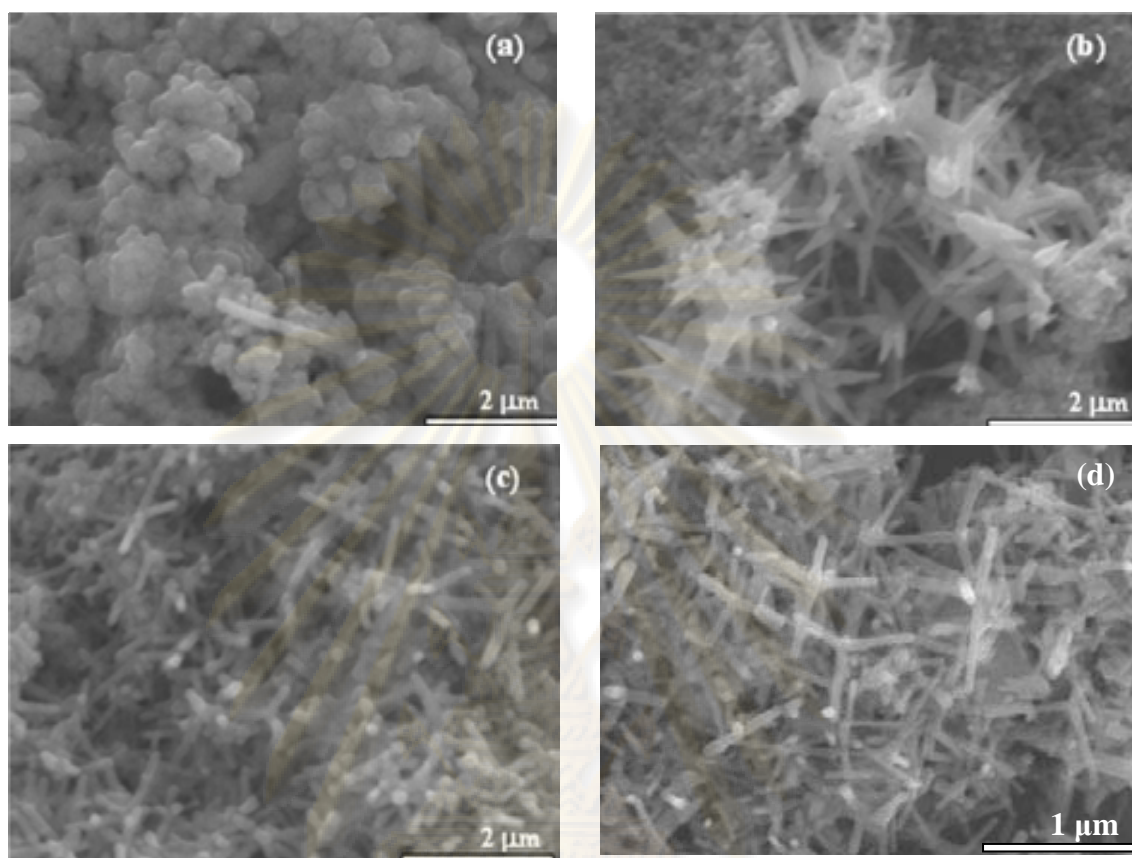


**Figure 4.4** SEM micrographs of ZnO nanoparticles collected by filter: (a)  $T_{\text{evp}}= 600^{\circ}\text{C}$ , (b)  $T_{\text{evp}}= 700^{\circ}\text{C}$ , (c)  $T_{\text{evp}}= 800^{\circ}\text{C}$ , and (d)  $T_{\text{evp}}= 900^{\circ}\text{C}$ .

Partial pressure of zinc vapor and oxygen were calculated as shown in Figure 4.5. The partial pressure of zinc vapor increases when the zinc evaporation temperature is increased. Under the Zn-rich conditions, cluster- and rod-type nanostructures are mainly observed. On the other hand, the tetrapods are grown only under the stoichiometric ( $\text{O}/\text{Zn} = 1$ ) and O-rich conditions, which strongly indicates that the  $\text{O}/\text{Zn}$  ratio played an important role to determine the shape of nanostructures [Jung et al. (2006)]. It has been reported that tetrapods were formed at the high temperature and the high oxygen flow [Singh et al (2007)]. As our results, tetrapods were found at evaporation temperature of 800-900°C whereas  $\text{O}/\text{Zn}$  ratio was set at about 1-2. Spherical ZnO could be grown in the condition with very low zinc partial

pressure. Therefore, morphology and size of ZnO nanoparticles are related to the zinc evaporation temperature.

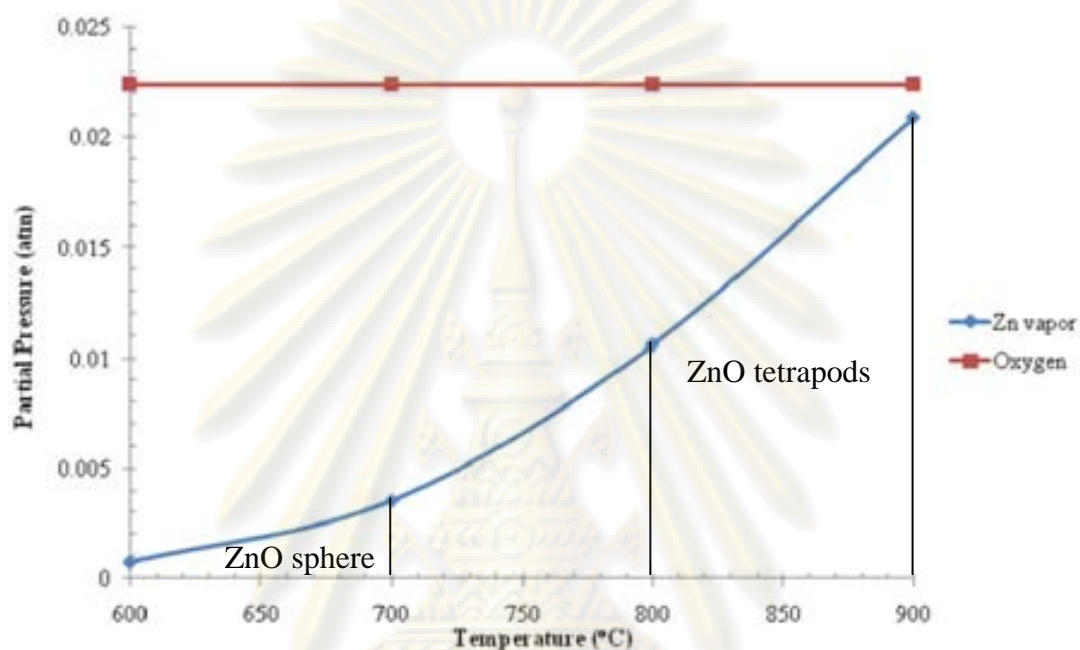


**Figure 4.5** Partial pressure of zinc vapor and oxygen by varying evaporation temperature.

Figure 4.6 shows SEM micrographs of the deposits formed at different zones of the reactor during the synthesis at evaporation temperature of 800°C. Powder deposited at location 1 prior to the outlet for the supplied air is microrods. It is a result from reaction between zinc vapor and oxygen back diffusing from the supplied tube. The location 2 is in the reaction zone, in which the partial pressure of zinc and oxygen is high. So, the powder at this location can grow into the tetrapods. Finally, at the position further away from the zinc source, the zinc concentration is slightly and the less quantity of zinc oxide is carried by nitrogen gas to deposit in this zone. Therefore, the powder at this location can grow into the irregular (Figure. 4.6 powder 3). Figure 4.7 shows SEM micrographs of the deposits formed in the dry and wet chamber zones at evaporation temperature of 700 and 800°C. The product at evaporation temperature

of 600°C deposits in very small amount that it could not be collected and characterized by SEM. The sphere and tetrapods were found at evaporation temperature of 700 and 800°C, respectively which are corresponding with the product collected at the filters. Therefore, the product in synthesis is uniform.

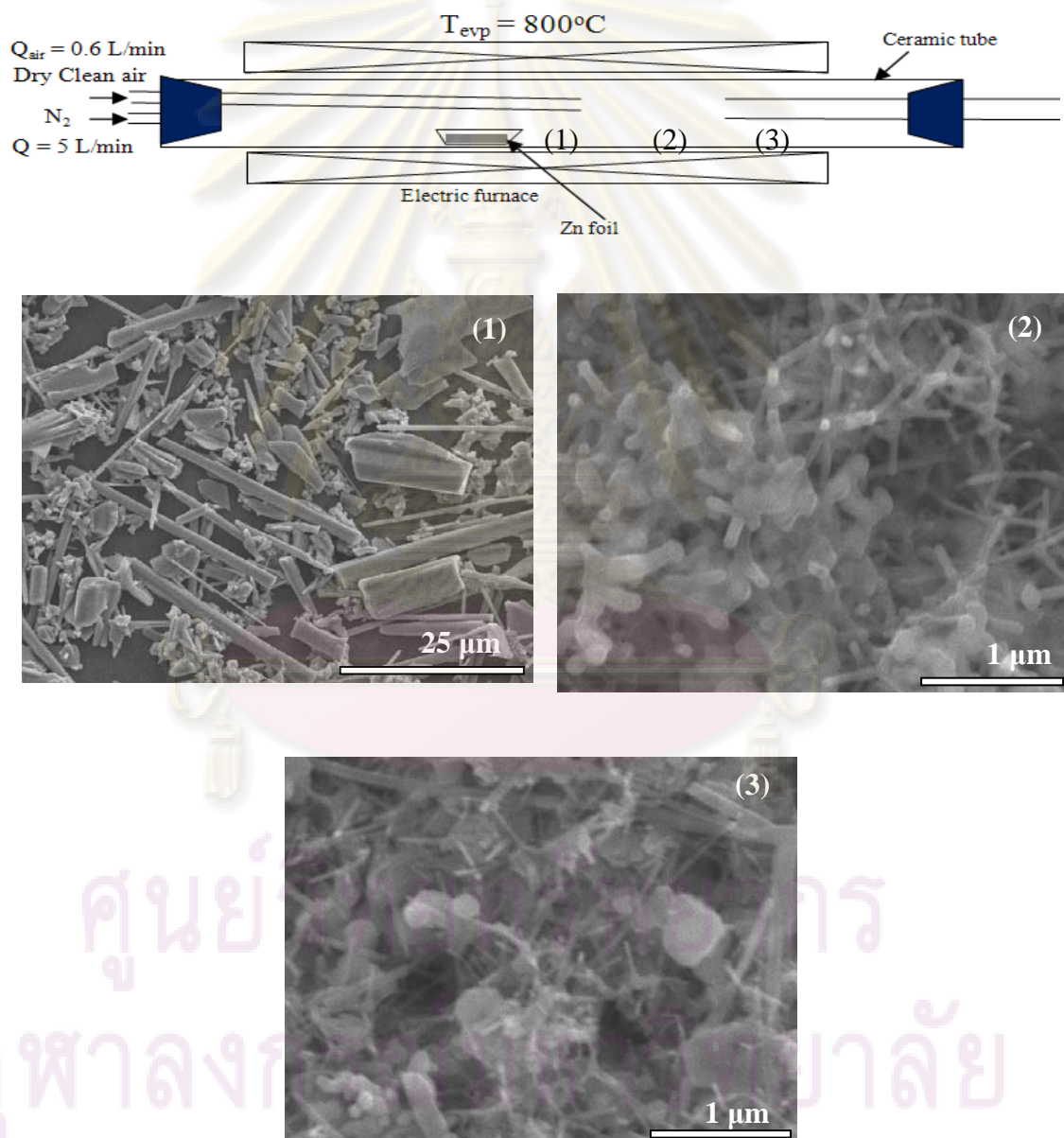


**Figure 4.6** SEM micrographs of the deposits formed in different zones of the reactor during synthesis of ZnO at evaporation temperature of 800°C.



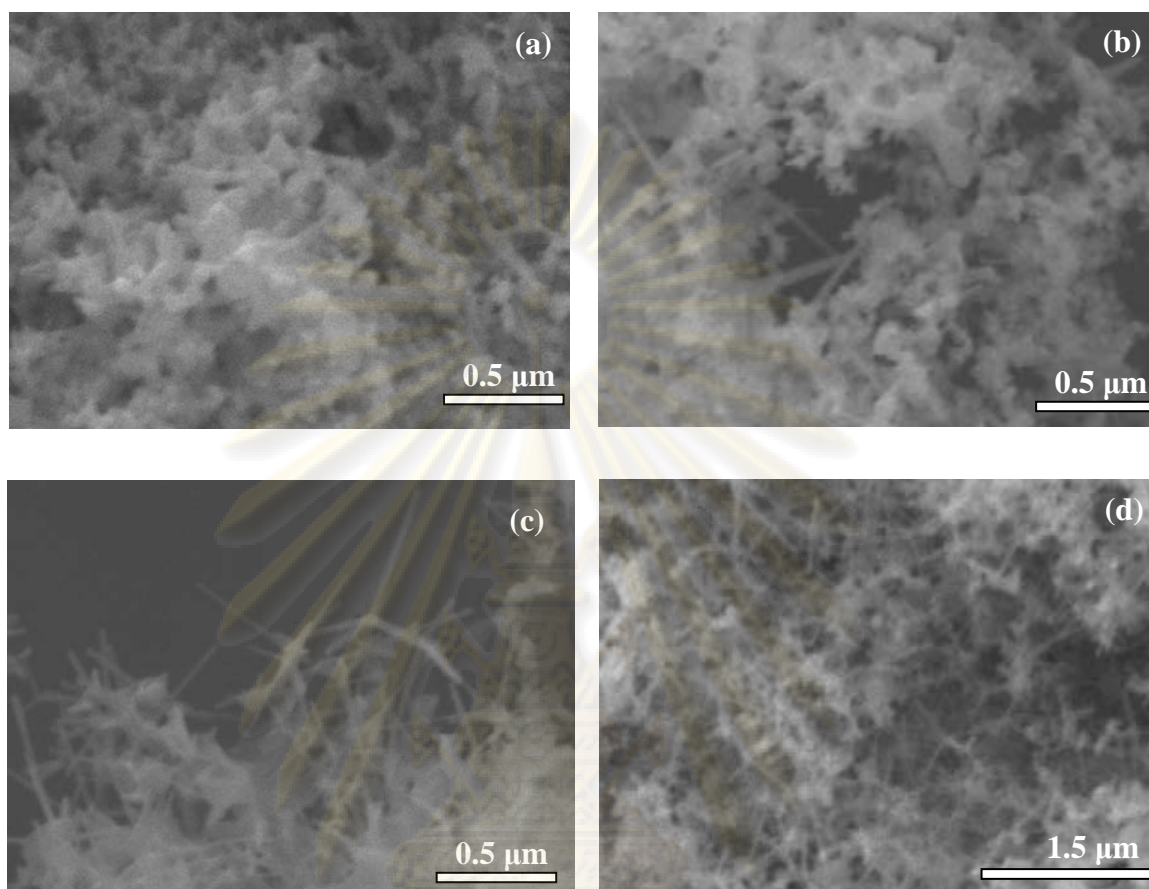


**Figure 4.7** SEM micrographs of the deposits formed in the dry and wet chamber zones (a) dry chamber  $T_{\text{evp}}=700^{\circ}\text{C}$ , (b) wet chamber  $T_{\text{evp}}=700^{\circ}\text{C}$  (c) dry chamber  $T_{\text{evp}}=800^{\circ}\text{C}$ , (b) wet chamber  $T_{\text{evp}}=800^{\circ}\text{C}$ .

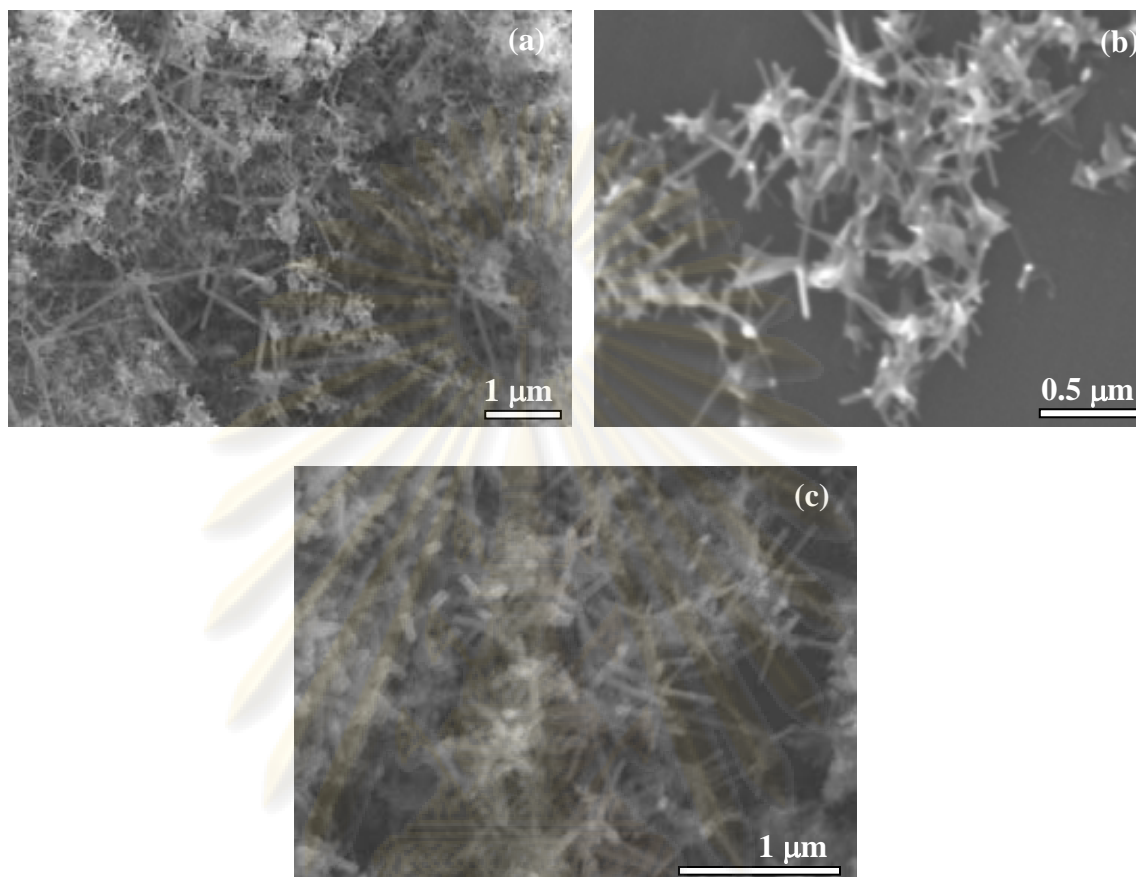
ศูนย์วิทยทรัพยากร  
จุฬาลงกรณ์มหาวิทยาลัย



## 4.2 Effect of Carrier Gas Flow Rate

The effect of carrier gas flow rate was studied by varying nitrogen flow rate from 3, 4, and 5 L/min respectively. The evaporation temperature was fixed at 800°C. Air was introduced into the reactor at fixed flow rate of 0.6 L/min.

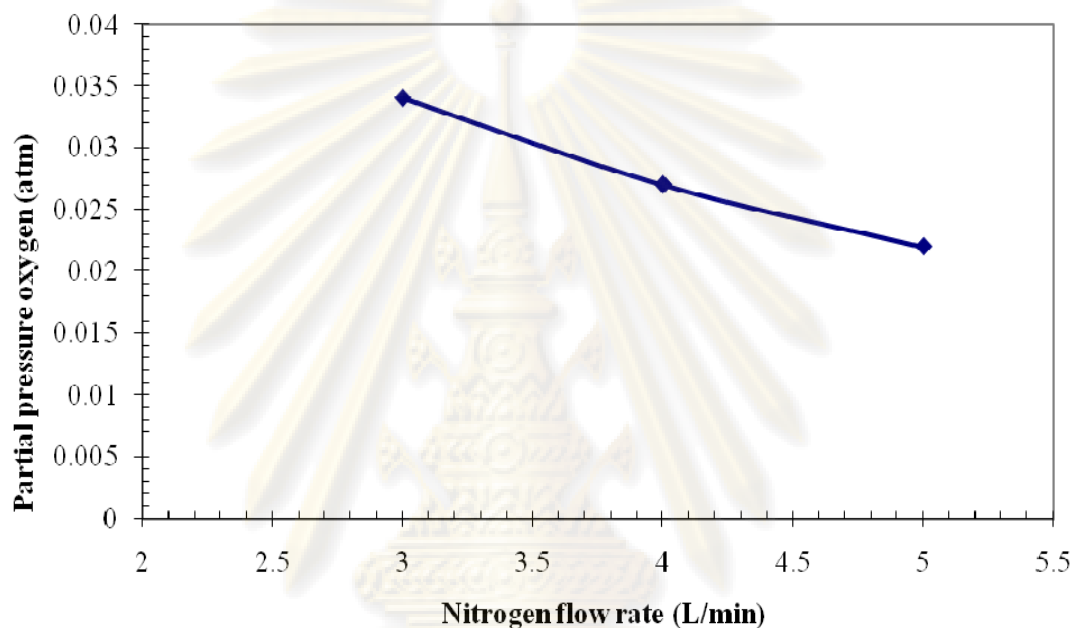
Figure 4.8 shows SEM micrographs of ZnO products that were synthesized at 800°C by using different flow rate of the carrier gas and captured by filters. At low flow rate of 3 L/min, it is found that the morphology of ZnO nanostructures is disordered, consisting of nanowires, multipods, tetrapods and small fraction of nanosheets. At the rate of 4 L/min, the main as-grown product is tetrapods and non-uniform. Few multipods are still found in the product (Figure. 4.8b). When the rate is increased to 5 L/min, tetrapod-like nanostructures are uniformly synthesized (Figure. 4.8c). The diameter of legs of the pods varies in the range from 60 to 80 nm. The length of the legs becomes slightly smaller when the flow rate of the carrier gas is increased because the retention time for the reaction is reduced. The growth time of ZnO is decreased which make the legs cannot grow to the large legs. It should be noted, however, that the length of the legs is not significantly affected by the flow rate. This result indicates that the growth in length of the legs takes place quickly at the early stage of the reaction. This is the result from the preferred growth along *c*-direction of ZnO crystal. Therefore, a high flow rate of the carrying gas, while the air flow rate is kept constant reduce the partial pressure of oxygen in the system, thus yielding a low supersaturation of ZnO, which favors the growth of tetrapods.



**Figure 4.8** SEM micrographs of ZnO nanoparticles synthesized at  $T_{\text{evp}} = 800^{\circ}\text{C}$  and fixed air flow rate of 0.6 L/min. The nitrogen flow rate was varied from (a) 3, (b) 4 and (c) 5 L/min.

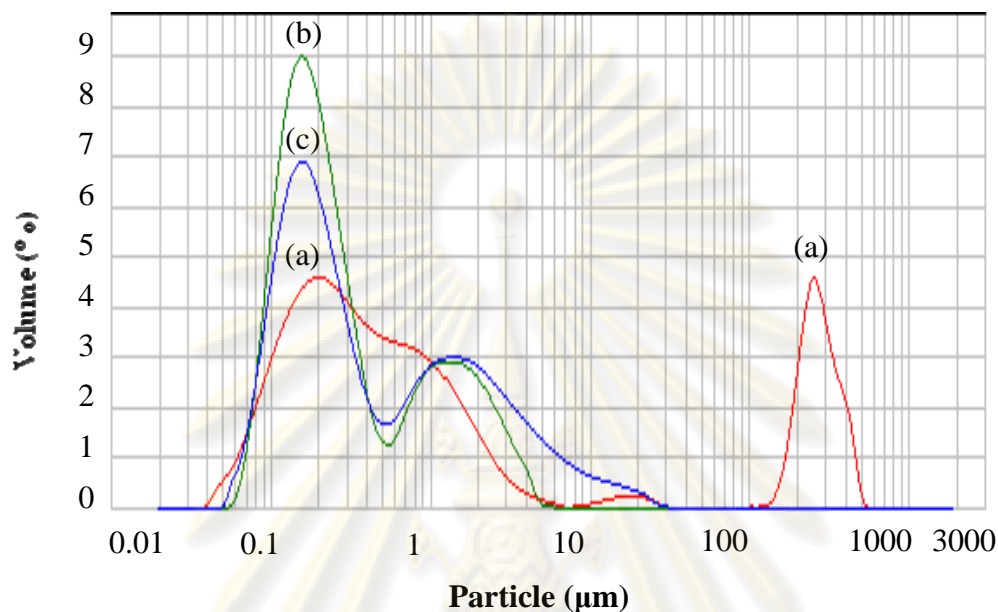
Figure 4.9 shows partial pressure of oxygen at different value of nitrogen flow rate (calculations are shown in Appendix A). The partial pressure of oxygen investigated was in the range of 0.027-0.034 atm. As partial pressure of oxygen is in the range of 0.022-0.027 atm, the morphology of ZnO product changes from non-uniform shape to tetrapods. In the other words, the tetrapods are grown under low oxygen partial pressure. Therefore, the morphology is likely linked to dynamic crystal growth processes at different oxygen partial pressure. At low oxygen partial pressure, ZnO crystal growth is slow. It probably undergoes toward thermodynamic equilibrium during the growth process, which would result in regular hexagonal legs. At high

oxygen partial pressure, the growth of ZnO crystals might be kinetically controlled, since the growth rates in the  $\langle 001 \rangle$  and  $\langle 100 \rangle$  directions depend on the oxygen partial pressure to a different extent. As a result, trumpet-shaped arms would form [Yan et al. (2003)].



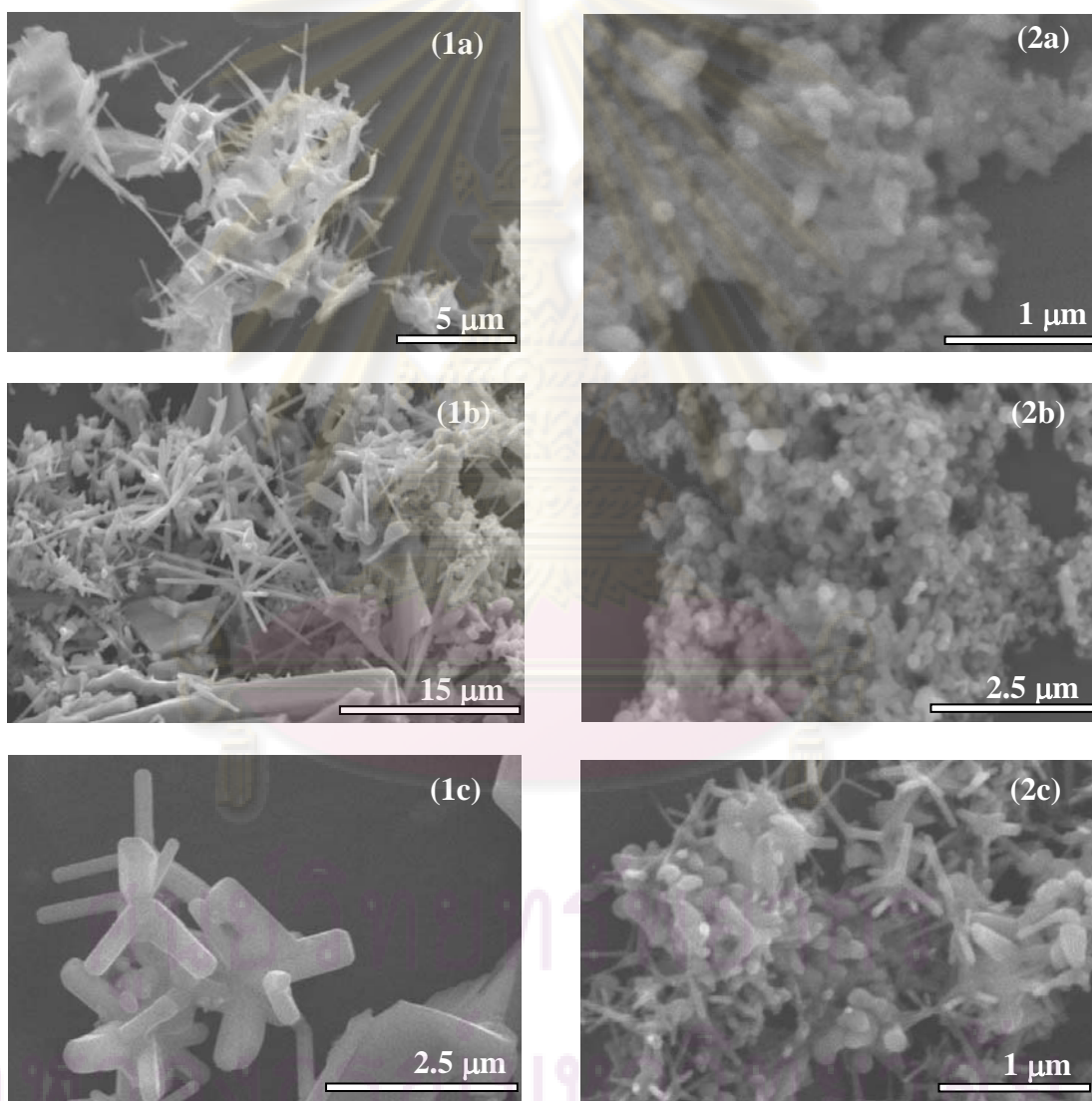
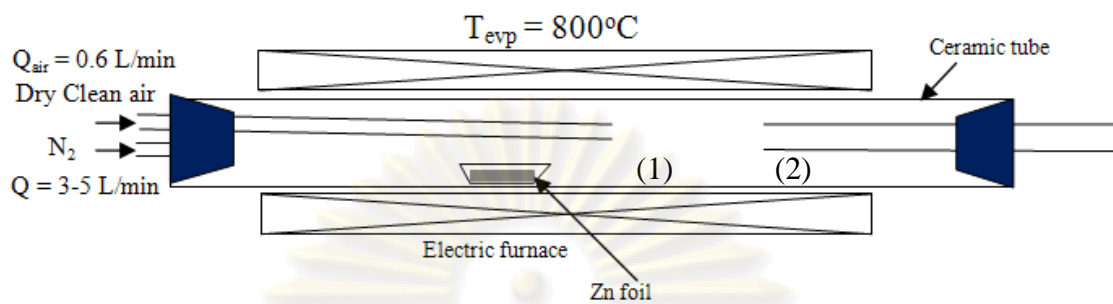
**Figure 4.9** Partial pressure of oxygen in the system as a function of nitrogen flow rate.

Figure 4.10 shows particle size distribution of ZnO nanoparticles collected at filters, synthesized by varying nitrogen flow rate. According to Figure 4.10a, particle size distribution of ZnO nanoparticles is polymodal in shape. It corresponds with SEM image (Figure 4.8a), which shows that ZnO nanoparticles synthesized at low nitrogen flow rate are polydispersed. For the results using higher nitrogen flow rate, particle size distribution is bimodal. At nitrogen flow rate 4 and 5 L/min, size of ZnO nanoparticles are only slightly different because the morphology of ZnO nanoparticles are tetrapods in both cases. The average size of ZnO nanoparticles synthesized using nitrogen flow rate of 3, 4 and 5 L/min is 0.513, 0.225 and 0.305  $\mu\text{m}$  respectively.



**Figure 4.10** Particle size distribution of ZnO nanoparticles synthesized using nitrogen flow rate of: (a) 3 L/min, (b) 4 L/min and (c) 5 L/min.

Figure 4.11 show SEM micrographs of the powder obtained in synthesis at the reaction and the further the zinc source. In the reaction zone (location 1), the morphology of the powder deposit is irregular shape when the nitrogen flow rate is low as shown in Figure 4.11 (1a-1b). For the higher nitrogen flow rate, the pods and tetrapods are found in this zone as shown in Figure 4.11 (1c). With the increase in the nitrogen flow rate, higher flux of zinc vapor is generated and also the amount of zinc vapor changes. The amount of zinc generation with the lower nitrogen flow rate is lower than that of the higher nitrogen flow rate. Consequently, the zinc oxide nuclei are less. The nuclei can grow into the irregular shape. At the position further away from the zinc source, the morphology of ZnO is sphere, which may be carried from the reaction zone to deposit in this zone.



**Figure 4.11** SEM micrographs of the deposits formed in different zones of the reactor during the synthesis using nitrogen flow rate of (a) 3 L/min, (b) 4 L/min and (c) 5 L/min.



Figure 4.12 shows SEM micrographs of the deposits in the dry and wet chamber zones formed by varying nitrogen flow rate. The products correspond with the product collected at the filters. The morphology of ZnO is disorder at nitrogen flow rate of 3 and 4 L/min and it changes to tetrapods when nitrogen flow rate is increased to 5 L/min.

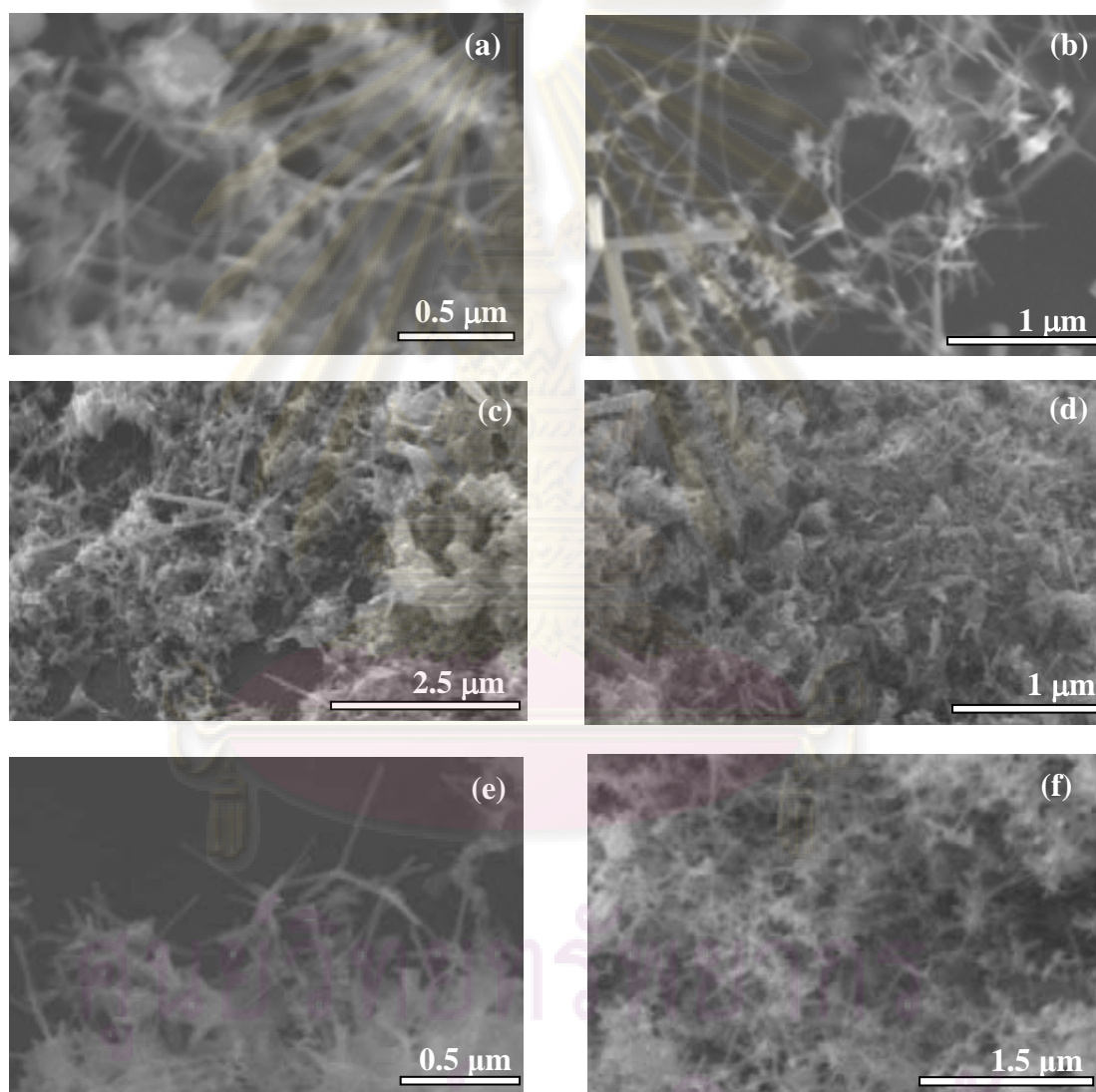


**Figure 4.12** SEM micrographs of the deposits formed in the dry and wet chamber zones synthesized using nitrogen flow rate of: (a-b) 3 L/min, (c-d) 4 L/min and (e-f) 5 L/min.



### 4.3 Effect of Oxygen Concentration

The effect of oxygen concentration was studied by controlling relative flow rates of both nitrogen gas and air that was mixed before supplying to the reaction zone as shown in Figure 4.13. The total flow rate which includes the mixing gas and the carrier entering the reaction zone was set to 5.6 L/min. The oxygen concentration was varied from 1.0 to 2.0 % by mole and the evaporation temperature was fixed at 800 °C.

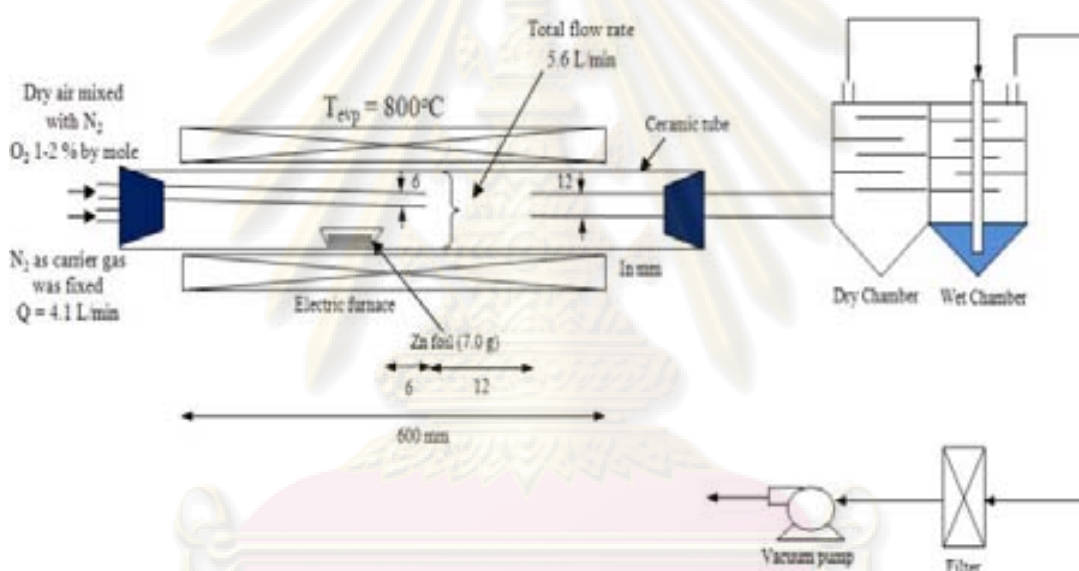


**Figure 4.13** Schematic diagram for experimental sets up for studying the effect of oxygen concentration.

Figure 4.14 shows SEM images of ZnO nanoparticles collected at filters prepared at different oxygen concentration. It can be observed that all the products are the mixture of two different shapes, i.e. a majority of tetrapods and few irregular shape particles. Several tetrapods are found when ZnO is synthesized using oxygen concentration of 1 % by mole. On the contrary, the irregular particles are slightly increased at oxygen concentration of 2 % by mole. The legs of tetrapods prepared at oxygen concentration of 1 % by mole are slightly longer than that prepared at oxygen

concentration of 2 % by mole, indicating the slight effects of oxygen concentration on shape of the product prepared in our experimental setup. The diameter and the length of the legs of the pods are in the range of 40-80 nm and 220-270 nm, respectively.

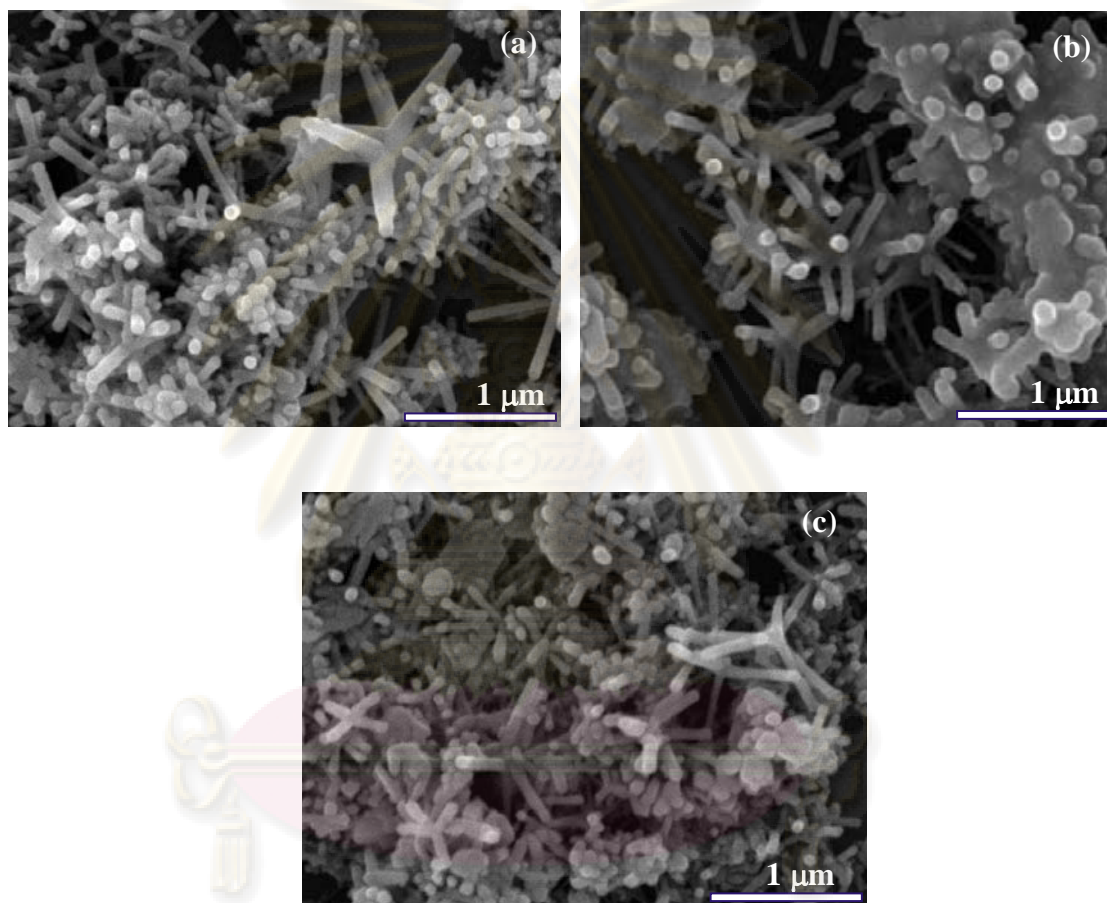
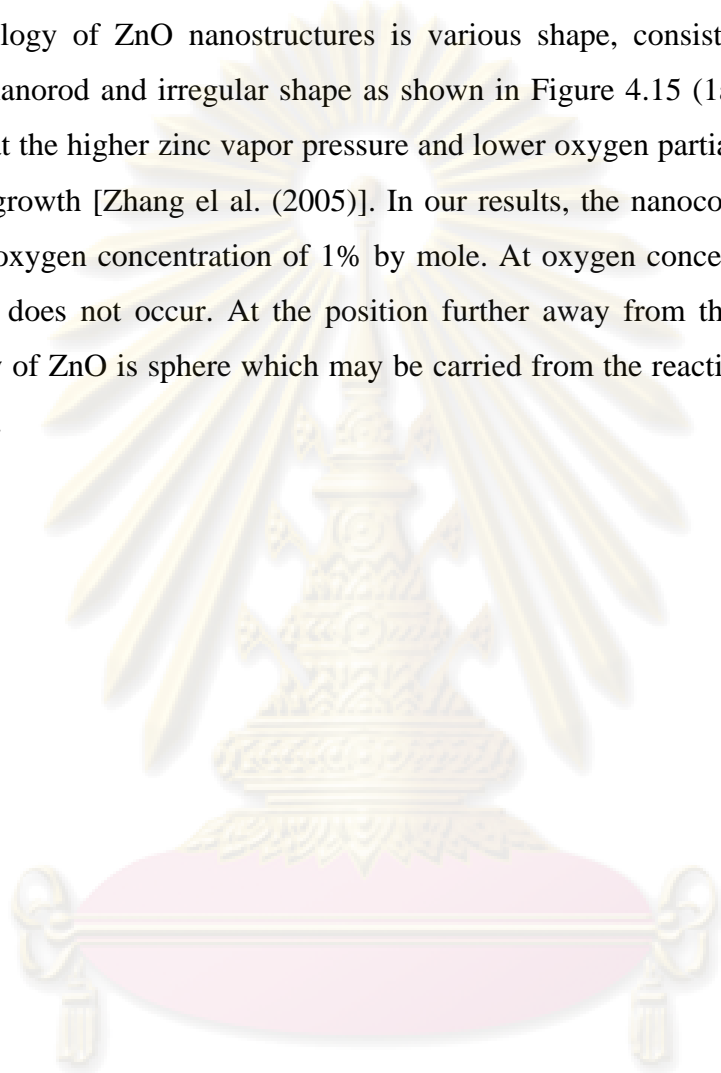


**Figure 4.14** SEM micrograph of ZnO nanoparticles synthesized at various with varying oxygen concentrations: (a) 1.0% (b) 1.5% and (c) 2.0 % by mole.

Figure 4.15 shows SEM micrographs of the deposits formed in different zones of the reactor varying oxygen concentration. In the reaction zone (location 1), the morphology of ZnO nanostructures is various shape, consisting of nanocomb, nanowire, nanorod and irregular shape as shown in Figure 4.15 (1a-1c). Zhang et al. reported that the higher zinc vapor pressure and lower oxygen partial pressure favored nanocomb growth [Zhang et al. (2005)]. In our results, the nanocomb is found when supply the oxygen concentration of 1% by mole. At oxygen concentration above 1% by mole, it does not occur. At the position further away from the zinc source, the morphology of ZnO is sphere which may be carried from the reaction zone to deposit in this zone.



ศูนย์วิทยทรัพยากร  
จุฬาลงกรณ์มหาวิทยาลัย

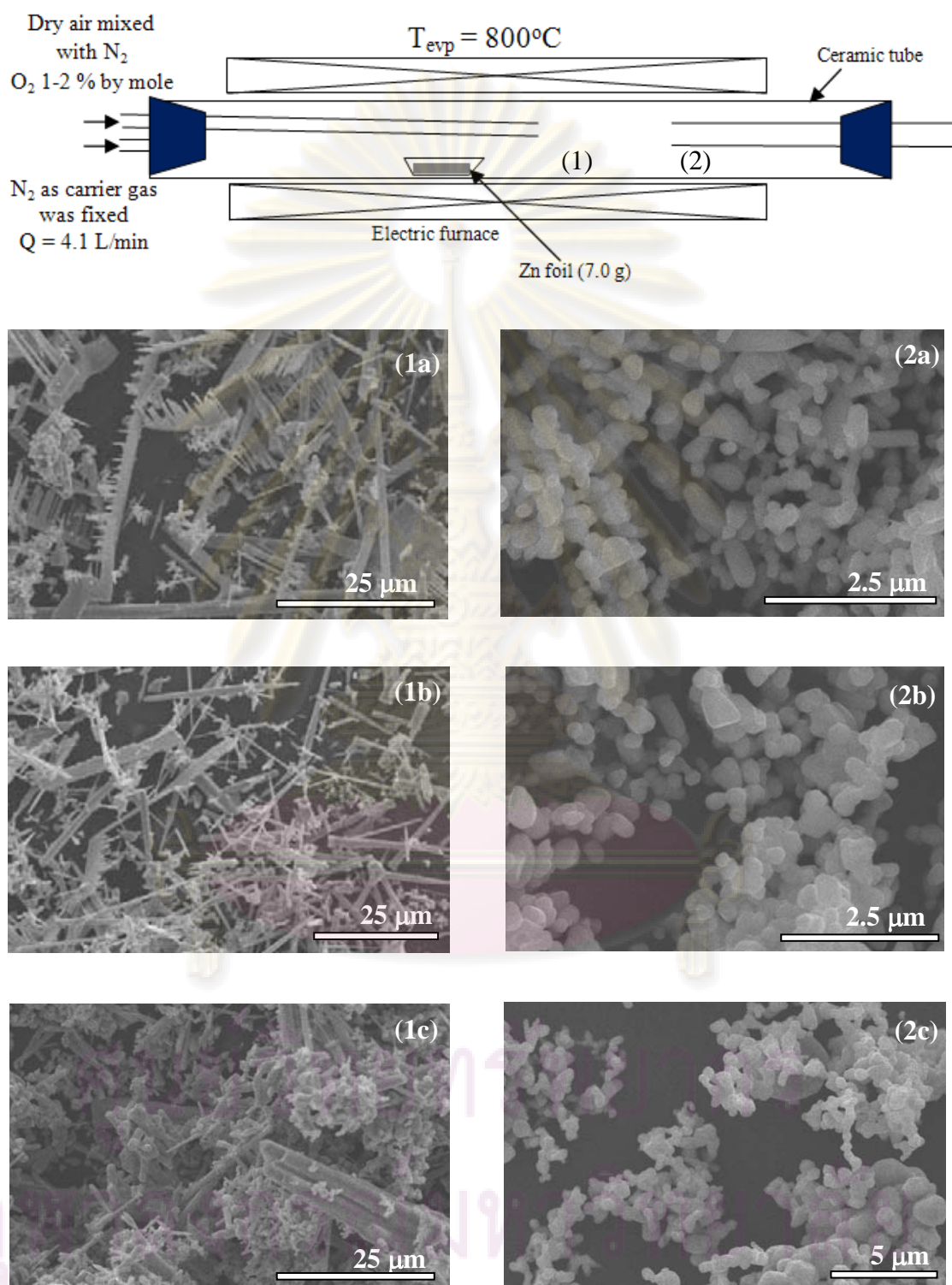


**Figure 4.15** SEM micrographs of the deposits formed in different zones of the reactor during the synthesis using oxygen concentration of (a) 1%, (b) 1.5% and (c) 2% by mole.



Figure 4.16 shows SEM micrographs of the deposits in the dry and wet chamber zones formed by varying oxygen concentration. The morphology of product at dry and wet chamber is similar. It is tetrapod with few nanosphere and nanorod. The morphology of ZnO nanostructures is non-uniform which may occur from the fluctuation of reactant vapor pressure in the system.

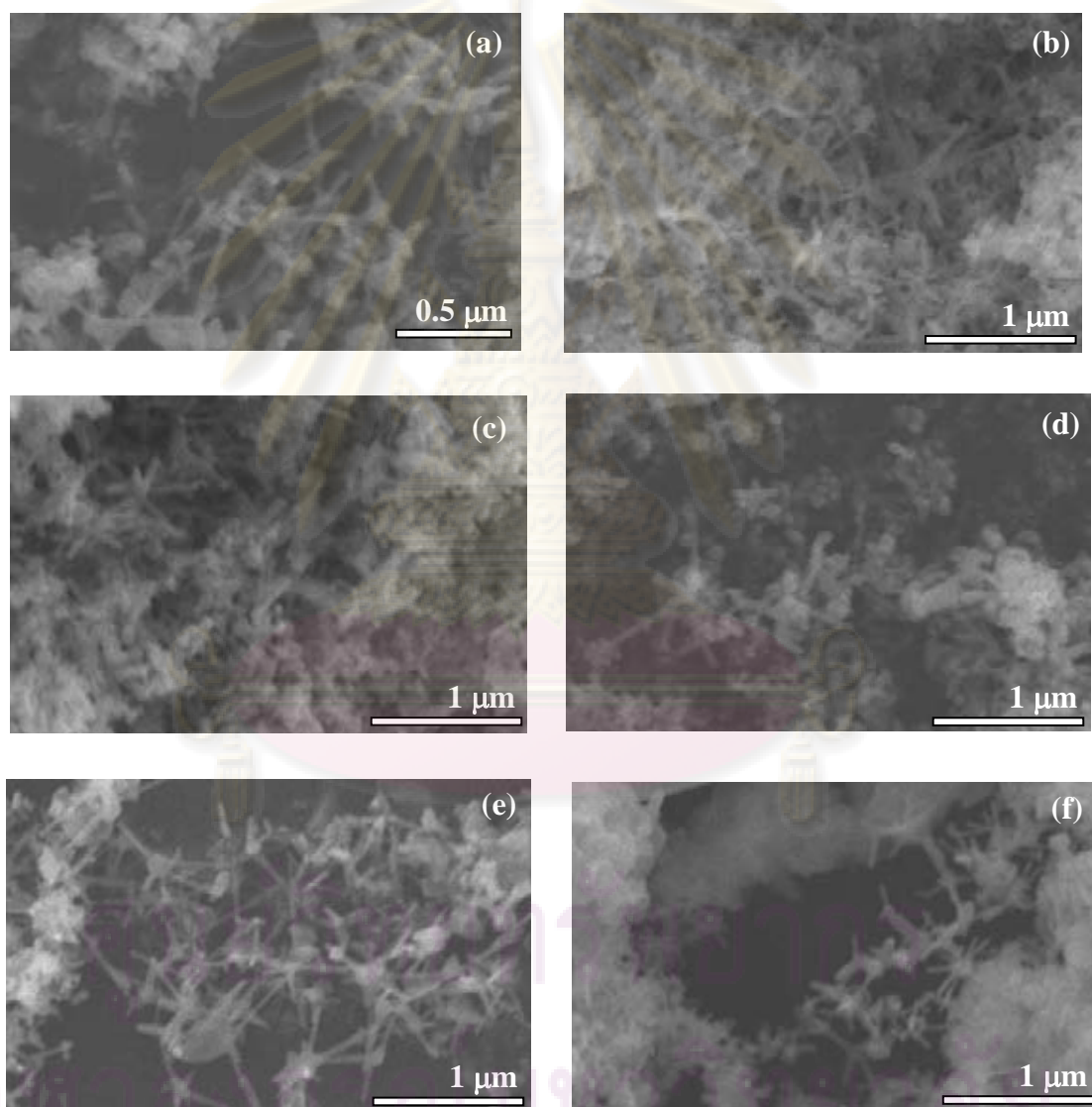


**Figure 4.16** SEM micrographs of the deposits formed in the dry and wet chamber zones synthesized varying oxygen concentration of: (a-b) 1%, (c-d) 1.5% and (e-f) 2% by mole.

#### 4.4 Effect of Amount of Zinc Vapor

The effect of amount of zinc vapor was studied by varying the cross sectional area of the alumina boat from 4, 12, to 20 cm<sup>2</sup> respectively. In our system, Generation of zinc vapor is mass transfer limited process, since the zinc vapor increases with increase in the cross sectional area. Zinc foil in the amount of 1 g was used as raw material. The reaction was conducted at 800°C for 5 min, during which air and nitrogen were supplied to the reactor at constant flow rate of 0.6 and 5 L/min, respectively. After the reaction, ZnO deposited at the different zones of the reactor was characterized by scanning electron microscope (SEM).

Figure 4.17 shows SEM micrographs of the deposits formed at different zones of the reactor when the cross sectional area of the alumina boat containing zinc foil is varied. Figure 4.17(a)-4.17(b) show the dendritic nanostructures formed at zone 1 located upstream of the supplied air outlet, when the cross sectional area of the alumina boat is 4 cm<sup>2</sup>. It can be seen that a large quantity of nanorods grow on a nanowire stem, and the end of the rod expand into hexagonal facet. They might take place the secondary rapid growth process [Zhuo et al. (2008)]. In addition, the nanowires are found in the reaction zone as shown in Figure 4.17(c). The nanocombs with needle-like teeth and expanding hexagonal caps at their tip are found at zone 1 when the cross sectional area of the alumina boat is increased to 12 cm<sup>2</sup>, as shown in Figure 4.17(d). A large quantity of needle-like teeth grows out of the nanowires. However, the ZnO nanoparticles using the cross sectional area of 12 cm<sup>2</sup> in the reaction zone are not found because they does not deposit in this zone. At the cross sectional area of the alumina boat of 20 cm<sup>2</sup>, we found the tetrapods at zone 2, which is located in the reaction zone, but we are not found product at zone 1. The tetrapods legs are short, but the hexagonal cross section can be clearly observed. In these experiments, increasing cross section area of the alumina boat results in an increase in the amount of zinc vapor evaporated within such a short period of the reaction. Furthermore, it is well realized that the concentration of zinc vapor decreases along the length of the reactor, due to the reaction with oxygen to form ZnO.



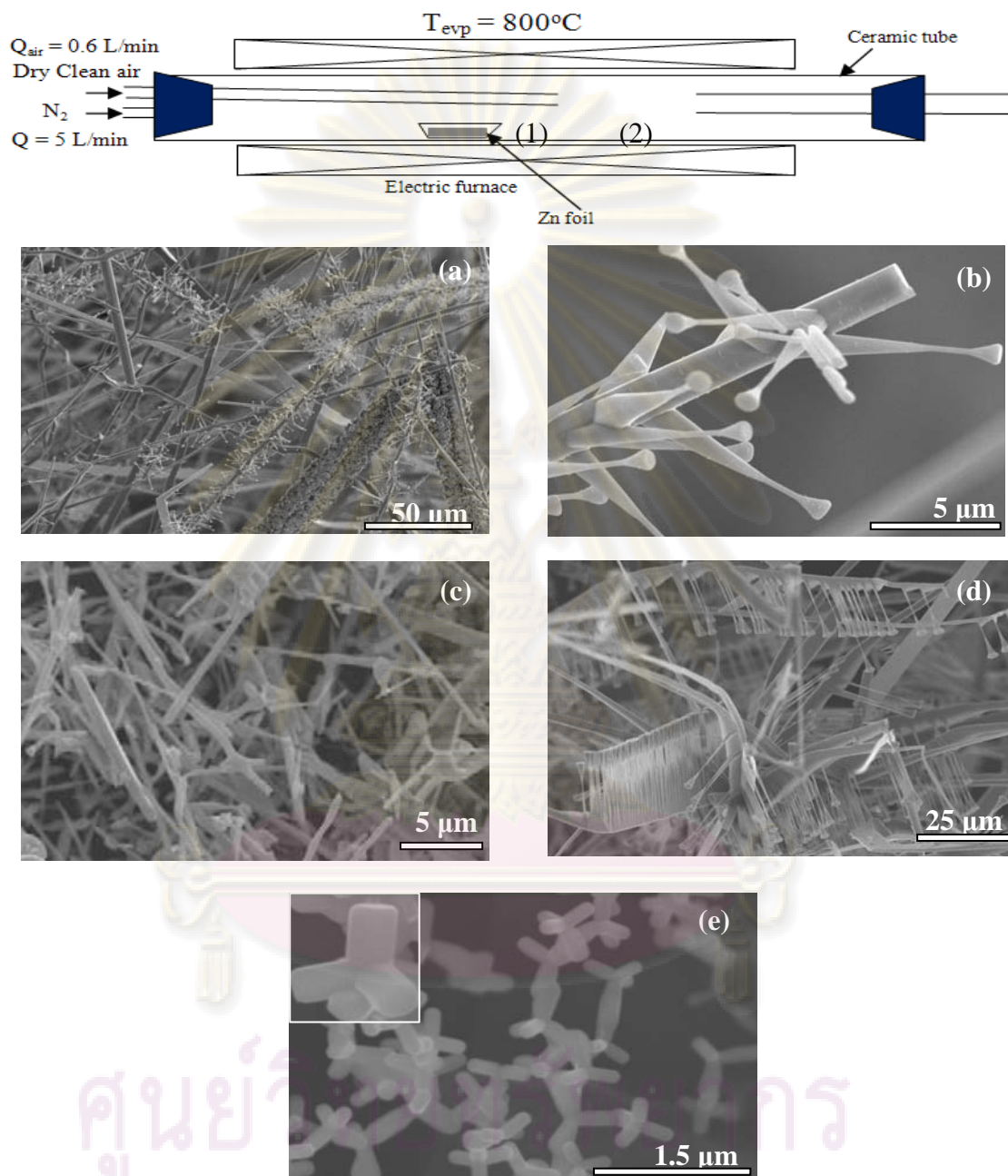


**Figure 4.17** SEM micrographs of the deposits formed in different zones of the reactor during the synthesis using oxygen concentration of (a-b) dendritic nanostructures, (c) nanowires, (d) nanocombs and (e) tetrapods.

In the growth of dendritic nanostructures, ZnO crystal growth might undergo the following process. Zn powder is vaporized and reacted with the back-diffused oxygen to form the primary ZnO nanowires as shown in Figure 4.18(a). The zinc vapor is generated continually. It adsorbs onto the surface of the nanowire substrates to form an adsorbed layer of Zn atoms. The reaction between the back-diffused oxygen and Zn atoms absorbed on the surface of the primary nanowire substrate takes place to form ZnO crystal particles. Then, they migrate to a suitable lattice to grow up. However, the crystal particles do not migrate to certain lattices and grow up directly. They undergo a growth process, which the nanorods grew on the nanowire substrates as shown in Figure 4.18(b)-4.18(d).

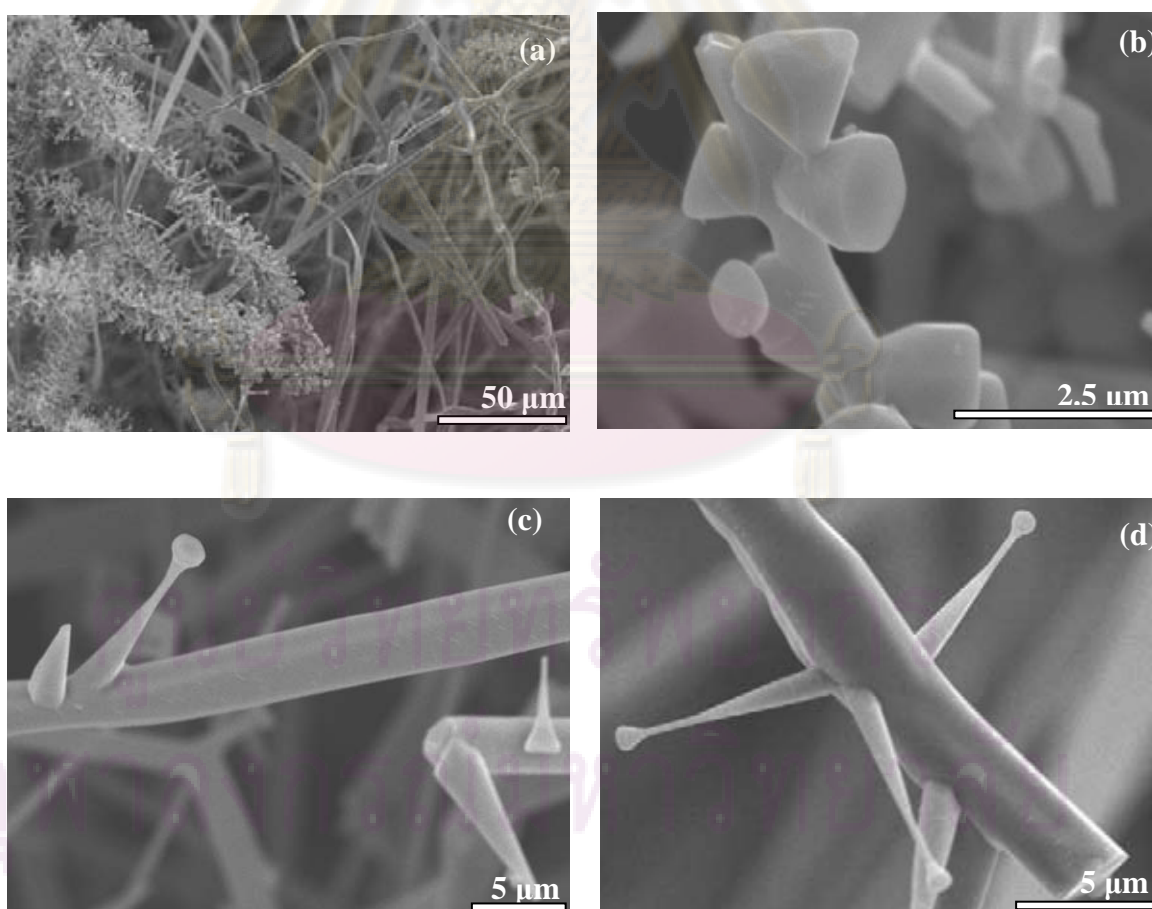


**Figure 4.18** SEM images of dendritic nanostructures. (a) nanowires, (b)-(d) nanorods grown on nanowire stem.

The rate of nucleation,  $J$ , e.g., the number of nuclei formed per unit time per unit volume, can be expressed in the form of the Arrhenius reaction velocity equation commonly used to describe the nucleation rate of a thermally activated process.

$$J = A \exp \left[ \frac{\Delta E_{des} - \Delta E_d - \Delta G_{crit}}{kT} \right] \quad (1)$$

$$\Delta G_{crit} = \frac{16\pi\sigma^3 v^2}{3k^3 T^3 (\ln S)^2} f(\phi) \quad (2)$$

$$f(\phi) = \frac{(2 + \cos \phi)(1 - \cos \phi)^2}{4} \quad (3)$$

$$\beta = \frac{J_1}{J_2} = \exp \{B[f(\phi_2) - f(\phi_1)]\} \quad (4)$$

$$B = \frac{16\pi\sigma^3 v^2}{3k^3 T^3 (\ln S)^2} \quad (5)$$

Where  $\Delta G_{crit}$  is the critical nucleus excess free energy;  $\Delta E_{des}$  is the desorption activation energy of desorption,  $\Delta E_d$  is the surface diffusion activation energy,  $k$  is the Boltzmann constant, and  $T$  is the temperature. The angle  $\phi$  is the angle of contact between the crystalline deposit and the foreign solid surface;  $\sigma$  is the interfacial tension,  $v$  is the molecular volume, and  $S$  is the degree of supersaturation. These equations indicate that the rate of nucleation was governed by four main variables:  $S$ ,  $T$ ,  $\sigma$ , and  $\phi$ . The necessary condition to form epitaxial growth is that the rate of nucleation in epitaxial direction is larger than nonepitaxial direction. We use  $J_1$  as the rate of nucleation in epitaxial direction  $\phi_1$ ,  $J_2$  as the rate of nucleation in nonepitaxial direction  $\phi_2$ , from the eq. (1), the ratio of the two nucleation rates  $\beta$  is given by ZnO dendritic nanostructures. When we have a relatively high supersaturation, the corresponding  $B$  and  $\beta$  decreased. In this situation, epitaxy has been restrained and the relationship between the secondarily grown nanorods and the primary ZnO nanowire is not epitaxial in the initial nucleation process. When the supersaturation decreases to a stable status, which may be a very quick process since the reactant zinc foil is reduced and the system was evacuated by a mechanical rotary pump. It approximately undergoes an equilibrium condition during the growth process, which

would result in regular-shaped hexagonal cylinder arms. The relatively high-saturated vapor pressure benefits the growth of 1D nanostructures. In the growth of nanowires, the relatively lower supersaturation is probably critical for whisker growth, which should be lower than that required for euhedral crystal growth, otherwise, two- or three-dimensional growth will occur. In the word nucleation is very important in the chemical vapor deposition process to synthesize nanoscale crystals. When the supersaturation  $S$  is high or a lot of “active centers” exist, the system can have a high rate of nucleation and achieve the fastest growth speed, and then the nucleus could not grow up along certain crystallographic directions and approximately parallel to each other. To study the growth mechanism of the branches after the initial nonepitaxial growth stage, the velocity of the (0001) plane is higher than that of the {1000} planes due to the different surface energy. Therefore, the growth pattern of secondary ZnO nanorods is dominated by a kinetic process, due to the increase in both the surface/interface defects and the system energy in the ZnO nanorods [Tong et al. (2006)].

Yan et al. (2008) indicated that the supersaturation and temperature are two crucial factors determining the morphology. Accordingly, the zinc supersaturation decreases rapidly along the direction of airflow because of the reaction with oxygen in the system. In the growth process of the nanostructure, the fluctuation of supersaturation will induce a change of the growing behavior and result in the formation of hierarchical structures. Accordingly, at a first stage of the reaction, the Zn supersaturation increases with the increasing temperature to maximum at desired temperature, and then decreases when it is consumed in the reaction with oxygen. As to the formation of nanocombs with needle-like teeth, the growth of this kind of nanocomb involved two steps. First, the zinc supersaturation is high in the initiate reaction, which may grow the backbone nanobelt as shown in Figure 4.19(a). In the growth period, the zinc supersaturation is decreased due to reduction of raw material. It may grow a row of nanorods as shown in Figure 4.19(b)-4.19(c).

As to the needle shape of a nanorod, the curtailment of the diameter from bottom to the tip can be ascribed to a gradual decrease of the reagent's supersaturation. On the top plane of the needle, there exist abundant defects (atomic steps, Zn clustering, etc), which favor the further absorption of reagent species and which induce the growth of finer hexagonal caps at the end.

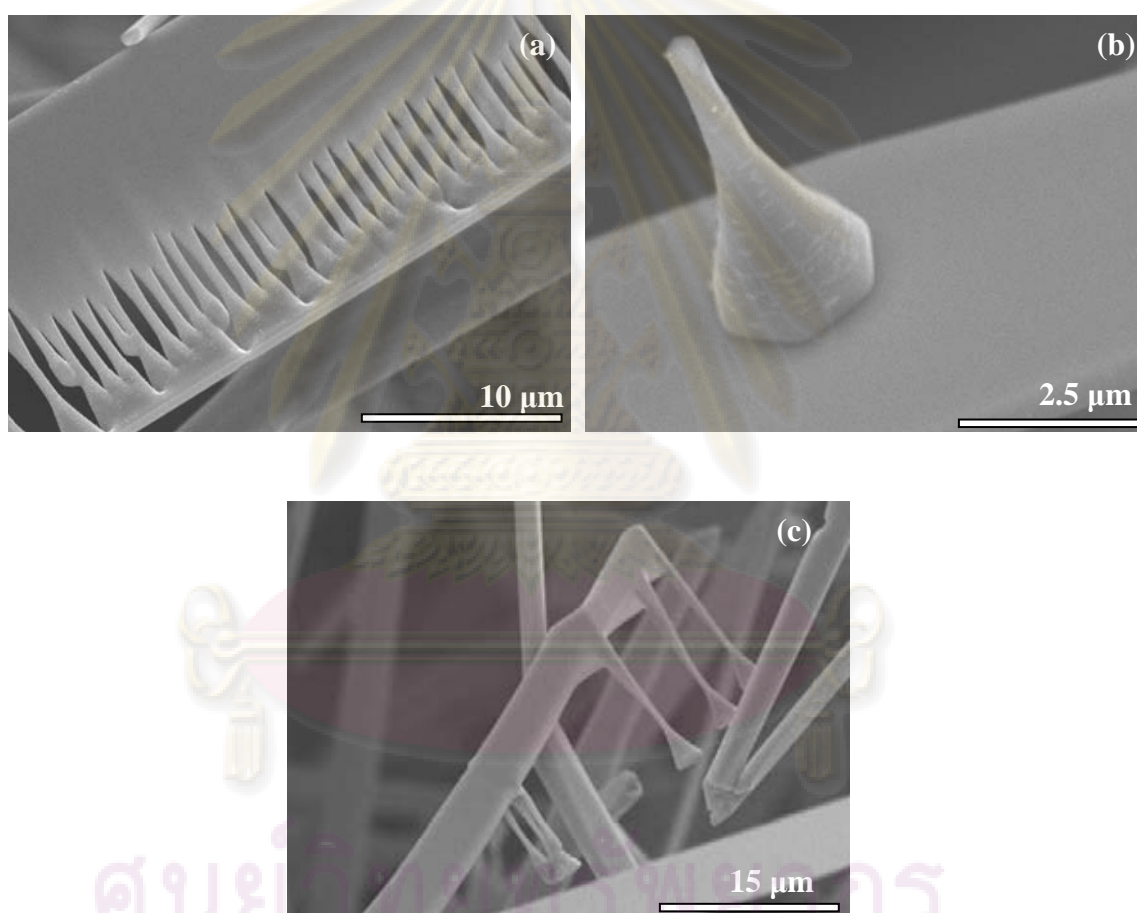


**Figure 4.19** SEM images of nanocombs (a) nanoblet, (b) needle-like teeth grown on nanowire, (c) nanocombs with needle-like teeth.



#### 4.5 Effect of Oxidation Time

In this section, 1 g of zinc foil was loaded in a alumina boat with the cross sectional area of 4 cm<sup>2</sup>. Then the furnace was heated to 800°C at a rate of 10°C/min. Next, air was supplied to the reactor with flow rate of 0.6 L/min for various feeding time, i.e. 1 and 30 min. During the reaction, nitrogen flow rate was kept constant at 0.6 L/min. ZnO deposited at the different zones of the reactor was characterized by scanning electron microscope (SEM).

Figure 4.20 shows SEM micrographs of the deposits formed in reaction zone of the reactor, when the reaction time was varied from 1 to 30 min. The microrods and multipods are found when the reaction time is limited to 1 min, as shown in Figure 4.20(a). Legs of the multipods is blunt at the end, with diameter of about 2-3 μm. Zheng et al. (2008) reported that the growth process was affected by vapor pressure, including Zn vapor and oxygen. The morphology of the legs could be controlled by adjusting the heating and cooling speed to change the vapor pressure. The high pressure of Zn vapor was beneficial to accelerate the growth along the six-symmetric directions of  $\pm[1\ 0\ \bar{1}\ 0]$ ,  $\pm[1\ \bar{1}\ 0\ 0]$ , and  $\pm[0\ 1\ \bar{1}\ 0]$  and suppressed the growth of ZnO along  $[0\ 0\ 0\ 1]$  direction. The growth process of the multipods nanostructures was more complicated, but the vapor concentration and the growth temperature were still the critical factors, which influenced the initial nucleation and the following legs growing. In our system, the concentration of Zn vapor is maximal in the initial stage and the feeding time of air is limited. Consequently, there is no redundant oxygen for continuing growth. Therefore, ZnO nuclei could accumulate and form the multiple facets nuclei which could form to multipods.

จุฬาลงกรณ์มหาวิทยาลัย



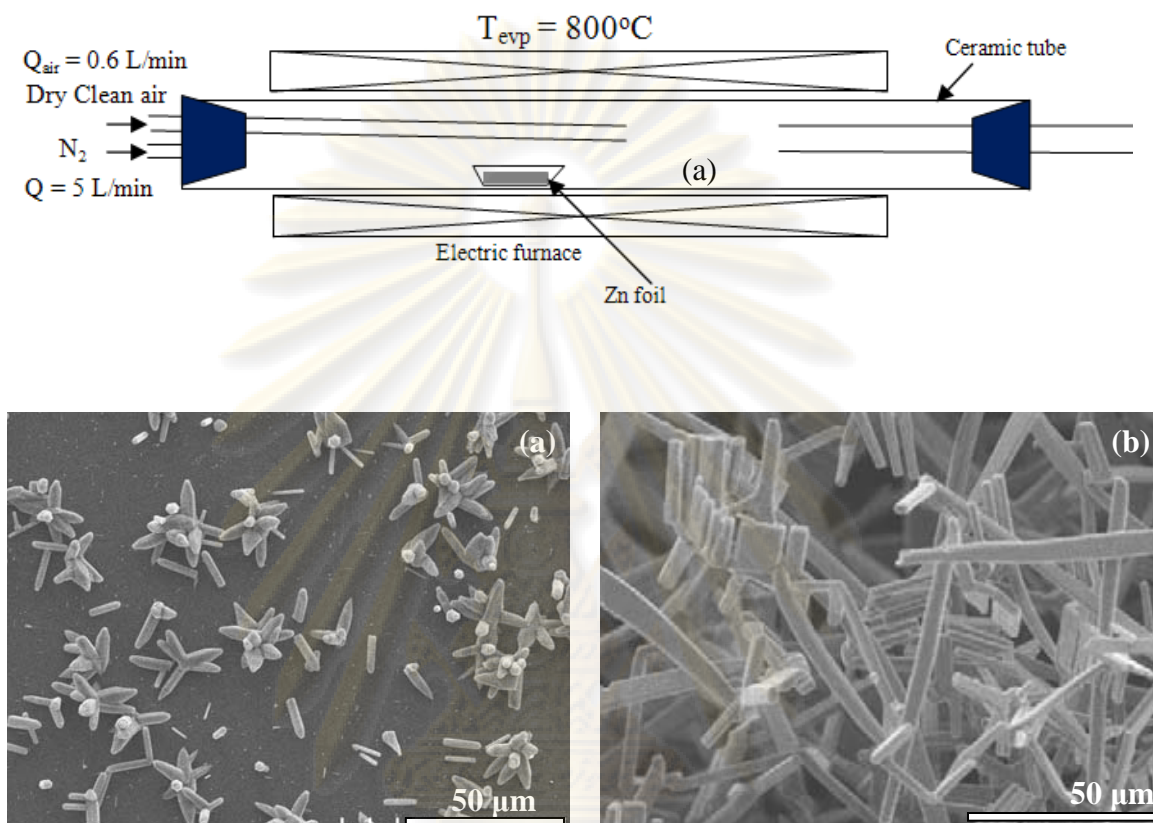


**Figure 4.20** SEM micrographs of the deposits formed in reaction zone of the reactor during the synthesis of ZnO for: (a) 1 min, (b) 30 min.

When the feeding time of air is limited to 30 min, the microrods and microwires are found at the reaction zone as shown in Figure 4.20(b). The diameter of microrods and microwires is about  $10 \mu\text{m}$ . Park et al. (2005) demonstrated the synthetic routes for the ZnO nanowires, that the nanowires were synthesized at condition which Zn vapor was very low and oxygen was high. In our system, air was supplied for 30 min which is sufficient for the Zn oxidation. The zinc vapor is slightly generated because of the small cross sectional area of the alumina boat. Therefore, the ZnO nanostructures grow continuously from nanorods and nanowires to microrods and microwires.

## CHAPTER V

### CONCLUSIONS AND RECOMMENDATIONS

#### 5.1 Conclusions

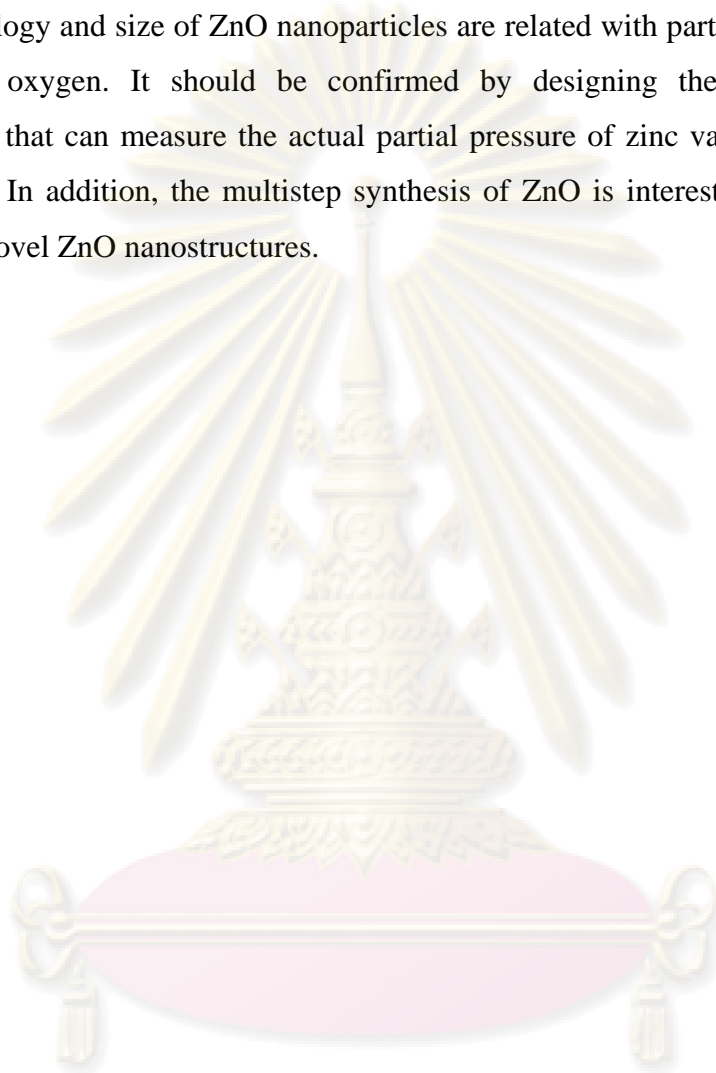
In this work, the ZnO nanoparticles could be synthesized by French process. The process parameters which affect the morphology and size of ZnO nanoparticles synthesized from French process include evaporation temperature, carrier gas flow rate, oxygen concentration, amount of zinc vapor and oxidation time. According to above mentioned experimental results, it can be concluded as follows.

1. The evaporation temperature and nitrogen flow rate have impact on the partial pressure of zinc and oxygen in the system, which affect on the morphology of ZnO nanostructures.
2. The morphology and size of ZnO nanostructures depend on the amount of zinc vapor and the oxidation time.
3. Tetrapods ZnO nanostructures can be synthesized under limiting condition of low oxidation.

ศูนย์วิจัยทรัพยากร  
จุฬาลงกรณ์มหาวิทยาลัย

## 5.2 Recommendations for future work

According to the experimental results in this work, it is hypothesized that the morphology and size of ZnO nanoparticles are related with partial pressure of zinc vapor and oxygen. It should be confirmed by designing the experiments and equipments that can measure the actual partial pressure of zinc vapor and oxygen in the system. In addition, the multistep synthesis of ZnO is interesting because it can create the novel ZnO nanostructures.



ศูนย์วิจัยทรัพยากร  
จุฬาลงกรณ์มหาวิทยาลัย

## REFERENCES

- Bacsa, R., Y. Kihn, M. Verelst, J. Dexpert, W. Bacsa and P. Serp. Large scale synthesis of zinc oxide nanorods by homogeneous chemical vapour deposition and their characterisation. Surface & Coatings Technology 201 (2007): 9200-9204.
- Cao, Guozhong. Nanostructures & nanomaterials : Synthesis, properties & applications. London : Imperial College Press, 2004.
- Chen, Z., Z. W. Shan, M. S. Cao, L. Lu and S. X. Mao. Zinc oxide nanotetrapods. Nanotechnology 15 (2004): 365-369.
- Cheng, W. D., P. Wu, X. Q. Zou and T. Xiao. Study on synthesis and blue emission mechanism of ZnO tetrapodlike nanostructures. Journal of Applied Physics 100 (2006): 054311-1 - 054311-4.
- Dai, Y., Y. Zhang and Z. L. Wang. The octa-twin tetraleg ZnO nanostructures. Solid State Communications 126 (2003): 629-633.
- Fan, H. J., Bertram, F., Dadgar, A., Christen, J., Krost, A., and Zacharias, M. Self-Assembly of ZnO Nanowires and The Spatial Resolved Characterization of Their Luminescence. Nanotechnology 15 (2004): 1401-1404.
- Gong, J. F., H. B. Huang, Z. Q. Wang, X. N. Zhao, S. G. Yang and Z. Z. Yu. A third kind growth model of tetrapod: Rod-based single crystal ZnO tetrapod nanostructure. Materials Chemistry and Physics 112 (2008): 749-752.
- Hao, Y. F., G. W. Meng, C. H. Ye and L. D. Zhang. Controlled synthesis of In<sub>2</sub>O<sub>3</sub> octahedrons and nanowires. Crystal Growth & Design 5 (2005): 1617-1621.
- Hao, Y. F., G. W. Meng, C. H. Ye, X. R. Zhang and L. D. Zhang. Kinetics-driven growth of orthogonally branched single-crystalline magnesium oxide nanostructures. Journal of Physical Chemistry B 109 (2005): 11204-11208.
- Jung, M. N., S. Y. Ha, H. S. Kim, H. J. Ko, H. Ko, W. H. Lee, D. C. Oh, Y. Murakami, T. Yao and J. H. Chang. The shape control of ZnO based nanostructures. Journal of Nanoscience and Nanotechnology 6 (2006): 3628-3632.

- Keishi Gotoh, Hiroaki Masuda, Ko Higashitani. Powder technology handbook. 2nd ed. New York: Marcel Dekker, 1997.
- Lao, J. Y., J. Y. Huang, D. Z. Wang and Z. F. Ren. Hierarchical oxide nanostructures. Journal of Materials Chemistry 14 (2004): 770-773.
- Leung, Y. H., A. B. Djuricic, W. C. H. Choy, M. H. Xie, J. Gao, K. W. Cheah, K. Y. K. Man and W. K. Chan. Synthesis and properties of ZnO multipod structures. Journal of Crystal Growth 274 (2005): 430-437.
- Li, Y., Meng, G. W., Zhang, L. D., Phillip, F. Ordered semiconductor ZnO nanowire arrays and their photoluminescence properties. Applied Physics Letters 15 (2000): 2011-2013.
- Liu, B. and Zhang, H. Hydrothermal Synthesis of ZnO Nanorods in The Diameter Regime of 50 nm. Journal of the American Chemical Society 125 (2003): 4430-4431.
- Mahmud, S., M. J. Abdullah, G. A. Putrus, J. Chong and A. K. Mohamad. Nanostructure of ZnO fabricated via French process and its correlation to electrical properties of semiconducting varistors. Synthesis and Reactivity in Inorganic Metal-Organic and Nano-Metal Chemistry 36 (2006): 155-159.
- Manzoor, U. and D. K. Kim. Size control of ZnO nanostructures formed in different temperature zones by varying Ar flow rate with tunable optical properties. Physica E-Low-Dimensional Systems & Nanostructures 41 (2009): 500-505.
- Park, J. H., Y. J. Choi and J. G. Park. Synthesis of ZnO nanowires and nanosheets by an O<sub>2</sub>-assisted carbothermal reduction process. Journal of Crystal Growth 280 (2005): 161-167.
- Ramgir, N. S., D. J. Late, A. B. Bhise, M. A. More, I. S. Mulla, D. S. Joag and K. Vijayamohan. ZnO multipods, submicron wires, and spherical structures and their unique field emission behavior. Journal of Physical Chemistry B 110 (2006): 18236-18242.
- Ren, S., Y. F. Bai, J. Chen, S. Z. Deng, N. S. Xu, Q. B. Wu and S. H. Yang. Catalyst-free synthesis of ZnO nanowire arrays on zinc substrate by low temperature thermal oxidation. Materials Letters 61 (2007): 666-670.

- Ronning, C., N. G. Shang, I. Gerhards, H. Hofsass and M. Seibt. Nucleation mechanism of the seed of tetrapod ZnO nanostructures. Journal of Applied Physics 98 (2005): 034037-1 – 034037-5.
- Ruangsanam, T. Effects of Metal-Doping on Zinc Oxide Nanoparticles Synthesized via Solvothermal Method. Master's Thesis. Department of Chemical Engineering, Chulalongkorn University, (2005).
- Sekar, A., S. H. Kim, A. Umar and Y. B. Hahn. Catalyst-free synthesis of ZnO nanowires on Si by oxidation of Zn powders. Journal of Crystal Growth 277 (2005): 471-478.
- Shen, L., H. Zhang and S. W. Guo. Control on the morphologies of tetrapod ZnO nanocrystals. Materials Chemistry and Physics 114 (2009): 580-583.
- Singh, J., A. Srivastava, R. S. Tiwari and O. N. Srivastava. Nucleation and growth of catalyst-free zinc oxide nanostructures. Journal of Nanoscience and Nanotechnology 5 (2005): 2093-2098.
- Singh, J., R. S. Tiwari and O. N. Srivastava. Synthesis of zinc oxide nanotetrapods and nanorods by thermal evaporation without catalysis. Journal of Nanoscience and Nanotechnology 7 (2007): 1783-1786.
- Sun, T. J. and H. S. Qiu. Fabrication of ZnO microtube arrays via vapor phase growth. Materials Letters 62 (2008): 1528-1531.
- Tong, Y. H., Y. C. Liu, L. Dong, D. X. Zhao, J. Y. Zhang, Y. M. Lu, D. Z. Shen and X. W. Fan. Growth of ZnO nanostructures with different morphologies by using hydrothermal technique. Journal of Physical Chemistry B 110 (2006): 20263-20267.
- Tseng, Y. K., H. C. Hsu, W. F. Hsieh, K. S. Liu and I. C. Chen. Two-step oxygen injection process for growing ZnO nanorods. Journal of Materials Research 18 (2003): 2837-2844.
- Wang, B. B., J. J. Xie, Q. Yuan and Y. P. Zhao. Growth mechanism and joint structure of ZnO tetrapods. Journal of Physics D-Applied Physics 41 (2008): 1-6.



- Wang, H. H. and C. S. Me. The effects of oxygen partial pressure on the microstructures and photocatalytic property of ZnO nanoparticles. Physica E-Low-Dimensional Systems & Nanostructures 40 (2008): 2724-2729.
- Wang, Z. L.. Zinc oxide nanostructures: growth, properties and applications. Journal of Physics-Condensed Matter 16 (2004): R829-R858.
- Wei, O. Y. and Z. Jing. Catalyst-free synthesis of macro-scale ZnO nanonail arrays on Si substrate by simple physical vapor deposition. Materials Letters 62 (2008): 2557-2560.
- Xu, C. X., X. W. Sun, Z. L. Dong and M. B. Yu. Self-organized nanocomb of ZnO fabricated by Au-catalyzed vapor-phase transport. Journal of Crystal Growth 270 (2004): 498-504.
- Xu, C. X., X. W. Sun, Z. L. Dong, M. B. Yu, T. D. My, X. H. Zhang, S. J. Chua and T. J. White. Zinc oxide nanowires and nanorods fabricated by vapour-phase transport at low temperature. Nanotechnology 15 (2004): 839-842.
- Xu, F., K. Yu, G. D. Li, Q. Li and Z. Q. Zhu. Synthesis and field emission of four kinds of ZnO nanostructures: nanosleeve- fishes, radial nanowire arrays, nanocombs and nanoflowers. Nanotechnology 17 (2006): 2855-2859.
- Yan, H. Q., R. R. He, J. Pham and P. D. Yang. Morphogenesis of one-dimensional ZnO nano- and microcrystals. Advanced Materials 15 (2003): 402-405.
- Yan, Y. G., L. X. Zhou, L. Q. Yu and Y. Zhang. Morphology evolution of hierarchical ZnO nanostructures modulated by supersaturation and growth temperature. Applied Physics a-Materials Science & Processing 93 (2008): 457-465.
- Yan, Y. G., L. X. Zhou and Y. Zhang. Synthesis of MgO Hierarchical Nanostructures Controlled by the Supersaturation Ratio. Journal of Physical Chemistry C 112 (2008): 19831-19835.
- Ye, C. H., X. S. Fang, Y. F. Hao, X. M. Teng and L. D. Zhang. Zinc oxide nanostructures: Morphology derivation and evolution. Journal of Physical Chemistry B 109 (2005): 19758-19765.

- Zhang, Y. H., J. Liu, T. Liu, L. P. You and X. G. Li. Supersaturation-controlled synthesis of two types of single-sided ZnO comb-like nanostructures by thermal evaporation at low temperature. Journal of Crystal Growth 285 (2005): 541-548.
- Zhang, Y. S., Yu, K., Jiang, D. S., Zhu, Z. Q., Geng, H. R., Luo, L. Q. Zinc Oxide Nanorod and Nanowire for Humidity Sensor. Applied Surface Science 242 (2005): 212-217.
- Zhao, Y. N., M. S. Cao, H. B. Jin, L. Zhang and C. J. Qiu. Catalyst-free synthesis, growth mechanism and optical properties of multipod ZnO with nanonail-like legs. Scripta Materialia 54 (2006): 2057-2061.
- Zheng, K., C. X. Xu, G. P. Zhu, X. Li, J. P. Liu, Y. Yang and X. W. Sun. Formation of tetrapod and multipod ZnO whiskers. Physica E-Low-Dimensional Systems & Nanostructures 40 (2008): 2677-2681.
- Zhiyong Fan and Jia G. Lu. Zinc Oxide Nanostructure: Synthesis and Properties. Journal of Nanoscience and Nanotechnology 5 (2005): 1561-1573.
- Zhuo, R. F., H. T. Feng, J. T. Chen, D. Yan, J. J. Feng, H. J. Li, B. S. Geng, S. Cheng, X. Y. Xu and P. X. Yan. Multistep synthesis, growth mechanism, optical, and microwave absorption properties of ZnO dendritic nanostructures. Journal of Physical Chemistry C 112 (2008): 11767-11775.

ศูนย์วิทยทรัพยากร  
จุฬาลงกรณ์มหาวิทยาลัย



APPENDICES

ศูนย์วิทยทรัพยากร  
จุฬาลงกรณ์มหาวิทยาลัย

## APPENDIX A

### CALCULATION OF PARTIAL PRESSURE

Partial pressure of zinc vapor and oxygen was calculated by using ideal gas mixtures. The mole fraction of an individual gas component in an ideal gas mixture can be expressed in terms of the component's partial pressure or the moles of the component:

$$x_A = n_A/n \quad (A1)$$

$$p_A = x_A \cdot p \quad (A2)$$

where :

- n = total moles of the gas mixture
- $p_A$  = partial pressure of gas component A in gas mixture
- $n_A$  = moles of gas component A in gas mixture
- $x_A$  = moles fraction of gas component A in gas mixture
- p = pressure of gas mixture

For example, in case of 0.6 L/min of air and 5 L/min of nitrogen

Zn raw material 7 g was exhausted in time 40 min under evaporation temperature 800 °C

$$\begin{aligned} \text{Rate of Zn generation} &= \frac{7 \text{ [g]}}{40 \text{ [min]} \times 65.38 \text{ [g/mole]}} \\ &= 2.68 \times 10^{-3} \text{ mole/min} \end{aligned}$$

$$\begin{aligned} \text{Mole of oxygen , } n_{O_2} &= \frac{0.6 \text{ [L/min]} \times 0.21 \times 1.429 \text{ [g/L]}}{32 \text{ [g/mole]}} \\ &= 5.63 \times 10^{-3} \text{ mole/min} \end{aligned}$$

$$\text{Mole of nitrogen, } n_{\text{N}_2} = \frac{0.6 \text{ [L/min]} \times 0.79 \times 1.251 \text{ [g/L]}}{28 \text{ [g/mole]}} + \frac{5 \text{ [L/min]} \times 1.251 \text{ [g/L]}}{28 \text{ [g/mole]}}$$

$$= 0.2450 \text{ mole/min}$$

$$\text{Total mole} = 2.5533 \text{ mole/min}$$

$$\text{Mole fraction of Zinc vapor, } x_{\text{Zn}} = \frac{2.68 \times 10^{-3}}{2.5533}$$

$$= 0.0106$$

$$\text{Mole fraction of oxygen, } x_{\text{O}_2} = \frac{5.63 \times 10^{-3}}{2.5533}$$

$$= 0.0222$$

$$\text{Mole fraction of nitrogen, } x_{\text{N}_2} = \frac{0.245}{2.5533}$$

$$= 0.9672$$

We assume that partial pressure inside reactor is 1 atm. Therefore, partial pressure of gas component is equal to mole fraction.

ศูนย์วิทยทรัพยากร  
จุฬาลงกรณ์มหาวิทยาลัย

## APPENDIX B

### TEMPERATURE PROFILE INSIDE REACTOR

Temperature profile inside the reactor was mapped, as shown in Figure B1. We found that the temperature inside the reactor slightly decrease in the desired temperature from 25 to 40 cm. Base on this data, the effective zone for evaporation was taken be 25 to 40 cm of the furnace, from the feed-side of the reactor.

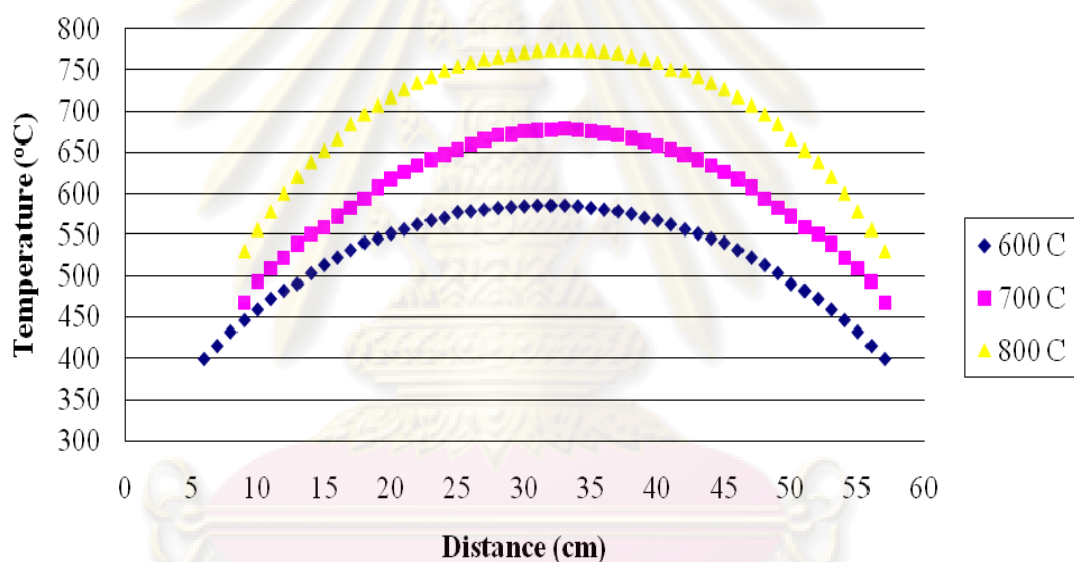


**Figure B1** Temperature profiles inside the reactor.

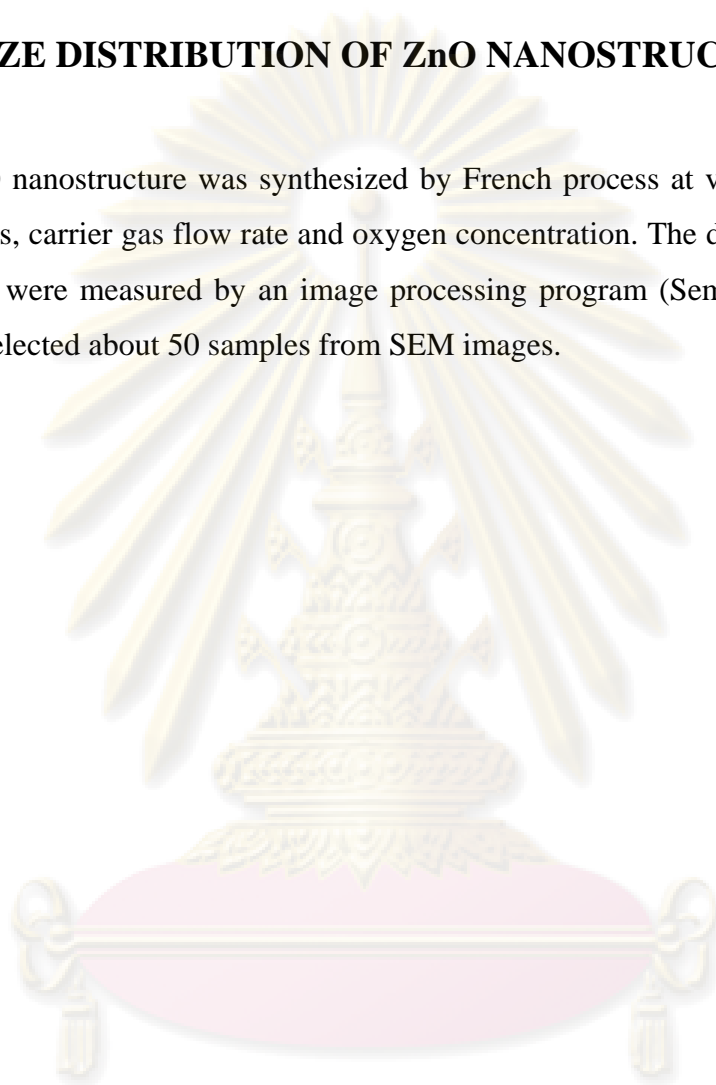
ศูนย์วิทยทรัพยากร  
จุฬาลงกรณ์มหาวิทยาลัย



## APPENDIX C

### SIZE DISTRIBUTION OF ZnO NANOSTRUCTURES

ZnO nanostructure was synthesized by French process at various evaporation temperatures, carrier gas flow rate and oxygen concentration. The diameter and length of particles were measured by an image processing program (SemAfore 4.0), which randomly selected about 50 samples from SEM images.



ศูนย์วิจัยทรัพยากร  
จุฬาลงกรณ์มหาวิทยาลัย

### C1 Effect of evaporation temperature

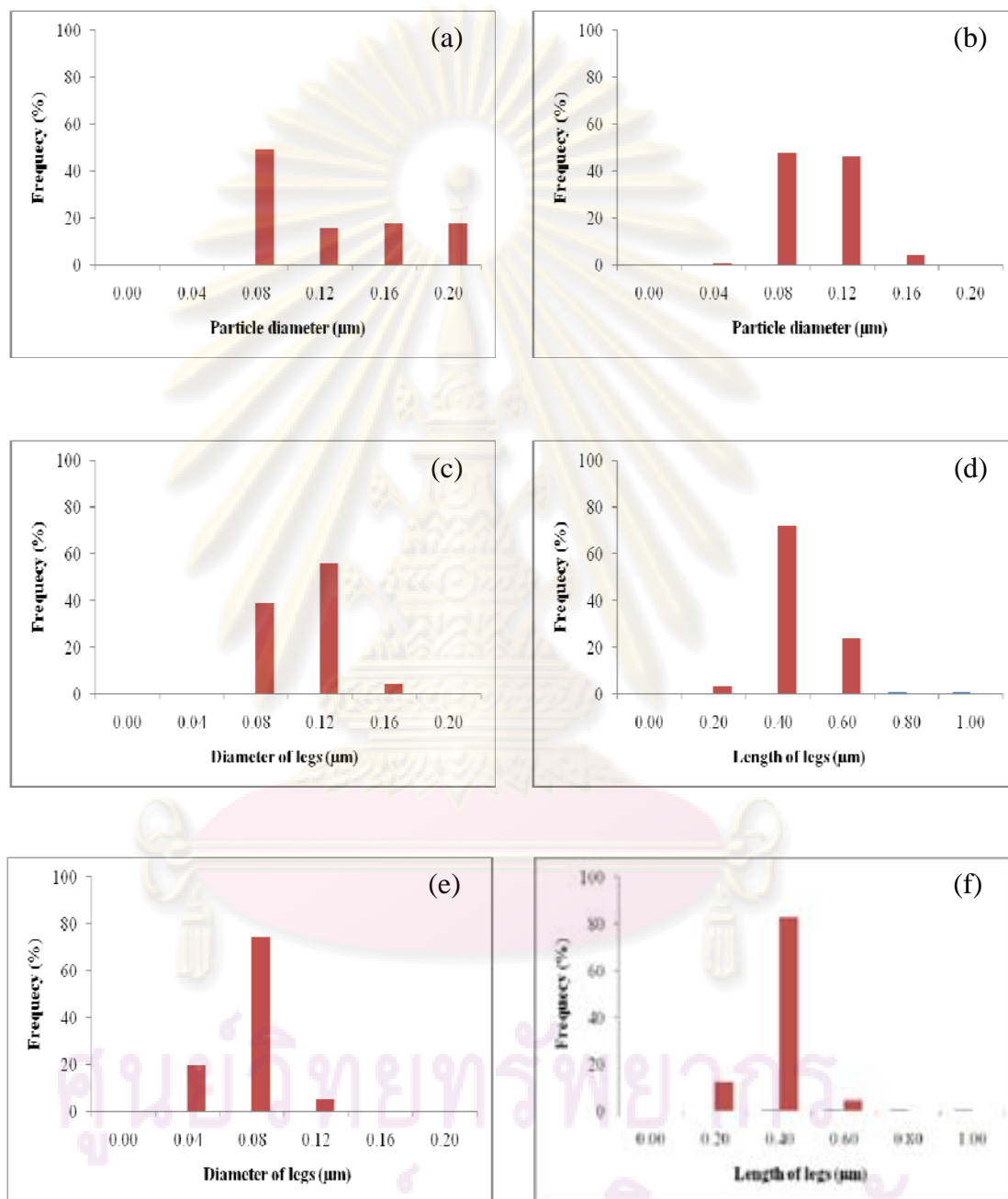


**Figure C1** Frequency distributions for diameter and length of particles varying evaporation temperature (a) sphere  $T_{\text{evp}} = 600^{\circ}\text{C}$ , (b) sphere  $T_{\text{evp}} = 700^{\circ}\text{C}$ , (c-d) tetrapods  $T_{\text{evp}} = 700^{\circ}\text{C}$  and (e-f) tetrapods  $T_{\text{evp}} = 800^{\circ}\text{C}$ .

### C2 Effect of carrier gas flow rate

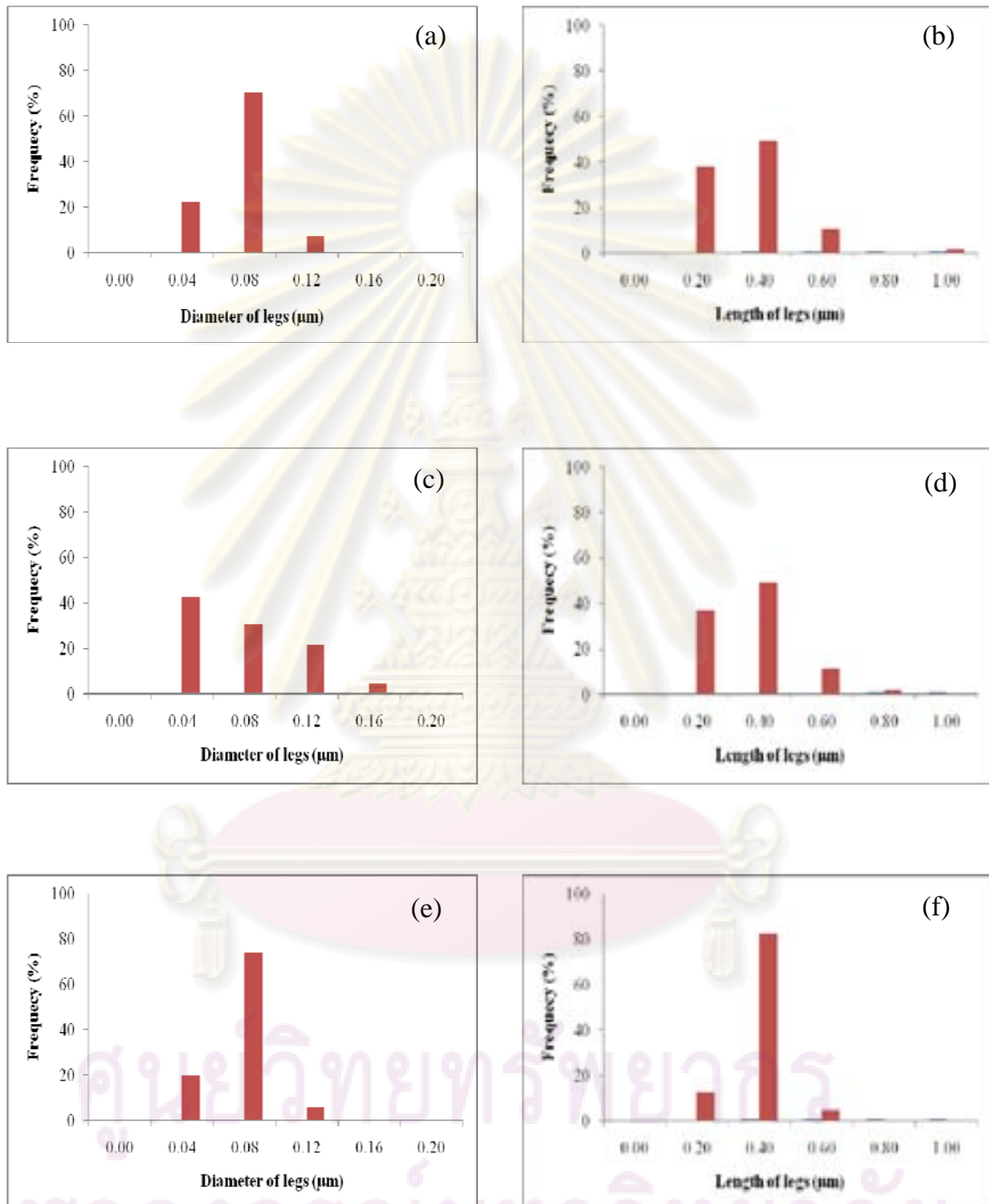


**Figure C2** Frequency distributions for diameter and length of particles using carrier nitrogen gas flow rate of: (a-b) 3 L/min, (c-d) 4 L/min and (e-f) 5 L/min.

### C3 Effect of oxygen concentration

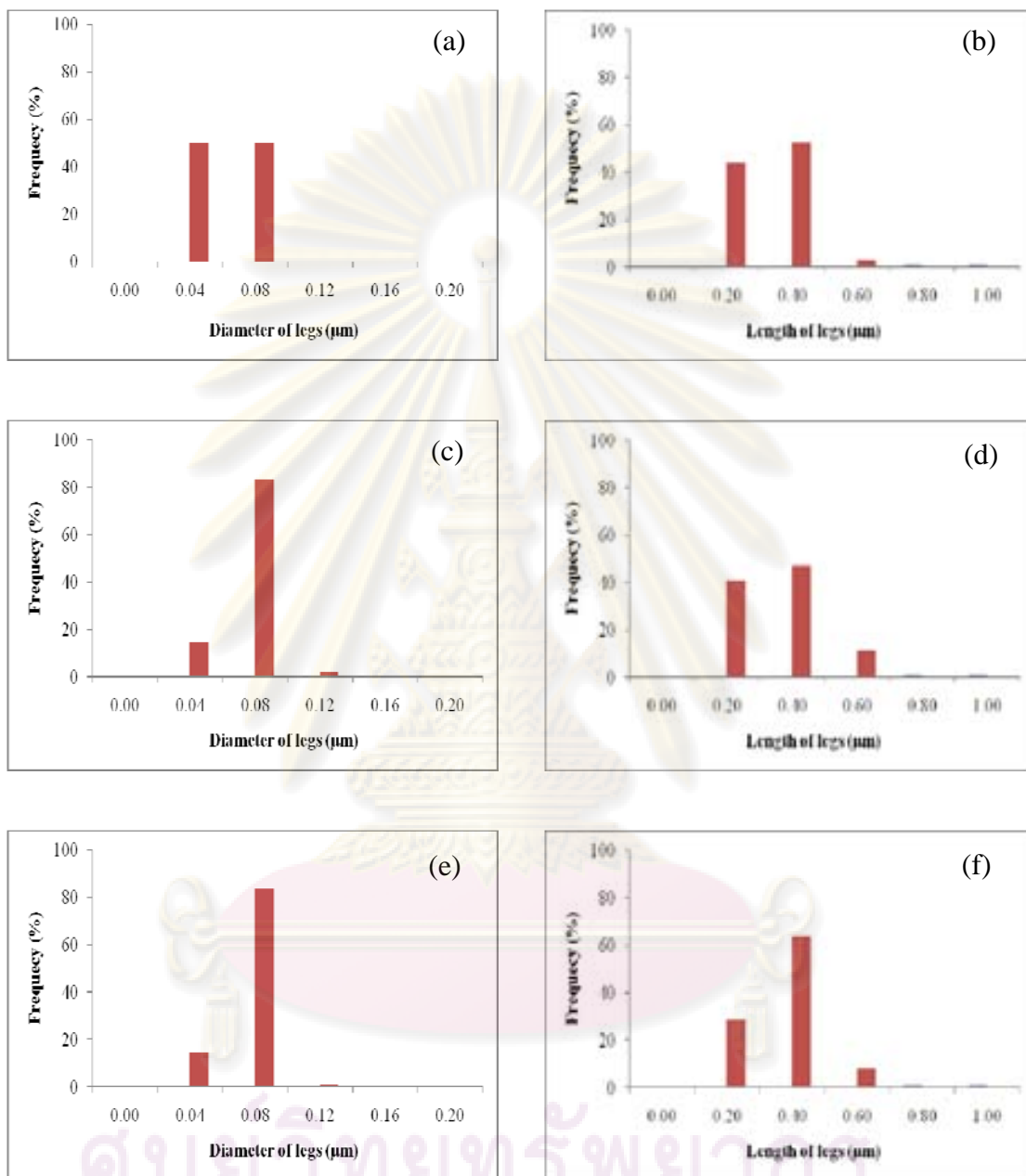


**Figure C3** Frequency distributions for diameter and length of particles using oxygen concentration of: (a-b) 1.0% by mole, (c-d) 1.5% by mole and (e-f) 2.0% by mole.

## APPENDIX D

### QUANTITY OF ZnO IN THE DIFFERENT POSITION

The quantity of ZnO in the different zones is shown in this section. The length of the system is divided into six zones, i.e. ahead reaction zone, reaction zone, dead zone, dry chamber, wet chamber and filters.

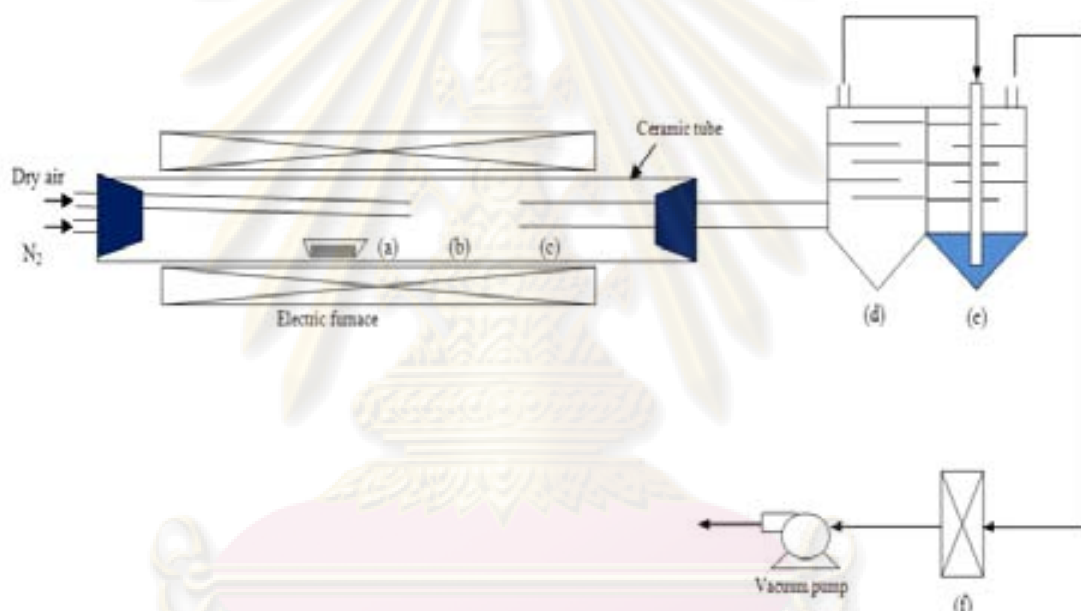


**Figure D1** Schematic diagram for product in the different zones: (a) ahead reaction zone, (b) reaction zone, (c) dead zone, (d) dry chamber, (e) wet chamber and (f) filters.

ศูนย์วิทยทรัพยากร  
จุฬาลงกรณ์มหาวิทยาลัย

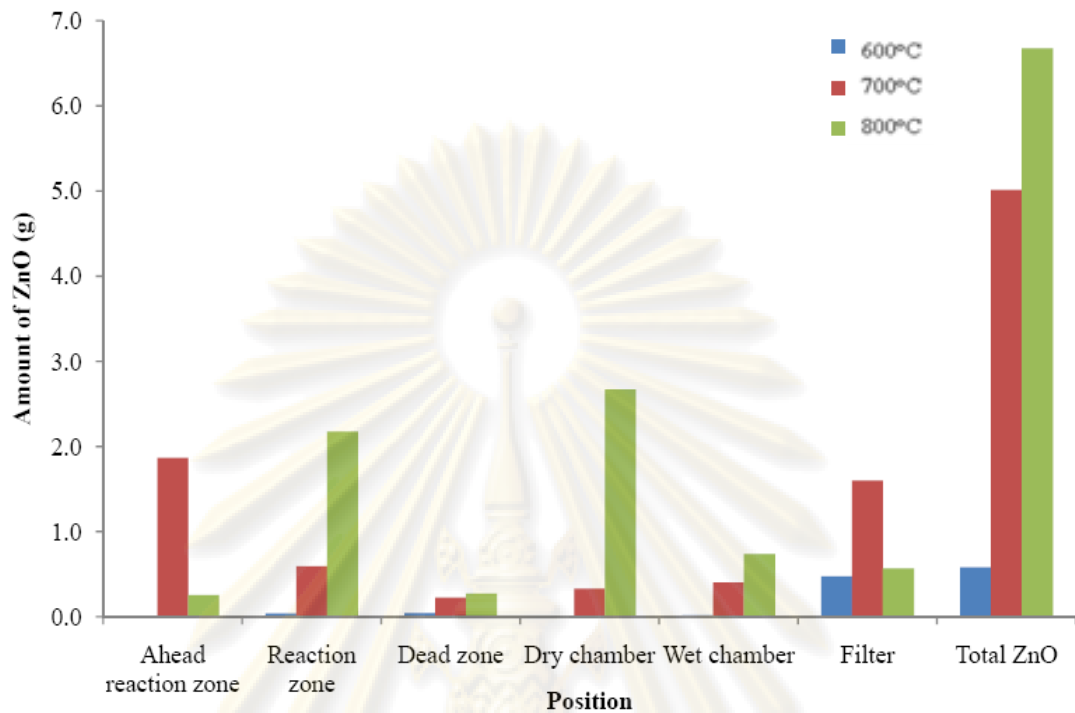


**Figure D2** The quantity of ZnO in the different position varying the evaporation temperature.

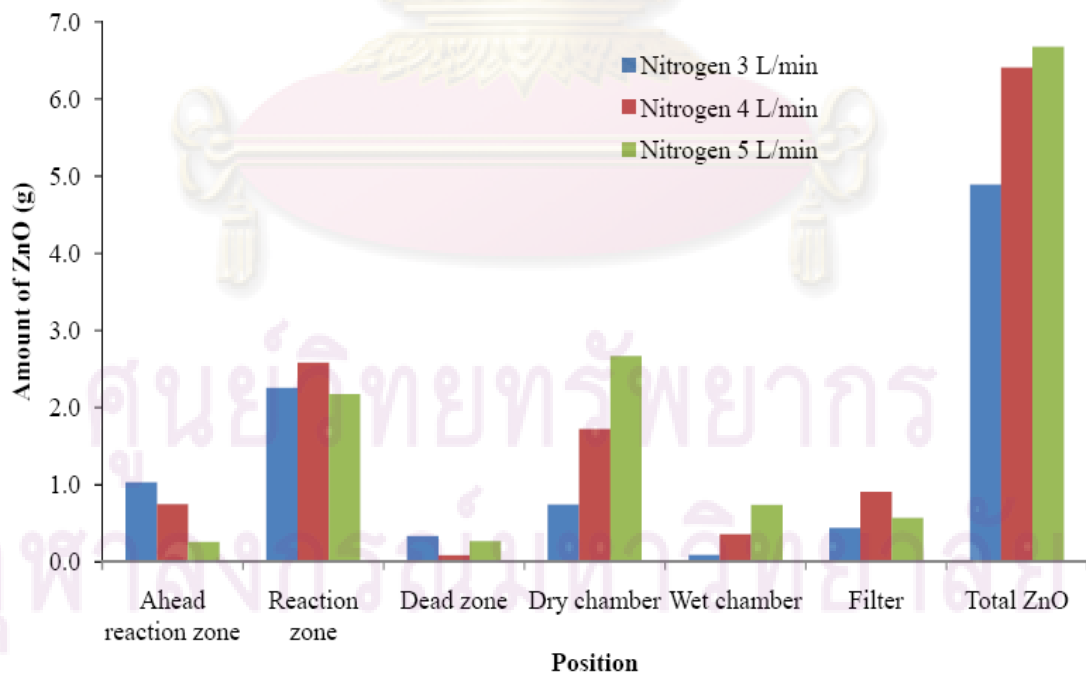


**Figure D3** The quantity of ZnO in the different position varying the carrier gas flow rate.



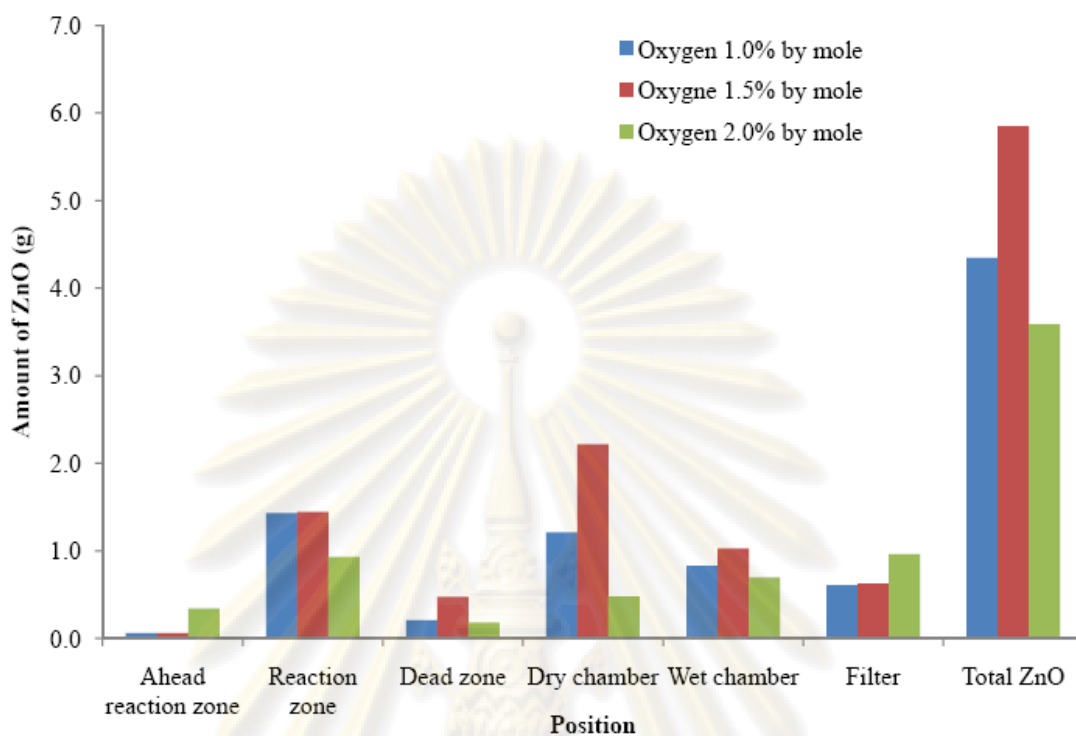


**Figure D4** The quantity of ZnO in the different position varying the oxygen concentration.

ศูนย์วิทยทรัพยากร  
จุฬาลงกรณ์มหาวิทยาลัย

**APPENDIX E****LIST OF PUBLICATION**

Chawalit Sommaneevat, Bussarakum Charnhuttakorn, Patamaporn Totemchokchaiyakarn and Varong Pavarajarn, “Synthesis of Zinc Oxide Nanopartilces by French Process”, The 5<sup>th</sup> Thailand Materials Science and Technology Conference, Bangkok, Thailand, September 16-19, 2008.



ศูนย์วิจัยทรัพยากร  
จุฬาลงกรณ์มหาวิทยาลัย



# 5<sup>th</sup> Thailand Materials Science and Technology Conference

"Materials Technology for Climate Change"

In conjunction with

- Seminar on Corrosion and its Prevention
- Tutorial on Powder X-ray Diffraction: The Rietveld Method applied to Quantitative Analysis and Microstructural Characterization
- Tutorial on Materials and Characterization for Advanced Solid Oxide Fuel Cells
- Thainox Metallurgy Award 2008

Organized by

MTEC NSTDA

September 16-19, 2008  
Miracle Grand Convention Hotel, Bangkok, Thailand  
[www.mtec.or.th/MSAT-5](http://www.mtec.or.th/MSAT-5)

Platinum Sponsors

Rigaku

Award Sponsors

SHIMADZU  
FUJIKURA  
TOYOTA  
COTTO TILES  
Polyplastics

ศูนย์วิจัยทรัพยากร  
จุฬาลงกรณ์มหาวิทยาลัย



### Synthesis of zinc oxide nanoparticles by French process

**Chawalit Sommaneevat**, Bussarakum Charnhuttakorn, Patamaporn Totemchokcharyakarn  
and Varong Pavarajam\*

Department of Chemical Engineering, Chulalongkorn University, Bangkok 10330

\*Corresponding author: Phone 0-2218-6890, Fax 0-2218-6877, E-mail: fchvpv@eng.chula.ac.th

#### Abstract

Zinc oxide nanoparticles can be synthesized by the conventional French process, which relies on the reaction between zinc vapor and oxygen in air. Morphology of the product ranges from granular nanoparticles to ZnO tetrapods. The flow rate of the carrier gas for zinc vapor as well as temperature of the reaction were found to be the key parameters controlling the morphology and size of the product.

#### 1. Introduction

Zinc oxide has been recognized as one of the most promising oxide semiconductor materials because of its good optical, electrical and piezoelectrical properties. It has received a considerable amount of attention over the last few years for many applications, such as electronics, paints, pharmaceutical uses, ceramics, photovoltaic cells, and gas sensors [1].

In the recent decade, a large variety of zinc oxide nanostructures such as rods, wires, belts, discs, tetrapods, mallets, tubes and cages, have been fabricated via several growth techniques that include molecular beam epitaxy, vapor phase transport, metalorganic chemical vapor deposition and vapor-liquid-solid (VLS) processes. It has also been found that electrical and optical properties of nanostructured zinc oxide depend sensitively on both size and shape of the particles. The value of nanosized ZnO is more than 10 times of the conventional micron-sized ZnO.

At present, the commercial zinc oxide is mostly manufactured via the French process, which is simply the oxidation of zinc vapor by air. Although this process is the cheapest and highly productive method to mass-produce ZnO, majority of the product is not nanosized and the shape of the product can not be well controlled.

In this study, we report process parameters that lead to efficient shape control in the synthesis of ZnO nanoparticles via the French process [2].

#### 2. Materials and Methods

In order to synthesize zinc oxide via the French process, pure zinc was put into an alumina boat and placed in a horizontal flow reactor. The whole system was sealed, evacuated and subsequently filled with nitrogen to eliminate residual oxygen in the system. Then, the reactor was heated up at constant rate of 10 °C/min to desired temperature. Once the reactor had reached the desired reaction temperature, nitrogen was supplied as the carrier gas for zinc vapor at the upstream end of the reactor, while air was separately fed into the middle of the reactor. The flow rate of air was kept at 600 cm<sup>3</sup>/min, while that of the carrier gas was varied in the range of 3-4 l/min. It should be noted that the end of the tube supplying air to the reactor was located beyond the position of the zinc-containing boat in the reactor so that air would not directly react with zinc metal in the boat. The reaction was conducted for 2 h. The products collected by the filter at the outlet of the reaction system, as well as the product remaining in the reactor were characterized by X-ray diffraction (XRD) and scanning electron microscopy (SEM).

#### 3. Results and Discussion

##### 3.1 Products characteristics

Figure 1 shows an example of the XRD patterns observed from all synthesized products. All diffraction peaks can be indexed to the known hexagonal wurtzite structure of ZnO. No diffraction peak from Zn or other impurity phases was found in any of the samples, confirming that the products were pure ZnO. The strong



intensity and the sharpness of the diffraction peaks indicate that the resulting products were ZnO with high crystallinity.

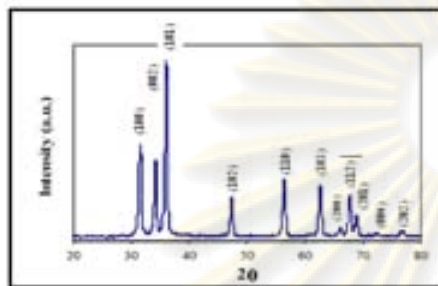


Figure 1. Sample of XRD pattern of the product.

Figure 2(a-b) show SEM micrographs of the ZnO products that were synthesized at 800 °C by using different flow rate of the carrier gas and captured by a filter. It was found that the products were collection of nanoparticles with different morphologies, including tetrapods, multipods, and small fraction of nanosheets. The diameter of legs of the pods varied in the range from 30 to 100 nm. The legs became smaller when the flow rate of the carrier gas was increased because the retention time for the reaction was reduced. It should be noted, however, that the length of the legs was not significantly affected by the flow rate. This result indicates that the growth in length of the legs took place quickly at the early stage of the reaction. This is the result from the preferred growth along *c*-direction of ZnO crystal.

In addition to the nano-pods collected by the filter downstream, ZnO microtubes was found deposited inside the reactor (Figure 2c). The microtubes had hexagonal cross-section with the average diameter about 8 μm and wall thickness of about 1.5 μm. The tube was several millimeters in length. Although the exact mechanism of the formation of the ZnO microtubes is not clear at the moment, it has been suggested that they are grown from ZnO<sub>2</sub> nuclei deposited in the system at the early stage of the reaction [3].

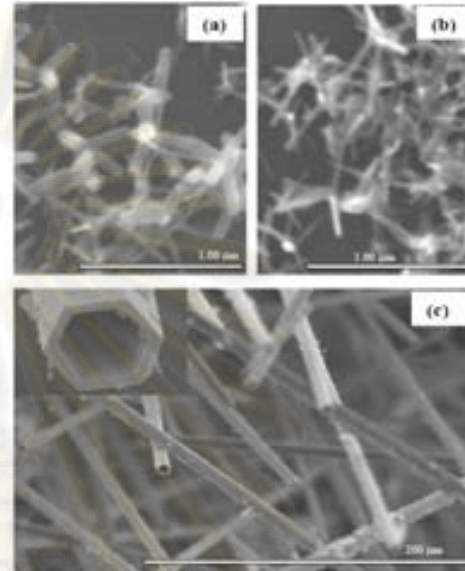


Figure 2. SEM micrographs of: (a) ZnO synthesized by using carrier gas flow rate of 3 l/min and collected by filter, (b) ZnO synthesized by using carrier gas flow rate of 4 l/min and collected by filter and (c) ZnO microtubes deposited inside the reactor.

Figure 3a shows a SEM micrograph of the products synthesized by increasing the flow rate of air to 1.5 l/min. Comparing with Figure 2a, it was found that the increase in oxygen concentration in the system caused spontaneous reaction throughout the reactor. The product was in the form of spherical nanoparticles instead of nano-pods because the increase in the air flow rate also decreased the resident time of the particle within the reactor and the crystal would not have enough time to grow.

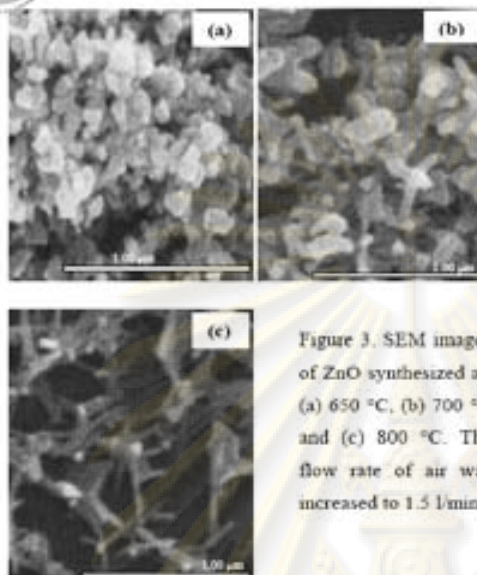


Figure 3. SEM images of ZnO synthesized at: (a) 650 °C, (b) 700 °C and (c) 800 °C. The flow rate of air was increased to 1.5 l/min.

The morphology of the product shifted from granular into tetrapods, as the reaction temperature was raised from 650 to 800°C. It should be noted that the highest temperature employed in this work was still lower than the boiling point of zinc. The increase in temperature not only affected the generation of zinc vapor, but also increase mobility of the growth species on the surface of the crystals, which allowed the growth along the preferential *c*-axis and results in product as tetrapods. The yield of the nanosized ZnO production is about 65 %.

### 3.2 Growth mechanism

The growth mechanism of ZnO nanostructures can be explained by the vapor-solid (VS) model. For the growth of tetrapods, several mechanisms have been proposed [4,5]. The main difference among these models is the difference in shapes, geometries, and crystallographic structures of the nuclei, which are subsequently overgrown during the growth process along fast growing planes.

In this work, zinc vapor was generated and formed atomic clusters of zinc that reacted instantaneously with oxygen supplied to produce primary particles of zinc oxide in the gas phase. These particles coalesced and aggregated to form larger particles. At the same time, the growth species, i.e. molecular cluster of ZnO, could also be formed on the existing ZnO nuclei, according to the VS model. The incorporation of the growth species to the ZnO crystal took place more spontaneously on the (0001) plane, which resulted in preferential growth along *c*-axis and the formation of nanorods or legs of tetrapods.

### 4. Conclusion

Nanoparticle of zinc oxide can be synthesized by modified French process. The products are ZnO with high crystallinity and low impurity. The flow rate of the carrier gas and temperature are the key parameters for controlling the morphology and size of the synthesized product.

### 5. Acknowledgement

The authors would like to acknowledge financial support from the Thailand Research Fund (TRF) under the TRF-Master Research Grant number MRG-OSMEP505E018.

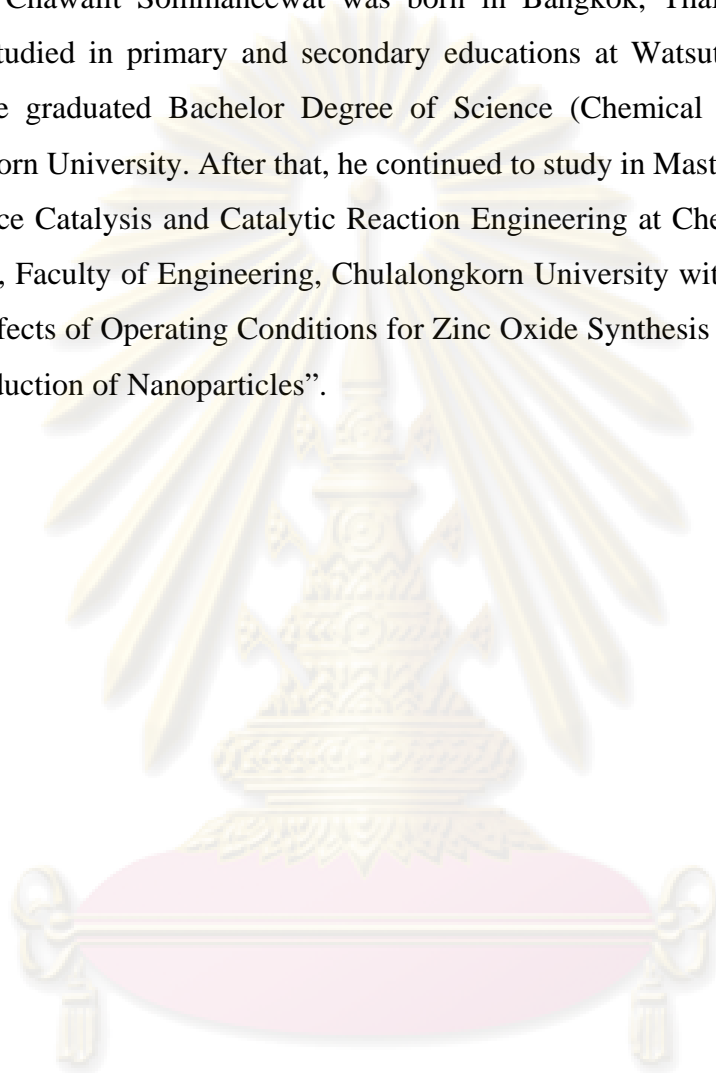
### References

- [1] S. Mahmud, M.J. Abdullah, et al., *Synthesis and Reactivity in Inorganic, Metal-Organic and Nano-Metal Chemistry* 36, 155-59 (2006).
- [2] R. Bacsa, Y. Kihn, et al., *Surface Coatings & Technology* 201, 9200-4 (2007).
- [3] T. Sun, J. Qiu, *Material Letters* 62, 1528-31 (2008).
- [4] K. Nishio, T. Ishiki, et al., *Philosophical Magazine* 76, 889-904 (1997).
- [5] C. Ronning, N.G. Shang, et al., *Journal of Applied Physics* 98, 034037-42 (2005).



## VITA

Mr. Chawalit Sommaneevat was born in Bangkok, Thailand, on June 24, 1984. He studied in primary and secondary educations at Watsuthivararam School. In 2007, he graduated Bachelor Degree of Science (Chemical Technology) from Chulalongkorn University. After that, he continued to study in Master degree in Center of Excellence Catalysis and Catalytic Reaction Engineering at Chemical Engineering Department, Faculty of Engineering, Chulalongkorn University with the master thesis entitled “Effects of Operating Conditions for Zinc Oxide Synthesis via French Process toward Production of Nanoparticles”.



ศูนย์วิทยทรัพยากร  
จุฬาลงกรณ์มหาวิทยาลัย